Division of Biomedical Engineering

Department of Human Biology

University of Cape Town

Implementation of Hadamard Encoding and Reconstruction of MEGA-Edited Spectroscopy (HERMES) for quantification of ɣ-aminobutyric acid (GABA) and glutathione (GSH)

Thesis presented for the degree of:

Master in Science (Biomedical Engineering)

Daniel Rimbault (RMBDAN003)

Supervisor: Ernesta Meintjes, Co-supervisors: Ali Alhamud, Richard Edden

Date: 27 August 2020

DECLARATION

I, Daniel Rimbault, hereby declare that the work on which this dissertation/thesis is based is my original work (except where acknowledgements indicate otherwise) and that neither the whole work nor any part of it has been, is being, or is to be submitted for another degree in this or any other university.

I empower the university to reproduce for the purpose of research either the whole or any portion of the contents in any manner whatsoever.

Signature: Signed by candidate

Date: 27/08/2019

Abstract

The present study aimed to accelerate and improve accuracy of ɣ-aminobutyric acid (GABA) and glutathione (GSH) quantification. These metabolites, present at low concentrations in the brain, are challenging to detect using MR spectroscopy due to the fact that their resonance frequencies overlap with those of other more abundant metabolites. The advanced spectral editing techniques involving J-difference editing that are required to resolve the overlapping signals of these low concentration metabolites are not routinely available on clinical MRI scanners.

In this work we implemented on a 3T Siemens Skyra MRI a novel MRS technique called Hadamard Encoding and Reconstruction of MEGA-Edited Spectroscopy (HERMES) to simultaneously detect GABA and GSH, developed a novel postprocessing technique that simultaneously models the sum and various difference spectra, and evaluated the performance of the sequence and processing method both in phantoms and in vivo.

HERMES was implemented by modifying the Siemens GABA-edited MEGA-PRESS WIP sequence to include two additional sub-experiments – one editing GSH with a single lobe pulse and one editing both GABA and GSH using a dual lobe pulse, and replacing the Siemens pulses with 'universal' pulses similar to those used in a previous implementation of HERMES on a Philips platform. Performance was assessed in a phantom and 22 healthy adults, 15 of whom provided usable data (7 male, mean age 25.6 ± 2.7 yr). Three of the subjects were scanned 3 times to assess reproducibility.

Data were processed and compared using a set of custom scripts in MATLAB. Following frequency and phase correction of individual averages with GANNET, we applied our custom simultaneous linear combination model that iteratively fit the concatenated sum and difference spectra using a least squares routine. SPM was used for tissue segmentation of structural images and FID-A to simulate high-resolution basis sets. The simultaneous modelling technique provided absolute quantification results for 15 metabolite moieties using internal unsuppressed water as a reference. The performance of the simultaneous fitting approach was compared to multiple independent fittings for HERCULES (Hadamard Editing Resolves Chemicals Using Linear-combination Estimation of Spectra) data that had been previously acquired on a 3T Philips Achieva MRI.

Although the HERMES sequence implemented on the Siemens platform as part of this project was able to successfully edit both GABA and GSH, and generate line shapes consistent with the work by Saleh et al. (2016), quantification accuracy was disappointing. In the phantom data, GSH and GABA concentrations were both roughly 50% of known levels. Since the actual concentrations in vivo were not known, we were not able to establish accuracy, but quantification agreement between the MEGA-PRESS and HERMES sequences was poor for most metabolites. Specifically, GABA levels were two to three times higher than expected values using both HERMES and GABA-edited MEGA-PRESS. Despite poor absolute agreement, concentrations from HERMES and MEGA-PRESS data were moderately correlated, and HERMES data showed lower coefficients of variation across subjects, suggesting that it may be more reliable. HERMES was also more reproducible across scanning sessions and participants for more metabolites than GABA- or GSH-edited MEGA-PRESS.

Our findings also showed that simultaneous fitting using the sum and difference spectra produces lower coefficients of variation for most metabolites than fittings to sum and difference spectra separately.

Table of Contents

List of Figures

List of Tables

1 Introduction

Magnetic resonance imaging (MRI) exploits the interactions that occur between different types of magnetic fields and an active element. Active elements in the human body that can be imaged include hydrogen (^{1}H), carbon (^{13}C), sodium (^{23}Na) and phosphorus (^{31}P). However, due to the abundance of ^{1}H in water in human tissues and its higher gyromagnetic ratio (γ) compared to other elements, ^{1}H is the most commonly imaged element in MRI.

While MRI is used to image ^{1}H in water, magnetic resonance spectroscopy (MRS) allows direct detection and quantification of different endogenous metabolites containing ^{1}H. Shielding by electrons of adjacent atoms causes small disturbances in the local B0 fields experienced by ^{1}H nuclei in different chemical environments, resulting in shifts in the precessional frequency known as the chemical shift. Metabolites that are typically detected in the human brain include N-acetylaspartate (NAA), creatine (Cr), choline (Cho), myo-inositol (Ins), and glutamate (Glu) (de Graaf 2007). These metabolites can be robustly detected on clinical MRI scanners with field strengths of 3 T, due to their adequate concentrations in human brain and their well distinguished chemical shifts. Recently, there has been increasing interest in measuring γ-aminobutyric acid (GABA) and glutathione (GSH) levels in the brain. GABA is the chief inhibitory neurotransmitter in the brain and plays a role in the menstrual cycle, acute differentiation, visual light-dark adaptation, alcohol and substance abuse, epilepsy, depression, and panic disorders. GSH is a major anti-oxidant in the brain and alterations in levels have been linked to damage in myelin, oligodendrocytes and mitochondria, Parkinson's Disease, Multiple Sclerosis (MS), and other neurodegenerative diseases.

1.1 Problem Identification

In vivo measurements of GABA and GSH are, however, challenging due to their low concentrations in the brain and the fact that their resonance frequencies overlap with those of other metabolites present in higher concentrations. As a result, GABA and GSH MRS require the application of advanced spectral editing techniques that are not routinely available on clinical MRI scanners.

The first aim of this project was to implement on a 3 T Siemens Skyra scanner an MRS technique called Hadamard Encoding and Reconstruction of MEGA-Edited Spectroscopy (HERMES) for measuring simultaneously GABA and GSH levels of tissue noninvasively. HERMES utilises the J-coupling phenomenon of adjacent hydrogen atoms in a molecule with a technique known as J-difference editing. The technique allows for the differential phase evolution of a desired hydrogen atom by inverting the atom coupled to it with an editing RF pulse in a distinct region of the spectrum (i.e. at a different frequency). By comparing the edited spectrum to an unedited spectrum from the same voxel, one can determine the portion of the signal that was contributed by the coupled proton of interest. This technique is usually employed using the MEGA-PRESS sequence for a single metabolite at a time. HERMES builds on this by encoding two editing schemes simultaneously using an orthogonal Hadamard matrix, which allows the resolution of two low concentration metabolites simultaneously. Although this technique has previously been implemented on a Philips Intera 3 T scanner at the Johns Hopkins University, it has not been implemented previously on a Siemens platform.

Historically, and particularly prior to 3 T scanners, clinical applications of MRS have been limited by poor sensitivity of metabolite quantification (Van Der Graaf 2010), especially for metabolites present in low concentrations. Although incorporating prior knowledge of the spin system evolution of different metabolites has improved the accuracy and stability of metabolite quantification from HERMES data, current approaches all consider difference spectra of specific metabolites in isolation. Here we implement a method that simultaneously models the sum and difference spectra of all metabolites and evaluate *in vivo* the reproducibility of the proposed approach for GABA and GSH quantification from HERMES data.

1.2 Objectives

The objectives of the research are as follows:

1. HERMES sequence development
   1.1. To modify the standard Siemens MEGA-PRESS pulse sequence (svs_edit work-in-progress (WIP) package) to perform HERMES acquisitions. This involves editing the source code of the pulse program and generating appropriate protocols.
   1.2. To standardise both pulse shapes and pulse timing to the Philips implementation as per Saleh et al. (2019).
   1.3. To install and validate the sequence on the 3T Siemens Skyra at the Cape Universities Body Imaging Centre (CUBIC) located at Groote Schuur Hospital adjacent to the UCT Faculty of Health Sciences.

2. Develop a Simultaneous modelling technique
   2.1. To produce a complete basis set for the HERMES sequence of expected metabolite spectra using density matrix simulations.
   2.2. To develop a novel data processing technique in the MATLAB environment that incorporates prior knowledge and simultaneously models all data to quantify metabolite levels.

3. Testing
   3.1. Compare spectral line shapes and quantification accuracy of HERMES and MEGA-PRESS acquisitions in phantoms.
   3.2. Compare HERMES and MEGA-PRESS line shapes and quantification *in vivo*.
   3.3. Assess quantification reproducibility *in vivo*.
   3.4. Compare performance of the simultaneous fitting routine to multiple separate fittings.

1.3 Thesis Outline

Following the general introduction in Chapter 1, Chapter 2 presents basic principles of MRI and MRS, as well as theory related specifically to editing and quantification of GABA and GSH. MRI pulse sequences are also introduced, including various design considerations.

Chapter 3 reviews the current and relevant literature, followed by a description of the methods employed in Chapter 4. Chapter 4 comprises three sections – the first describes the sequence development, the second the development of the simultaneous modelling tool, and the last the experiments performed to test performance of both the sequence and modelling tool.

Chapter 5 presents the results in 4 sections – phantom tests, in vivo tests, assessment of reproducibility, and comparison of simultaneous fitting to separate independent fitting. Chapter 6 presents a discussion of the results and chapter 7 some final conclusions and recommendations for future work.

2 Background Theory

Figure 2-1 shows a typical ^{1}H MRS spectrum where signals from different metabolites are plotted as a function of their frequency shift relative to a reference frequency. The chemical shift in parts per million (ppm) is defined as

$$Chemical\ shift\ (ppm) = \frac{Frequency - Reference\ Frequency}{Reference\ Frequency} \times 10^{6}.$$

The fact that the spectrum contains several metabolites in a small chemical shift range leads to considerable spectral overlap, impeding spectral peak assignment and quantification, especially of metabolites present in low concentrations. For example, the GABA peak at 1.9 ppm can only be distinguished from NAA using advanced editing pulse sequences such as MEGA-PRESS (Mescher-Garwood Point Resolved Spectroscopy) (Mullins et al. 2014). Furthermore, GSH is extremely difficult to isolate due to its frequency overlap with glutamate, glutamine, GABA, Cr+PCr, aspartate, and NAA (Govindaraju et al. 2000), even at high magnetic field strengths such as 14 T. A significant drawback of MEGA-PRESS is that it usually only edits one metabolite at a time, and from a single brain region. Recently, the Hadamard Encoding and Reconstruction of MEGA-Edited Spectroscopy (HERMES) approach (Chan et al. 2016) was introduced, that separately edits more than one metabolite with overlapping signals within a single acquisition.

HERMES typically achieves single volume localisation using Point Resolved Spectroscopy (PRESS) (Chan et al. 2016) (Saleh et al. 2016), and water suppression with a vendor-specific water suppression scheme (in the case of Siemens this is an optimised CHESS scheme (Ernst & Hennig 1995)). Additionally, J-difference editing is implemented using MEGA (Terpstra et al. 2006), but is multiplexed for multiple metabolite signals using Hadamard Encoding. These concepts are described in greater detail in the following sections.

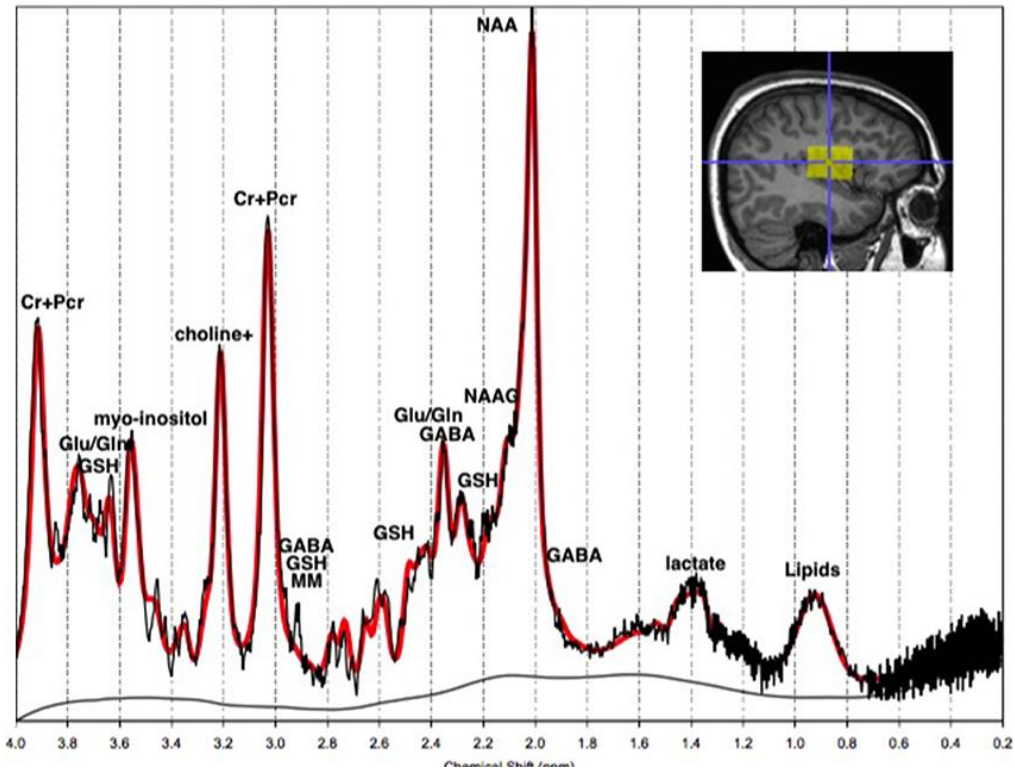

Figure 2-1 - ^{1}H-MRS spectrum acquired at 3T from the left temporal lobe of a healthy adult (Ford & Crewther 2016)*. The Y-axis gives the signal amplitude at different chemical shifts, and the integrated areas under specific peaks give the relative concentrations of said metabolites.*

2.1 Properties of GABA and GSH

2.1.1 γ-Aminobutyric acid (GABA)

GABA (γ-aminobutyric acid) is the chief inhibitory neurotransmitter in the brain. Figure 2-2 shows its chemical structure and MR spectrum. GABA has six observable protons. At 3T field strengths, triplet resonances are observable at 3.01 and 2.28 ppm, while a quintet is observable at 1.9 ppm (de Graaf 2007).

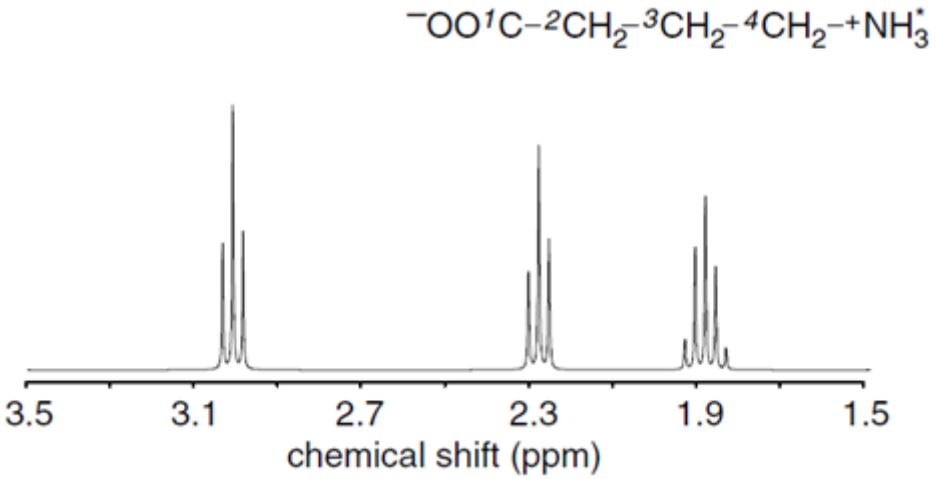

Figure 2-2 - The magnetic signature of GABA obtained from simulation (de Graaf 2007)

2.1.2 Glutathione (GSH)

GSH is a major antioxidant in the brain. Figure 2-3 shows its chemical structure and MR spectrum. Glutathione has a singlet at 3.77 ppm, two separate multiplets at 2.15 and 2.55 ppm, and three doublet-of-doublets at 2.93, 2.98, and 4.56 ppm.

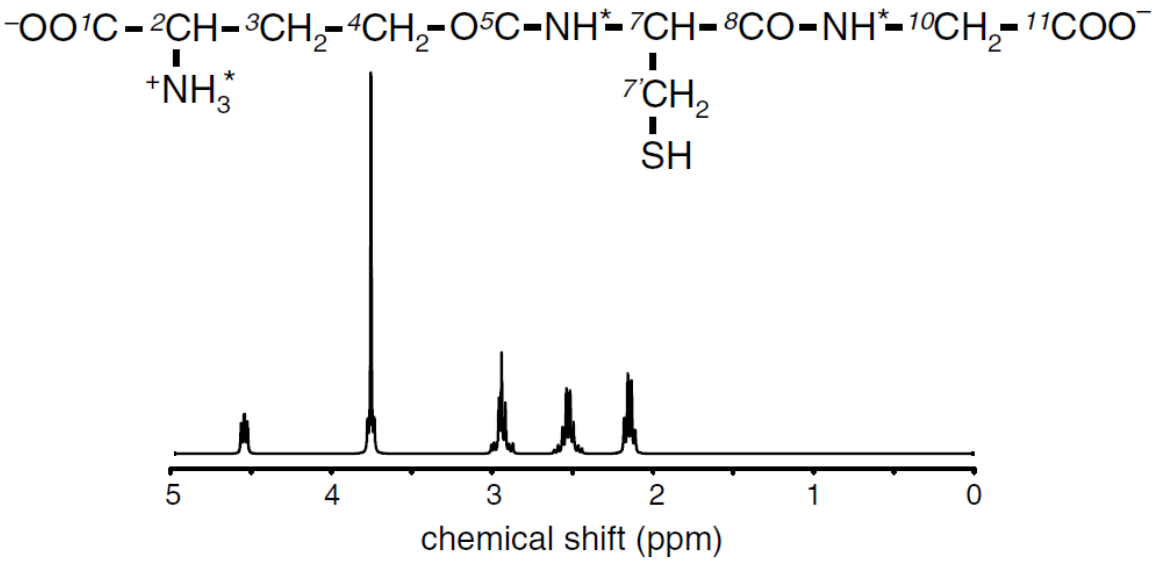

Figure 2-3 - The magnetic signature of GSH obtained from simulation (de Graaf 2007)

GABA and GSH are both considered low concentration metabolites, with concentrations ranging from 1.3 to 1.9 mM for GABA and 2 mM for GSH. Their signals overlap with the stronger creatine peak at 3 ppm, with creatine concentrations typically ranging from 5.1 to 10.6 mM, depending on the brain tissue type (Govindaraju et al. 2000). Since both GABA and GSH have coupled ^{1}H nuclei with split peaks, they can be isolated using J-difference editing. Although several sequences have been proposed to detect GABA, including 2D H NMR spectroscopy (Ryner et al. 1995a), double Band Selective Inversion with Gradient Dephasing (double BASING) (Star-Lack et al. 1998), and double-quantum filter experiments (Mclean et al. 2002), the most commonly used is the MEGA-PRESS sequence (Mescher et al. 1998). HERMES implements a multiplexed experiment that can be thought of as two simultaneous MEGA-PRESS acquisitions. Both HERMES and MEGA-PRESS are single voxel spectroscopy (SVS) techniques.

2.2 Single Voxel Spectroscopy (SVS)

Single voxel spectroscopy (SVS) acquires signal from a single region of space, typically with a volume ranging from 1 to 8 ml. Various methods have been developed to localise the signal during SVS, including Stimulated Echo Acquisition Mode (STEAM) (Frahm et al. 1987), Point Resolved Spectroscopy (PRESS) (Bottomley 1987), Localization by Adiabatic Selective Refocussing (LASER) (Garwood & Delabarre 2001), and Spin Echo Full Intensity Acquired Localised Spectroscopy (SPECIAL) (Fuchs et al. 2013). While the use of 6 adiabatic full-passage (AFP) pulses by LASER improves spatial localisation, this comes at the cost of longer echo times compared to PRESS and STEAM (de Graaf 2007). In the current work, we use PRESS localisation due to its higher signal to noise ratio compared to STEAM, and the fact that it is the technique employed in the MEGA-PRESS WIP we were adapting. PRESS excites the ^{1}H nuclei using a slice selective 90° RF pulse, followed by two 180° RF pulses that are selective for mutually orthogonal slices, and crusher gradients between the RF pulses. PRESS has the advantage that it recovers the full available magnetisation and achieves reasonably fast echo times (TE < 35 ms) (Blüml & Panigrahy 2013). Figure 2-4 shows the generic PRESS pulse sequence.

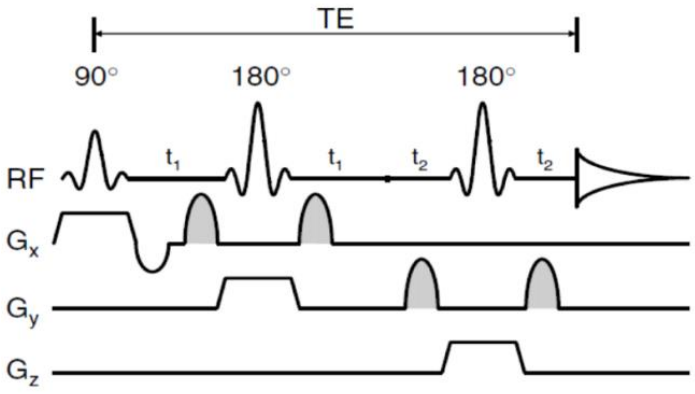

Figure 2-4 – PRESS pulse sequence showing three radiofrequency pulses and gradient pulses in the x, y, and z directions (de Graaf 2007)

A key scanner detail that impacts the quality of the MR spectrum obtained is shimming. Shimming is the process of correcting inhomogeneities in the B0 field. All scanners undergo passive shim correction during commissioning, which corrects some zero- and first-order inhomogeneities. In addition, most scanners feature active shimming with dedicated shim coils, similar to the gradient coils, which allow for small adjustments to the field following the acquisition of a field map. Second-order shim correction is standard on Siemens Skyra and Prisma scanners, while this is an option on Siemens Vida scanners. Figure 2-5 illustrates the difference between first- and second-order shim fields.

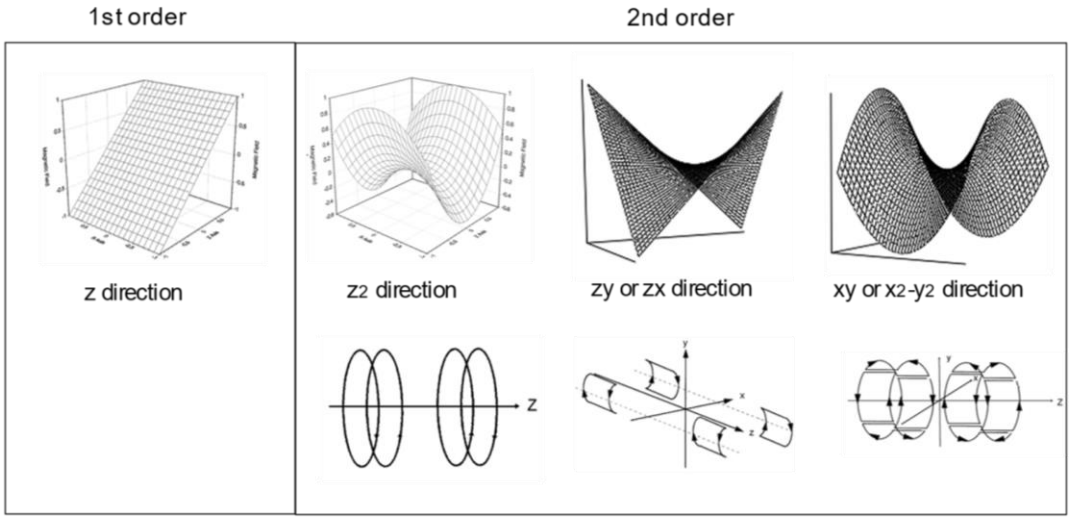

Figure 2-5 - Illustration of 1st and 2nd order shim fields, with gradient coil generalised geometry adapted from (Wendt 2000)

Using the shim coils, the equation representing the corrected B0 field becomes

$$B0_{corrected} = B0_{uncorrected} + A_{11}x + A_{12}y + A_{13}z + A_{21}z^2 + A_{22}zy + A_{23}zx + A_{24}xy + A_{25}(x^2 - y^2),$$

where A_{11}, A_{12} and A_{13} are three linear/1st order coefficients, and the remaining five are second-order coefficients. If there were 3rd order correction, an additional five terms would be required. Using the shim coils, most MRI scanners automatically perform manual shimming before the start of a spectroscopy acquisition. Once the field maps have been generated, the scanner records the full width half maximum (FWHM) (Figure 2-6) of the water peak and prompts the user to accept or reject the shim.

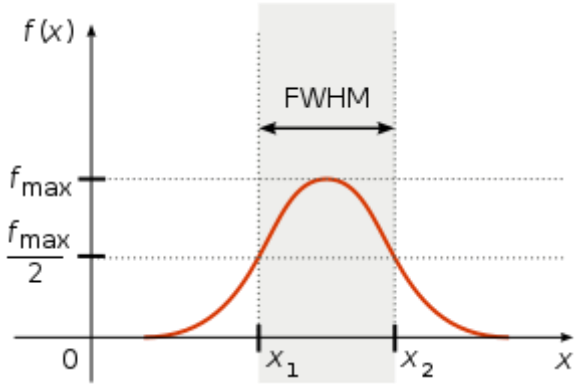

Figure 2-6 - Generalised illustration of the Full Width Half Maximum (FWHM) of a signal (Nordmann 2007)

The water FWHM is a useful measure of field homogeneity, as water protons should in a perfectly homogeneous field all precess at the same frequency due to the absence of local shielding effects. As such, any differences in precessional frequency can be attributed to local B0 field inhomogeneities.

2.2.1 Water Suppression in MRS

The most abundant molecule in brain tissue is water. Hydrogen nuclei in water generate an MRI signal at 4.7 ppm relative to Tetramethylsilane (TMS) that is three orders of magnitude larger than the signal from most other hydrogen-containing metabolites (Figure 2-7). Vibration induced signal modulations of this signal cause sidebands to the water peak that also distort the surrounding spectrum (de Graaf 2007). As such, accurate quantification of other metabolite concentrations requires that the water signal be suppressed.

Methods for water suppression include binomial pulse sequences (Sklenar & Starcuk 1982), frequency selective refocussing such as MEGA (Mescher et al. 1996), relaxation-based methods such as WET (Water Suppression Enhanced through T1 effects) (Ogg et al. 1994), and frequency selective excitation methods such as Chemical Shift Selective Saturation (CHESS) (Haase et al. 1985), SWAMP (Suppression of Water and Adiabatic-Modulated Pulses) (de Graaf & Nicolay 1998), and VAPOR (Variable Power Radiofrequency Pulses with Optimised Relaxation Delays) (Tkáč et al. 1999). SWAMP and VAPOR are variations of CHESS that have been optimised for different applications. All CHESS-based methods involve selectively exciting and then dephasing with crusher gradients the water signal prior to the MRS acquisition. Different MRI vendors employ different water suppression techniques. Siemens uses a three pulse optimised CHESS scheme referred to as 'Strong Water Suppression'.

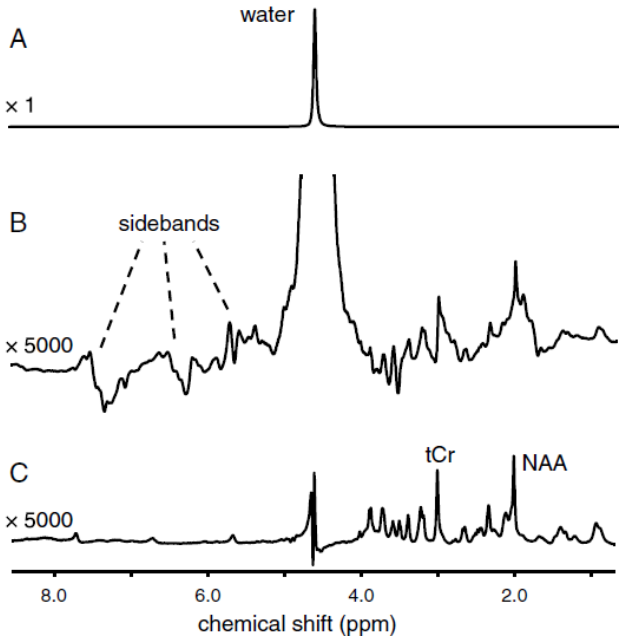

Figure 2-7 – MRS spectrum of brain tissue; A) spectrum with unsuppressed water signal scale x1, B) spectrum with unsuppressed water signal scale x5000 showing sidebands, C) spectrum with water signal suppressed scale x5000 (de Graaf 2007).

2.2.2 Spectral Editing

Spectral editing is the technique implemented to separate overlapped metabolites. Spectral editing utilizes scalar coupling between spins to separate scalar-coupled and uncoupled spins.

2.2.3 J-coupling (scalar coupling)

Energy states of nuclei depend on their quantised angular momentum. Since the spin quantum number (S) of a ^{1}H nucleus is ½, its nuclear spin is aligned either parallel (lower energy alpha (α) state) or antiparallel (higher energy beta (β) state) to the external magnetic field and its spectral peak corresponds to the characteristic frequency of the energy difference between the α and β states. In an isolated atom, the Fermi contact energetically favours an antiparallel orientation between nuclear and electronic spins. As such, the electron spin will be aligned antiparallel to the nuclear spin.

However, when the proton is covalently bonded to another atom (I) also with nuclear spin ½, it is possible for the nuclear spins of both atoms to be aligned either antiparallel (ββ) or parallel (αα) to the external magnetic field. In such situations, the Pauli exclusion principle dictates that the two bonding electrons have to be antiparallel to each other and as such cannot both be antiparallel to the nuclear spins as well. This forces one of the two nuclear-electronic spin pairs to be parallel, which is energetically less favourable, thus slightly increasing the energy levels of the ββ and αα states of the two-spin system by an amount proportional to the scalar coupling constant (J_{IS}). In contrast, when the nuclear spins of the two species are antiparallel to each other (i.e. the αβ and βα states), the electron spins of both species can be antiparallel to their respective nuclear spins and still be antiparallel to each other. Since this is energetically favourable, the corresponding energy levels of the two-spin system are decreased by an amount equal to the energy increase of the ββ and αα states. As such, for the S nucleus in the two-spin system, the energy difference between the β and α states is now increased or decreased by half the value of J_{IS} depending on whether nuclear spin I is, respectively, antiparallel (β) or parallel (α) to the external field. The energy differences are illustrated in Figure 2-8.

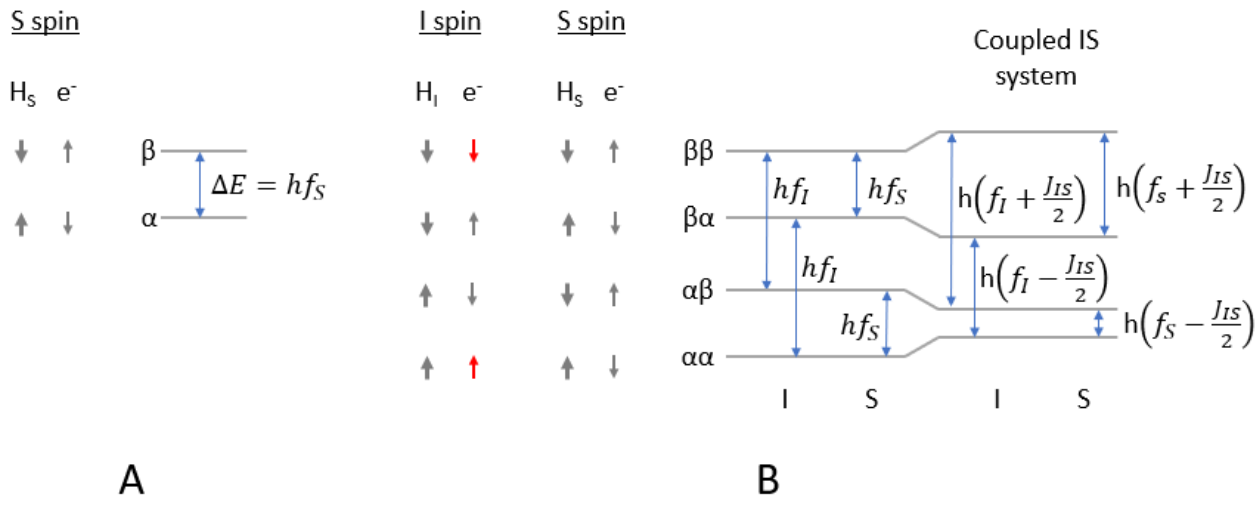

Figure 2-8 - A) The energy difference between nuclear spins aligned parallel (lower energy α state) and antiparallel (higher energy β state) to the external magnetic field (pointing vertically up in this example) is proportional to the precessional frequency of the nucleus. In this case, of an isolated S-spin, the electron and nuclear spins will be antiparallel. B) The four combinations of a weakly coupled IS spin system. For the ββ and αα combinations, the nuclear and electron spins of the I-spin are parallel (highlighted in red), which is energetically less favourable thus slightly increasing the energy levels of these states. In contrast, for the αβ and βα states, the electron and nuclear spins of both nuclei I and S are anti-parallel, thus lowering the energy levels corresponding to these states. These changes alter the energy that is released when nuclear transitions occur, depending on whether the nucleus under consideration (I or S) is coupled with a nucleus that is in a β (giving a slightly higher frequency/left shift) or α (giving a slightly lower frequency/right shift) state.

The spectral peak of nucleus I (or S) is therefore divided into two peaks of equal intensity separated by J_{IS} (Figure 2-9). These splittings that arise from magnetic interactions between electron and nuclear spins are termed scalar or J-J couplings.

Two peaks of equal intensity, however, only arise when the difference between the resonance frequencies of the two nuclear species I and S is much greater than the scalar coupling between them. This is typically true for heteronuclear couplings and in such cases the spin system is said to be weakly coupled. For homonuclear interactions, the frequency difference may be similar to the scalar coupling constant giving rise to strongly coupled spin systems. The $\alpha\beta$ and $\beta\alpha$ spin states now become mixed resulting in more complicated spectra with higher order effects.

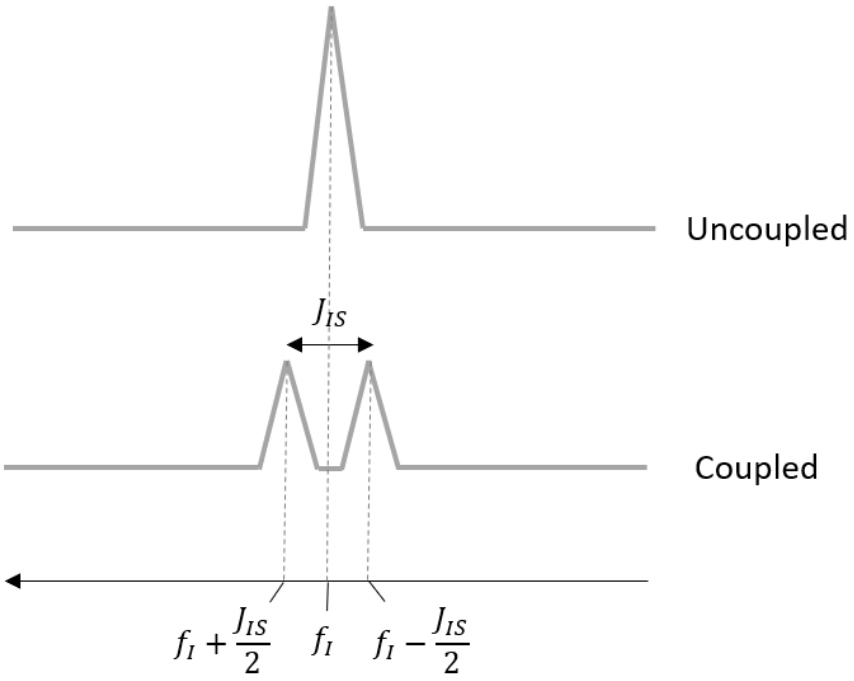

Figure 2-9 – Figure illustrating the I-spectrum of an uncoupled and weakly coupled IS system. The splitting of the peak to form a doublet can be seen in the coupled spectrum.

2.2.4 J-difference editing using MEGA

MEGA is a frequency selective refocusing method, originally used as a water suppression technique (Mescher et al. 1996), that employs J-difference editing to distinguish coupled peaks from overlapping uncoupled peaks in an MRS spectrum. MEGA features one sub-experiment (OFF) with a 90 degree excitation and a frequency-nonselective 180 degree refocusing pulse (i.e. a normal spin echo experiment) (top row Figure 2-10A), and a second sub-experiment (ON) with two 180 degree pulses selective for the S spin inserted symmetrically around the frequency-nonselective refocussing pulse — one mid-way between the excitation RF and frequency-nonselective refocusing pulse and the other between the refocusing pulse and acquisition (Figure 2-10A, bottom row).

In the latter acquisition, the selective 180 degree pulses invert the S spin population only. For coupled spins, this will cause slower rotating I spins attached to S spins in the α-state before the 180 degree pulse to become faster rotating I spins attached to S spins in the β-state after the selective 180 degree pulse, and vice versa. Since the selective 180 degree pulse only inverts the sense of rotation of the coupled I spin but does not reset its phase, the I-spin coherences will be perfectly refocused at TE/2. As such the two different I-spin populations

of a coupled two-spin system will be completely in-phase at TE/2 when the frequency-nonselective refocusing pulse is applied, and again at TE when the signal is acquired. It is worth noting here that the evolution of coupling during TE is fully refocussed, thus maximizing editing efficiency, when the two editing pulses are separated by TE/2. In the presence of the two selective 180 degree RF pulses, the coupled I spins are therefore in-phase with each other at TE, as well as resonances from uncoupled spins (Figure 2-10B, bottom row). The modulation of the I-spin signal (and the signal from uncoupled spins) is therefore given by

$$I_y e^{-TE/T_2},$$

where I_y is the component of the thermal equilibrium magnetisation of spin I (I_z) that was flipped by the RF pulse into the transverse plane.

In contrast, during the spin echo acquisition, the two I-spin populations of a coupled two-spin system will acquire a net phase shift relative to uncoupled spins that depends on the echo time TE. This is due to the fact that the frequency-nonselective 180 degree refocusing pulse inverts both the acquired phases of the I spins and the S-spin population. While resetting the acquired phase of an uncoupled spin population results in the spin population being back in-phase at TE, the fact that the sense of rotation is also inverted for I spins coupled to S spins, causes the two I-spin populations (one coupled to S spins in the α-state and the other to S spins in the β-state) to acquire a net phase difference relative to each other, as well as a phase shift relative to uncoupled spins. The signal modulation of the I spin is then given by

$$\left[I_y \cos(\pi J_{IS} TE)\right] e^{-\frac{TE}{T_2}},$$

where J_{IS} is the scalar coupling constant. Notably, for TE = $1/J_{IS}$, the two I-spin populations will be in-phase with each other, but 180 degrees out-of-phase with resonances from uncoupled spins (Figure 2-10B, top row).

Subtraction of the spectra with the coupled spins being in-phase and out-of-phase allow the coupled spins to be observed, while adding the two spectra give the uncoupled resonances. In this way, the signals from coupled spins (such as GABA and GSH) that are hidden by larger uncoupled signals can be isolated. In the case of GABA detection, the narrow band editing pulses are applied at 1.9 ppm, and for glutathione at 4.56 ppm.

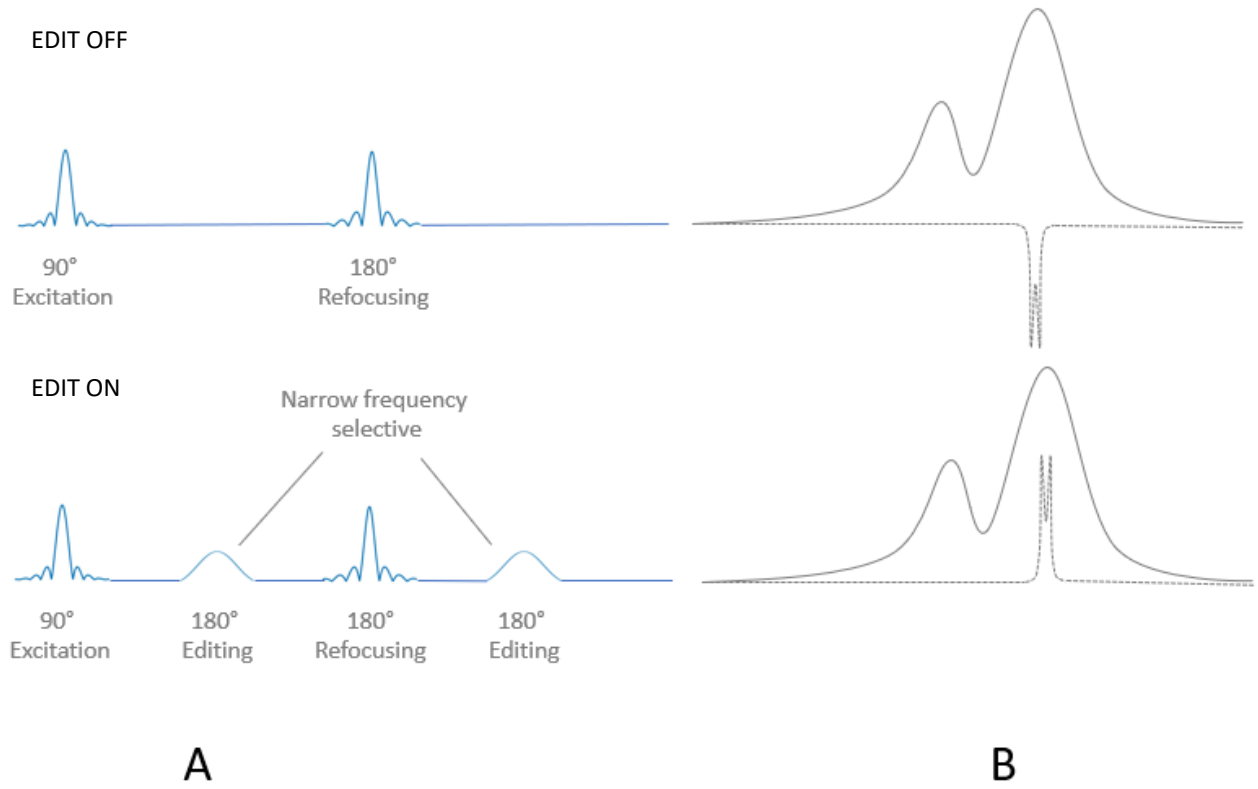

Figure 2-10 – Illustration of J-difference editing for resolution of an I-spin weakly coupled to an S-spin. A) The two RF pulse sequences. The top sequence is the 'EDIT OFF' sequence where no frequency selective editing pulses are applied. The bottom sequence is the 'EDIT ON' sequence where a pair of frequency selective editing pulses are added. B) The acquired spectra from both sequences. The dotted line shows the signal of the coupled I-spins. For the 'EDIT OFF' acquisition, the I-spins are out-of-phase with uncoupled spins, while they are in phase for the 'EDIT ON' acquisition.

MEGA-PRESS (Mescher et al. 1998) is a spatial localisation variation of MEGA, which features an additional 180 degree refocussing pulse. Figure 2-11 shows the MEGA and MEGA-PRESS sequences. Timing details will be discussed in greater detail later.

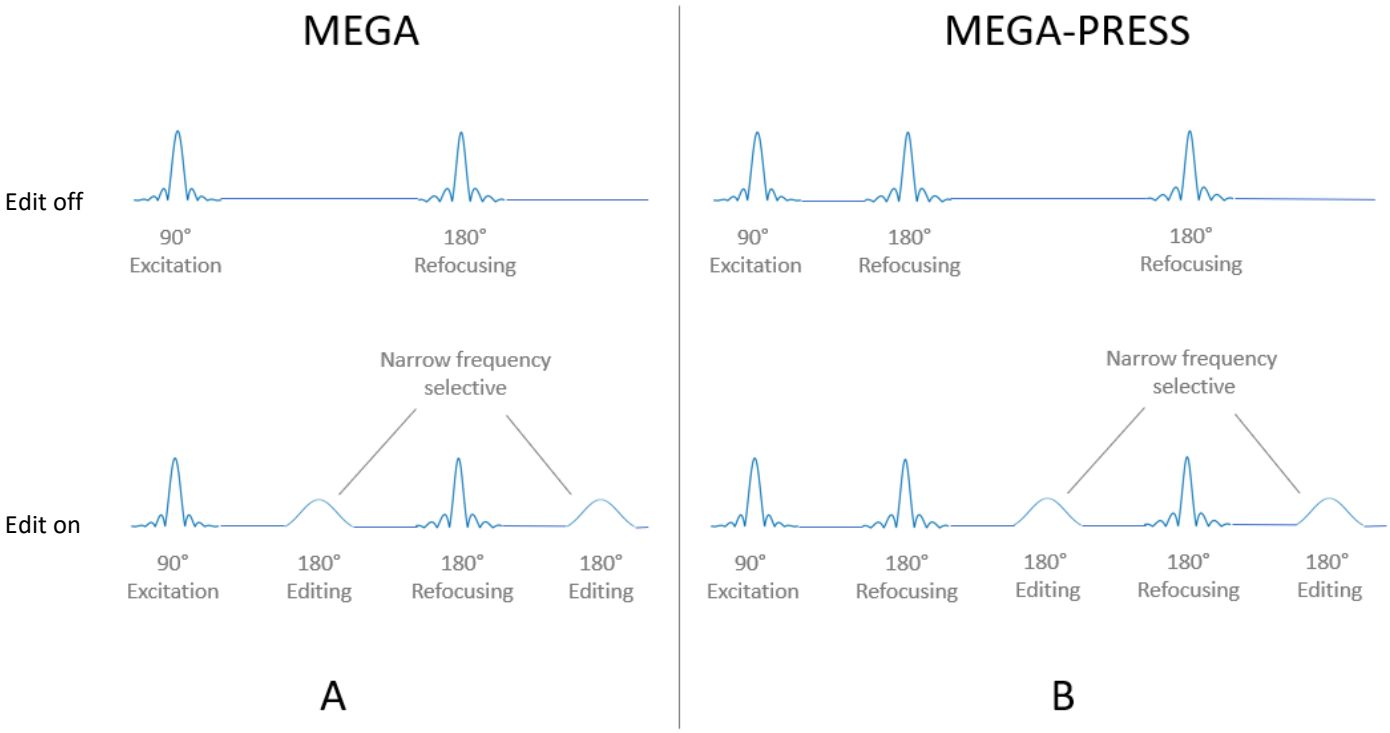

Figure 2-11 - Figure illustrating the generalised MEGA and MEGA-PRESS sequences.

2.2.5 Hadamard Encoding and Reconstruction of MEGA-Edited Spectroscopy (HERMES)

Hadamard encoding is a technique that is typically used for simultaneous multivoxel localization, such as for instance when spectra need to be acquired from *n* different slices. Essentially, the acquisition is repeated across the volume containing the *n* slices, *n* times – each time with the signals from different slices being selectively inverted. For instance, for four spatial slices, all four slices are acquired with the same phase in the first experiment, the last two slices are selectively inverted in the second experiment, the 2nd and 4th slices are inverted in the third experiment, and the 2nd and 3rd in the last experiment. The Hadamard matrix in this case is

$$H = \begin{pmatrix} +1 & +1 & +1 & +1 \\ +1 & +1 & -1 & -1 \\ +1 & -1 & +1 & -1 \\ +1 & -1 & -1 & +1 \end{pmatrix},$$

in which +1 and -1 denotes no inversion and selective inversion, respectively. Multiplying the four separately acquired spectra with the Hadamard matrix (which is equivalent to adding and subtracting different combinations of the spectra from the four experiments), allows the spectra from the individual slices to be reconstructed. Specifically

$$H_n {H_n}^T = nI_n,$$

where *H* is the Hadamard encoding matrix, *I* is the identity matrix, and *n* is the size of the matrix.

Hadamard encoding was first combined with spectral editing techniques to simultaneously quantify N-acetyl aspartate (NAA) and N-acetyl aspartyl glutamate (NAAG) by Chan *et al*. (Chan et al. 2016). Saleh *et al* (2016) subsequently used HERMES to simultaneously quantify GABA and GSH. When employing the Hadamard encoding matrix to distinguish signals from two different separately-coupled molecules J and K, four separate sub-acquisitions are performed. In the first, selective refocusing pulses (editing pulses) are applied at the frequencies of both spin systems coupled to the J and the K molecules, respectively, so that the resonances of

both the J and K spins at TE are in-phase with that from other non-coupled metabolites. In the second acquisition, editing pulses are applied only at the frequency of the spins coupled to the J molecule. This causes the resonances from the two J-spin populations to be in phase with uncoupled resonances, while those of the coupled molecule K will be out of phase. The 3rd acquisition has editing pulses applied only at the frequency of the spin system coupled to the K molecule, and the last acquisition has no editing pulses applied (Figure 2-12).

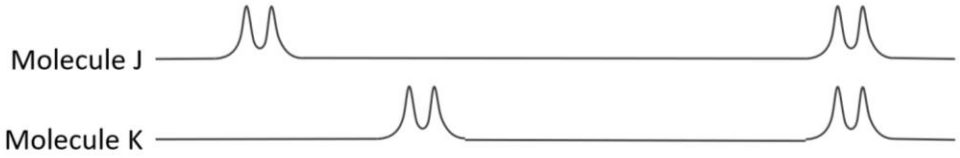

Experiment	Editing Pulses		Encoding Matrix	Signal	
	J	K	H	J	K
A	ON	ON	1 1		
B	ON	OFF	1 -1		
C	OFF	ON	-1 1		
D	OFF	OFF	-1 -1		

Figure 2-12 - Figure showing the HERMES Hadamard encoding matrix for two coupled molecules with overlapping signal for one of their spins. Reproduced from Chan et al. (2016).

The signals from either molecule J or K can then be isolated by adding the two ON-scans and subtracting the two OFF-scans of that molecule, i.e.

$$Signal_J = A + B - C - D$$

$$Signal_K = A - B + C - D$$

Note that when editing for J as shown above, the K signal experiences $ON + OFF - ON - OFF$, and therefore none of signal K is expected i.e. columns in the Hadamard matrix are orthogonal. This can be generalised by;

$$M = H^T \times N,$$

where **M** is a vector of the reconstructed spectra (dimension 2), **H** is the Hadamard matrix (dimension 4x2), and **N** is the vector of the recorded spectra (dimension 4).

2.2.6 Hadamard Editing Resolves Chemicals Using Linear-combination Estimation of Spectra (HERCULES)

HERCULES is an adapted version of the GABA and GSH edited HERMES sequence, which applies editing pulses at 1.9 and 4.56 ppm for GABA and GSH, respectively. It features an additional editing pulse at 4.18 ppm in the two GSH OFF sub-experiments. This is intended to provide additional differentiation of the signals of NAA and NAAG. Figure 2-13 demonstrates the editing schemes for HERMES and HERCULES.

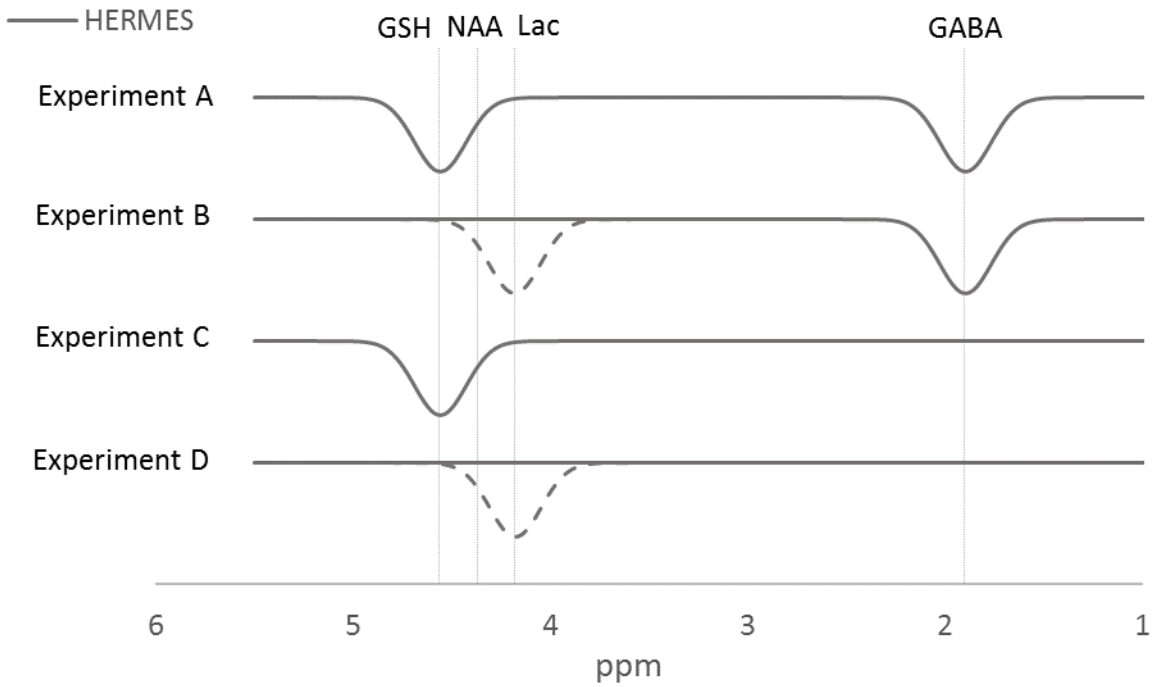

Figure 2-13 – The editing pulse scheme of the four HERMES and HERCULES sub-experiments. The solid lines show the frequency profile of the editing pulses applied in HERMES. In HERCULES editing pulses are applied at the frequencies shown by both the solid and the dashed lines (i.e. including the additional pulses at 4.18 ppm in the GSH "Off" experiments) (Oeltzschner et al. 2019).

2.3 Pulse Sequences

An MRI/MRS pulse sequence diagram is a simple way of showing how the radiofrequency (RF), for excitation, and magnetic field gradients, for spatial encoding, are applied during an MRI experiment. The vertical axis represents amplitude for each type of event and the horizontal axis time. Sequence development involves altering an existing sequence or building one from scratch using manufacturer functions, to perform an MR experiment that differs from available commercial sequences or work-in-progress sequences (WIPs). The sections below describe some of the elements of pulse sequences that required modification as part of the current project.

2.3.1 Siemens Integrated Development Environment for Applications (IDEA)

While much of the source code for the various MRI manufacturers is protected trade secrets, the big four MRI manufacturers (Siemens, Philips, GE, Toshiba/Canon) all provide certain portions of their source codes to partner institutions under research agreements. UCT has a master research agreement with Siemens, which allows the sharing of limited source code on a project by project basis. Siemens regularly updates the scanner software and releases new versions when updates are substantially different. Siemens scanner software is traded under the name 'syngo MR'. Currently installed on the Skyra at UCT (and the latest version) is VE11C. Sequences can be visualised, edited, and compiled using Siemens Integrated Development Environment for Applications (IDEA), which is also distributed under the master research agreement.

IDEA is distributed with an extensive User Manual which provides guidance on the use of functions within the environment for debugging and testing sequences, and for compiling binaries for scanner installation. Syngo MR version is an important detail when it comes to sharing sequences between research sites.

The following table shows the version numbers and scanners of institutions collaborating on this research;

Figure 2-14 - Siemens Integrated Development Environment for Applications (IDEA) logo

Table 2-1 - List of collaborating universities for this research, along with scanner hardware and software details

Scanning centre	Affiliated university	Scanner model	Software version
CUBIC	University of Cape Town	Skyra 3T	VE11C
The Centre for Molecular Imaging (CTMI)	The Johns Hopkins University	Prisma 3T	VE11B

Siemens sequences are written in the C++ object orientated programming language. Sequences are built using Siemens functions (often closed source) and usually build on previous sequences. Siemens has a commercial PRESS sequence, under the trade name 'svs_se'. There is a MEGA-PRESS WIP, under the trade name 'svs_edit', where interleaved editing pulses have been added. This WIP sequence is available to research institutions doing editing research (most commonly GABA editing). Due to the limitations of the sequence preparation protocol, the editing pulse file plays out in each measurement, and not only in the EDIT ON measurements as required. To overcome this, the svs_edit WIP applies the pulse in the OFF measurement at 7.5 ppm. At this frequency there are no coupled signals in the metabolite range so that the spectra are comparable to a measurement with no editing pulses. Figure 2-15 shows two sequential measurements of the svs_edit sequence. Although the two measurements appear identical, the editing pulses are tuned to different frequency bands according to the scheme described in the HERMES section previously.

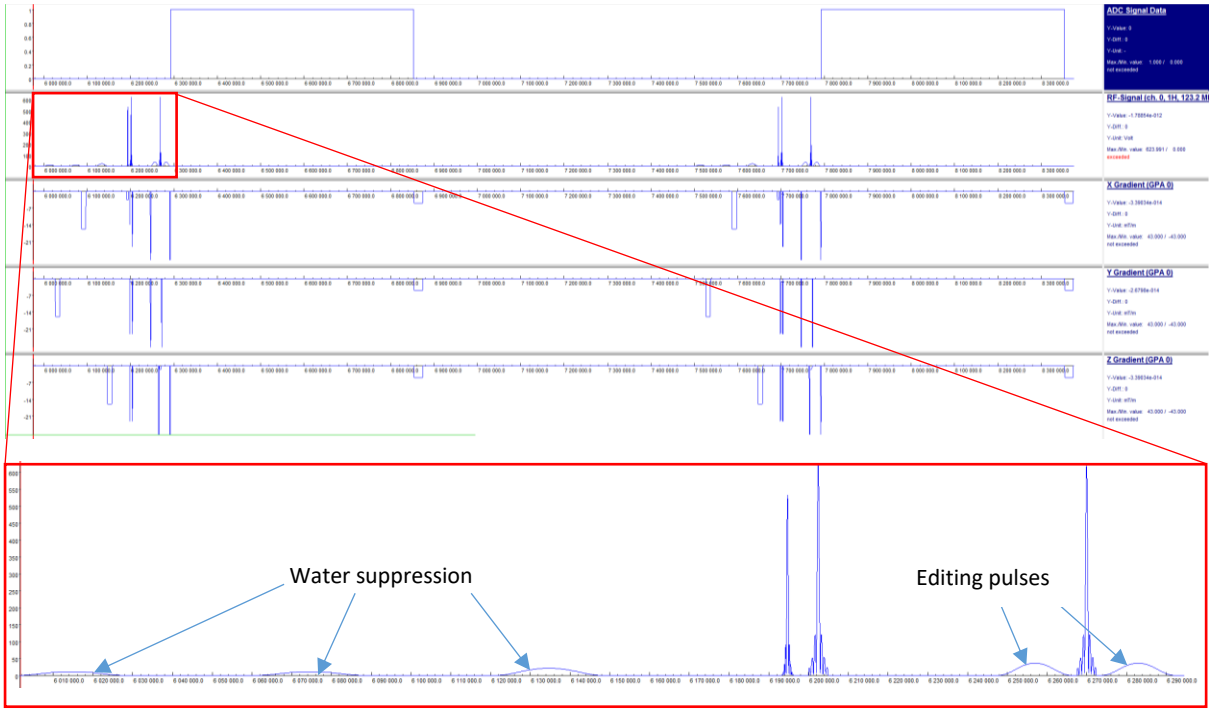

Figure 2-15 - Two sequential acquisitions using svs_edit (MEGA-PRESS) and zoomed in annotated section showing the water suppression and editing pulses. Despite appearing identical, the editing pulses of the two measurements are tuned to different frequencies.

2.3.2 RF pulses

Nuclear spins are excited during an NMR experiment by briefly applying a radiofrequency (RF) pulse at the Larmor frequency in a coil perpendicular to the main magnetic field. This pulse gives rise to a time-varying orthogonal magnetic field denoted, in general, by B1. Since an alternating field is made up of two counter-rotating fields, one of which will rotate at the same speed and in the same direction as the nuclear spins precess, the B1 field can be fixed to a reference frame (x', y', and z') rotating at the Larmor precession frequency of the nucleus. The following graphs in this document (and in general in MR literature) show how the magnitude of the B1 field varies in the rotating reference frame. Two considerations for RF pulses are the frequency and phase response profiles. Pulses can either uniformly excite all frequencies in the NMR spectrum (like excitation and frequency-nonselective refocussing pulses) or excite limited frequency ranges (like water suppression and editing pulses).

Pulse response can be calculated using either Fourier Transform Theory, the Bloch Equations, or optimisation procedures. Fourier Transform theory is most commonly used but does not accurately calculate off-resonance responses since it is a linear operation i.e. $FT(\alpha) + FT(\beta) = FT(\alpha + \beta)$, while NMR signal excitation is non-linear i.e. $M_{xy}(\theta_1) + M_{xy}(\theta_2) \neq M_{xy}(\theta_1 + \theta_2)$. However, since at excitation angles less than 30° $sin\theta \approx \theta$, Fourier Transform Theory provides reasonable predictions for small excitation angles. Some of the most widely used RF pulse classes are described below.

Sinc pulses

The non-normalised and normalised sinc functions are defined, respectively, as follows:

$$sinc(x) = \frac{\sin(x)}{x}, \text{ and}$$

$$sinc(x) = \frac{\sin(\pi x)}{\pi x},$$

giving the profiles shown in Figure 2-16.

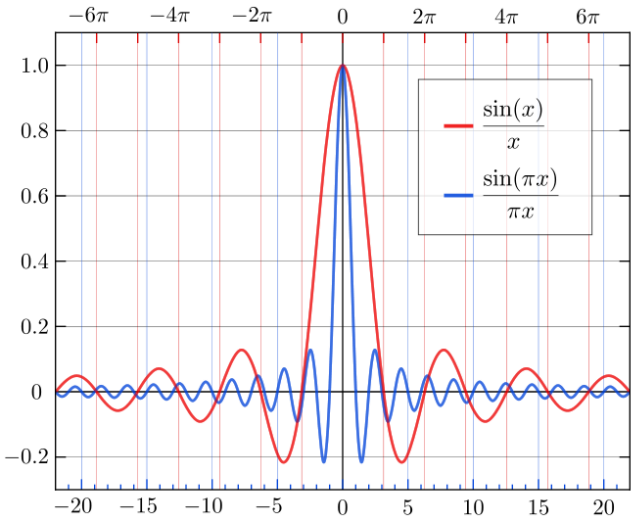

Figure 2-16 - Normalised (blue) and non-normalised (red) sinc functions (Johann 2011)

For application in NMR this is scaled by the desired B1 field strength and separated into lobe number (n) and pulse duration (T). Notably, pulse duration defines the truncation of the pulse too since a sinc function asymptotically decays according to

$$B_1 = B_{1max} \frac{\sin\left(\frac{2n\pi t}{T}\right)}{\frac{2n\pi t}{T}} \qquad \text{for} \qquad -\frac{T}{2} \leq t \leq \frac{T}{2}.$$

The frequency domain representation of the above sinc pulse is shown in Figure 2-17 for 30°, 90°, and 180° rotations at resonance.

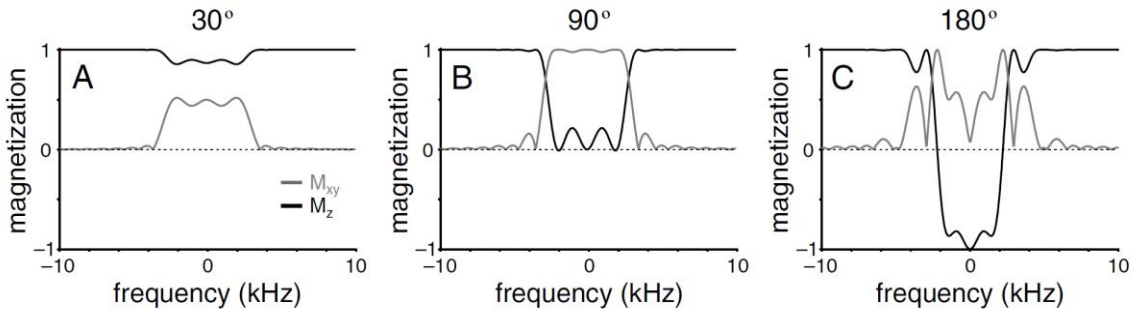

Figure 2-17 - Magnetisation response of a sinc pulse for 30°, 90°, and 180° rotations at resonance as determined by the Bloch Equations (de Graaf 2007)

Gaussian pulses

Gaussian RF pulses are typically used for MRS editing and water suppression. They are convenient to work with since the Fourier Transform is a Gaussian shape in the frequency domain. A Gaussian function is defined by

$$B_1(t) = B_{1max} e^{-\beta\left(\frac{2t}{T}\right)^2} \qquad \text{for} \qquad -T/2 \leq t \leq T/2,$$

$$\text{where} \quad \beta = -\ln\left(\frac{B_1\left(\frac{T}{2}\right)}{B_{1max}}\right), \text{ and}$$

B_{1max} is the maximum strength of the field. β is defined as the truncation percentage and depends on the pulse length T. Figure 2-18 shows a typical inversion pulse and its magnetisation response.

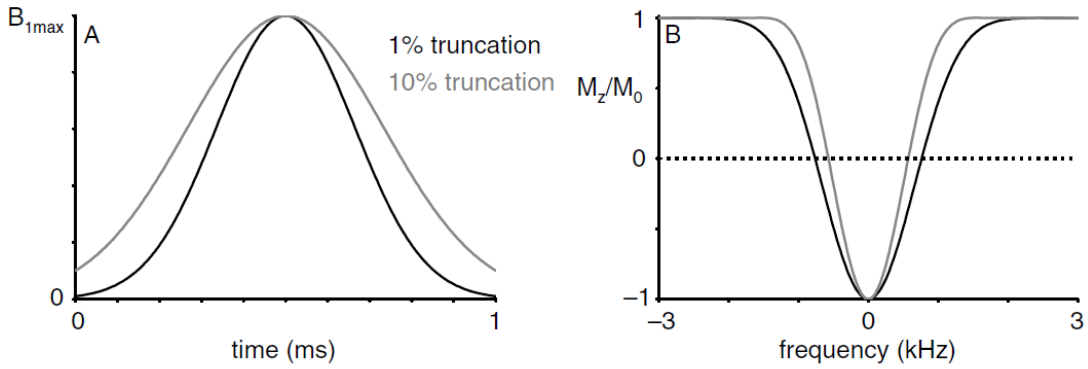

Figure 2-18 – Magnetisation response of a Gaussian inversion pulse for 1% and 10% truncation of the asymptotic time domain profile (de Graaf 2007).

Multifrequency pulses

HERMES and MEGA-PRESS require multifrequency editing pulses. These can be generated by simple addition of two complex pulse profiles. Separation of frequency selection is an issue if separation between editing frequencies is less than 4kHz.

Asymmetric pulses

As an alternative to a sinc pulse for excitation, one can truncate the second half of a sinc pulse more than the first, making it asymmetric. Asymmetric pulses have a more uniform excitation profile and allow shorter echo times (because most of the flipped magnetisation is near the end of the pulse) than symmetric sinc pulses (Stagg & Rothman 2013). However, they have the disadvantage that the high frequency modulation is present for all echo times, whereas for symmetric pulses this can be avoided by optimisation (de Graaf 2007). Figure 2-19 shows the frequency response of a Gaussian pulse, and both symmetric and asymmetric sinc pulses.

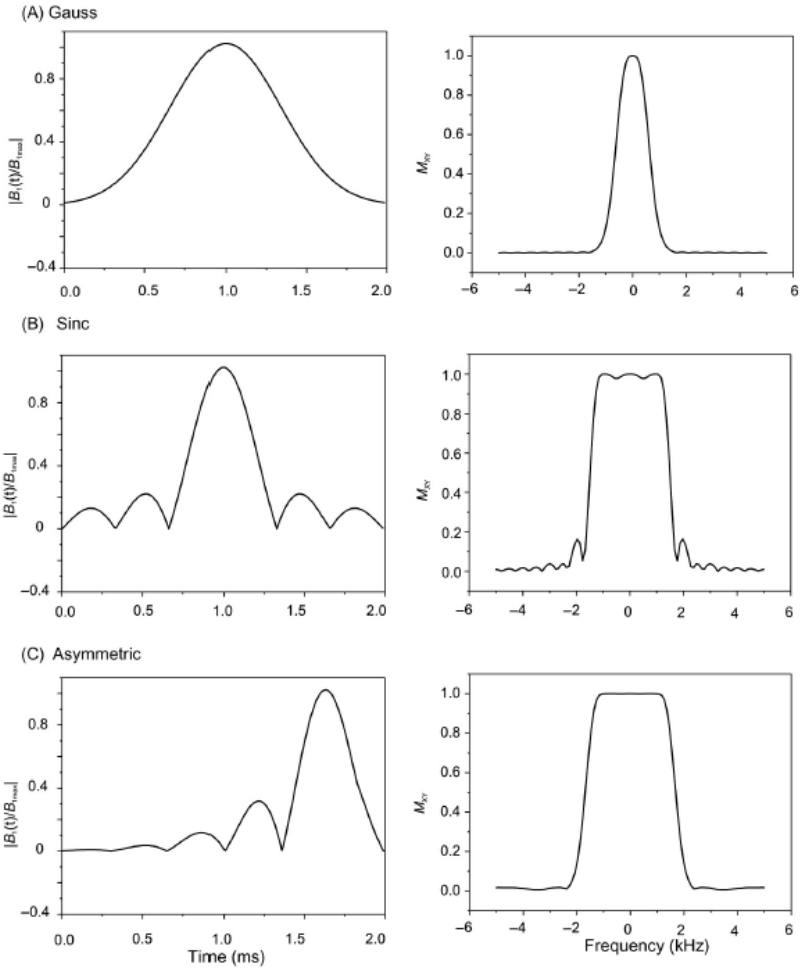

Figure 2-19 - Magnetisation responses of Gaussian (A), Sinc (B), and Asymmetric (C) excitation pulses (Stagg & Rothman 2013).

R Value

An important parameter that is useful in pulse design is the R value, which remains constant for a given RF pulse and nutation angle, and is defined as

$$R = T \times \Delta w,$$

where T is the pulse length and Δw is the bandwidth of the resultant magnetisation measured either at M_{xy} for excitation or M_z for inversion.

2.3.3 Sequence timing

Spin echoes occur at a time after refocusing that is equal to the time between excitation and refocusing, as this is when the spin system reaches maximum phase coherence. Figure 2-20 illustrates the timing of the echoes in a case where there are two refocusing pulses, such as in the PRESS sequence.

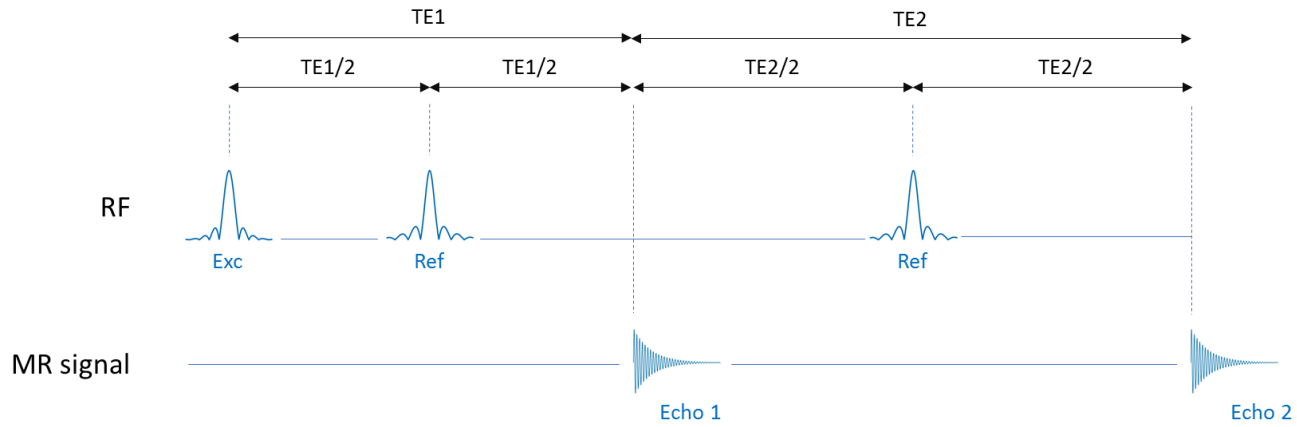

Figure 2-20 - RF pulses and echo timing for the PRESS sequence.

For the timings TE1 and TE2 as defined in Figure 2-20, the total echo time (TE) for the PRESS sequence is given by

$$TE = TE1 + TE2.$$

Furthermore, the time between the two refocussing pulses (Ref) equals half the total TE, i.e.

$$T_{Ref2} - T_{Ref1} = \frac{TE1}{2} + \frac{TE2}{2} = \frac{TE}{2}$$

For edited spectroscopy, two additional frequency selective refocussing pulses are applied – one between the first and second refocussing pulses, and another between the second refocussing pulse and the second echo (Figure 2-21).

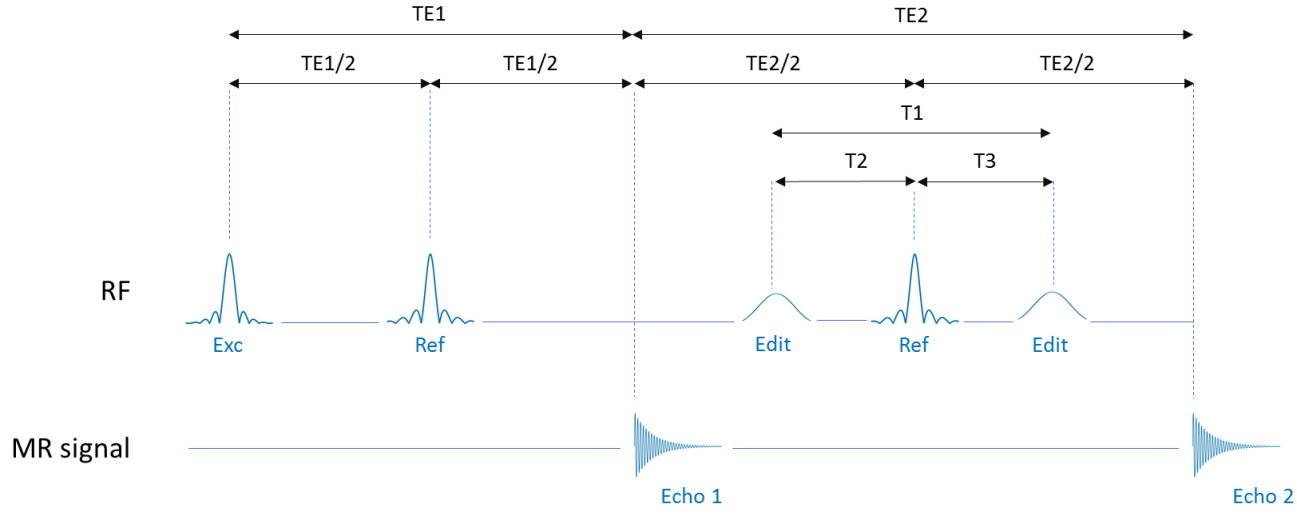

Figure 2-21 - RF pulses and echo timing for the MEGA-PRESS or HERMES sequences

As mentioned previously, coupling evolution during TE will only be completely refocussed if the time between the two editing pulses is half the total echo time. i.e.

$$T1 = \frac{TE1 + TE2}{2} = \frac{TE}{2}$$

However, since this limits the maximum duration of the editing pulses, it is common to place the first editing pulse equally between the two refocussing pulses, and to place the second editing pulse equally between the second refocussing pulse and the echo (Mullins et al. 2014). In that case,

$$T2 = \frac{\left(\frac{TE1}{2} + \frac{TE2}{2}\right)}{2} = \frac{TE1}{4} + \frac{TE2}{4} = \frac{TE}{4} \quad , \qquad and$$

$$T3 = \frac{TE2}{4}.$$

This timing, where the editing pulses are not symmetric about the second refocussing pulse and are not separated by TE/2, results in sub-optimal editing efficiency.

2.4 Post-processing of MRS data

The following sections aim to briefly introduce some of the key concepts related to post-processing of the signal acquired during an SVS acquisition, and two widely used packages for modelling MRS data. Although most vendors include processing on the scanner platforms, offline processing is more common.

Averaging, frequency and phase correction

Typically, the MRS signal is acquired repeatedly, once per ADC (analogue to digital conversion) event, and then averaged to improve the signal to noise ratio (SNR). The number of measurements is usually a multiple of four to allow for phase cycling (explained below), with edited protocols generally needing more measurements (e.g. 320) than unedited protocols (e.g. 64).

Due to the finite time (up to 10 minutes) required for a complete acquisition, the physical conditions of the voxel may, however, change between measurements. Frequency and phase correction are therefore performed routinely to correct changes in the precessional frequencies and phases between individual measurements that may arise from drift, changes in the local B0 field, and motion.

Baseline correction

While the signals from the metabolites of interest are sharp resonances in the frequency domain spectrum, these are superimposed on broader resonances from other elements. Baseline correction involves subtracting from the spectrum either a straight line or spline that is fit to the residual. These baseline signals can often be attributed to known physical contaminants such as plastic in the receiver coil, or macromolecules. Macromolecule signals are created by long chain organic molecules in the tissue and give a gently curved signal rather than the sharp peaks of the small metabolites of interest. The signals from macromolecules can be greatly reduced by selecting a relatively long echo time.

Line broadening

Due to several factors, including prevailing noise, the MRS spectrum may feature lines that are not perfectly smooth. Since this can influence the quantification outputs, spectra are often ‘smoothed’ using line broadening. This can be done either in the frequency domain by convolution of the acquired signal with a Gaussian or Lorentzian function or in the time domain by multiplication of the FID by a Gaussian or Exponential envelope.

Quantification

Metabolite quantification has historically been performed by measuring either the height of a peak, the height of a line fitted to the peak, or by measuring the area under the peak curve using numerical integration. While these methods provide some success, more sophisticated quantification techniques are now common. The most popular of these is linear combination modelling, which considers an MR spectrum as a mathematical combination of the individual spectra of the distinct metabolites and chemicals in the solution/voxel. The set of individual spectra is referred to as the basis set. Appropriate basis sets can be simulated for the particular pulse sequence conditions.

Phase-cycling

Phase-cycling is performed both in the simulation and the actual play out of the sequence on the scanner to remove unwanted coherences. Phase cycling involves alternating in successive measurements between one of four axes when applying the editing or refocussing pulses.

Absolute quantification

Absolute quantification uses either an internal or an external concentration reference. The metabolite concentration [m] in mmols/kg_{ww} is given by

$$[m] = \left(\frac{S_m}{S_r}\right)[r]C_n C_{av} C_{gain},$$

where S_m is the signal strength of the metabolite, S_r is the signal strength of the reference, [r] is the concentration of the reference in mmols/kg_{ww}, C_n is the correction for the number of nuclei in the metabolite signal compared to the reference, C_{av} is the correction for the number of measurements, and C_{gain} is the correction for the receiver gain setting. Since the concentration of pure water (55.5 mols/kg_{ww}) and the typical water content of different brain tissues are known, it is often used as a reference. The water fraction in grey matter is assumed to be 0.82, in white matter 0.73, and in CSF 0.98 (de Graaf 2007).

Examples of Post-processing Software

LCModel

LCModel, released by Stephen Provencher in 2001 (Provencher 2018), was the first processing tool to model the signal as a linear combination of metabolite spectra. The latest release, version 6.3, provides support for modelling MEGA-PRESS data, and while still primarily designed for brain MRS, includes features for muscle, lipid, and some other tissues. Since LCModel is not open source and is limited by the basis sets provided, it cannot easily be used for custom sequences and pulse shapes. Analyses are performed in the frequency domain, but time-domain data can be processed after first being Fourier Transformed.

JMRUI

Also in 2001, Naressi released a Java-based MRS analysis tool called jMRUI (Java Magnetic Resonance User Interface) (Naressi et al. 2001). Although initially free to use, it is now licensed. Like LCModel it incorporates prior knowledge, with the main difference being that data are quantified in the time domain rather than the frequency domain. jMRUI can process both free induction decays (FIDs) and echoes, and 1D or 2D data, allowing it (unlike LCModel) to be used for quantification of 2D NMR data. It features both interactive and non-interactive time domain algorithms that are based on non-linear least squares (NLLS) fitting, such as AMARES (Advanced

Method for Accurate, Robust, and Efficient Spectral fitting) (Vanhamme et al. 1997) and VARPRO (VARiable PROjection) (van der Veen et al. 1988).

3 Literature Review

This literature review will look at GABA and glutathione detection, post processing, and some select previous studies reporting values which will be useful for comparison with this research.

3.1 Acquisition techniques

A range of detection techniques have been developed for low concentration metabolites like GABA and GSH. The following paragraphs will discuss a few of these as they relate to each other.

In a review paper in 2017 Harris states that for GABA detection, although both MEGA-PRESS and double-quantum filter experiments have produced robust and repeatable measurements, MEGA-PRESS receives most of the attention. For glutathione detection, MEGA-PRESS, polarization transfer, and double quantum filtering methods have been developed. While polarisation techniques have not yet been applied to *in vivo* measurements of glutathione, double-quantum filter experiments have also successfully edited the 4.56 ppm cysteine moiety (Harris et al. 2017).

Two other widely implemented editing methods use the BASING (Star-Lack et al. 1997) and double-BASING (Star-Lack et al. 1998) sequences. These sequences were originally developed to dephase and remove unwanted water and lipid signals using a frequency selective inversion pulse, surrounded by crushing gradients on either side. It was then modified to additionally selectively invert the lactate doublet at 1.3 ppm and the choline singlet at 3.2 ppm. While single BASING does not apply pulses in an interleaved/alternating fashion, but instead simply selectively refocuses a coupled signal thereby improving its visibility (Harris et al. 2017), double-BASING does employ an alternating pulse scheme making it a J-difference editing technique. The pulse sequence is similar to MEGA-PRESS and only differs in the placement of the gradients. In fact the terms double-BASING and MEGA-PRESS are often used interchangeably (Harris et al. 2017), and in reality scanner vendors develop editing sequences with slightly different timing details to either.

Three methods have been employed to accelerate editing. The first and simplest happens as a consequence of a standard MEGA-PRESS experiment, namely co-editing. Co-editing occurs when another spin system, other than the spin system of interest, is coupled to the same editing target spin. This spin system will therefore also be edited, resulting in another signal in the difference (DIFF) spectrum that does not overlap with the coupled signal of interest. For example, when targeting the 1.9 ppm GABA peak, glutamine and glutamate are co-edited, giving rise to the Glx coupled signal at 3.75 ppm. This signal is evident in any GABA MEGA-PRESS DIFF spectrum and is therefore also commonly quantified.

The second method expands upon MEGA-PRESS by simultaneously editing two non-overlapping coupled spins. Since these spins are part of two different spin systems, editing pulses simultaneously applied at the two different target frequencies will result in both spins being edited (Terpstra et al. 2006). This method cannot be applied to GABA and GSH detection as their coupled signals are strongly overlapping at 3 ppm.

The third method resolves the edited signals from two overlapping coupled spins by editing two different target spins and using Hadamard encoding. HERMES and HERCULES are both examples of this. Harris et al. (2017) summarises these acceleration methods.

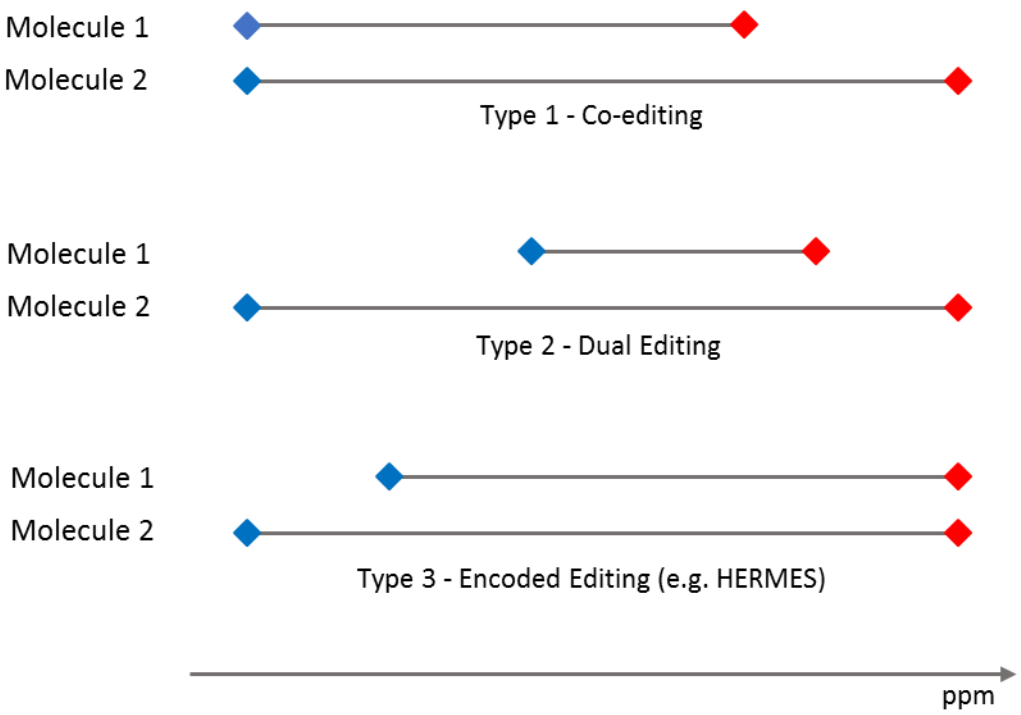

Figure 3-1 - Three types of editing acceleration shown, namely: Type 1 - co-editing, Type 2 - dual editing, and Type 3 – encoded editing. Blue ends show the frequency location of the editing target spin, and red ends show the frequency location of the detected spin. Reproduced from (Harris et al. (2017).

GABA can also be detected using 2D ^{1}H NMR spectroscopy. 2D spectroscopy separates overlapping signals by detecting and encoding a second frequency dimension that contains information based on the coupling of various resonances, in addition to the usual chemical shift information. This has been demonstrated with spatial localisation in phantoms and *in vivo* for a number of previously developed 2D NMR sequences, including 2D J-resolved MR spectroscopy (2D J-PRESS), 2D zero-quantum, 2D double quantum, Correlation Spectroscopy (COSY), and Spin-echo Correlation Spectroscopy (SECSY) (Ryner et al. 1995a). Measurements with 2D J-PRESS in phantoms containing NAA, alanine, choline, myo-inositol, glutamate, glutamine, GABA, taurine, glucose, and aspartate (Ryner et al. 1995b), and *in vivo*, have demonstrated strong coupling in many metabolites. There have also been Hadamard encoded variants of the 2D approach called COSY and Total Correlation Spectroscopy (TOCSY) (Kupce & Freeman 2003b), and a multi-dimensional approach builds on these (Kupce & Freeman 2003a).

There have been some developments on these techniques recently, such as the development of Localised Diagonal Suppressed Spin-echo Correlation Spectroscopy (LDISSECT) (Banerjee & Chandrakumar 2014) by adding a 90 degree pulse to a standard SECSY experiment. Or the 'selective pure shift TOCSY' (Poggetto et al. 2016) method, which is designed to help in the identification of the components of complex mixtures such as peppermint oil. However, no recent studies could be found which assess the reproducibility of GABA or GSH measurements using these methods, or that directly compare one of these 2D NMR methods to edited 1D spectroscopy. J-Difference editing is still the most widely used method for GABA and GSH detection (de Graaf 2007; Harris et al. 2017).

Despite the widespread use of MEGA-PRESS, another consideration is the differences in acquisition methods between MRI vendors; since vendor-native MEGA-PRESS sequences differ in terms of RF pulse shapes, timing, durations, and amplitudes, it is difficult to compare quantification between vendors. As such, Saleh and colleagues (Saleh et al. 2019) recently developed a standardised MEGA-PRESS sequence with HERMES functionality for scanners from each of the four major MRI vendors (Siemens, Philips, GE, and Canon). The universal sequence was validated primarily with GABA and lactate phantom data, and some *in vivo* data. The

universal sequence showed increased intraclass correlation (ICC) between data obtained from scanners of different vendors compared to the vendor-native sequences, increasing from 0.91 to 0.96 for GABA, and 0.74 to 0.98 for lactate. This is a promising first step towards sequence standardisation and application of MEGA-PRESS towards future clinical applications.

3.2 Post-processing of MRS data

Quantification packages

The previous chapter introduced the two leading commercial MRS quantification software packages; LCModel and JMRUI. Another commonly used quantification package is GANNET which was first published in 2014, and was designed specifically for J-difference edited MRS data (Edden et al. 2014). GANNET is written in MATLAB and is still free to use. It does not have a user interface but provides automated outputs and plots. GANNET quantifies data in the frequency domain. It can process data from all four of the major MRI vendors and performs recombination of averages from raw data. GANNET performs automated frequency and phase correction and can quantify relative to water reference data.

All three packages can process MEGA-PRESS data, but only GANNET can process HERMES data. Other sequences with complex editing schemes have typically been processed by custom scripts. GANNET quantifies signals by fitting a spline to the edited signal of interest in either MEGA-PRESS or HERMES data, but therefore only considers the difference spectra (i.e. half of the data in the case of MEGA-PRESS, or a quarter of the data in HERMES).

Basis sets

The most commonly used basis set simulation library is FID-A; an open source simulation toolkit, designed to generate and process basis sets for linear combination modelling of MRS data (Simpson et al. 2017). The toolkit is split into four sets of functions, namely; inputOutput, processingTools, rfPulseTools, and simulationTools.

The simulation toolbox calculates expected spectra for metabolite spin systems by calculating successive evolutions of the density matrix. The simulation toolkit contains a set of metabolite spin system definitions based on published values. This includes the J-coupling constants of each proton to every other proton, and the frequency shits of the protons. The expected signal of a sequence can then be calculated by combining excitation (sim_excite.m), delays (sim_evolve.m), rotation (sim_rotate.m) for ideal rotations, and rotations with a given RF pulse (sim_shapedRF.m). These can all be represented by a Hamiltonian transformation;

$$\sigma(t) = e^{-\mathcal{H}t}.\sigma(0).e^{\mathcal{H}t}$$

Where σ is the density matrix, $\mathcal{H}$ is a Hamilton operator, and t is the time. There are also a range of processing tools which are useful in handling the spectra and combining them as required. For example op_ampScale.m is used to scale a spectra by some factor.

3.3 Previous GABA studies

There has been extensive work relating to brain GABA levels. The following paragraphs present a selection of studies which relate to the goals of this research, such as with respect to reproducibility of GABA quantification, hardware and software consideration for improved quantification results, etc.

Much work has been done in assessing the reproducibility of GABA measurements using edited spectroscopy, with one recent study examining improvements related to coil channel numbers, macromolecular

contamination, and test retest reliability (Shungu et al. 2016). Among other things, the authors documented improved sensitivity using head coils with more channels and reported for an 8-channel coil a coefficient of variation of 1.25% for GABA+ relative to unsuppressed water in a cohort of seven adults (ages 25.9 ± 2.7 years; four women). The authors compared their own results to findings from several other studies that also used MEGA-PRESS, and in some instances STEAM, to measure GABA. This table has been reproduced here (Table 3-1). Notably, the coefficients of variation reported by Shungu et al. using the 8-channel coil are lower than values reported by other studies.

MEGA-PRESS GABA detection has also recently been applied in a large multi-site, multi-vendor, study where 272 healthy adults were scanned using the vendor native MEGA-PRESS sequences for Siemens, Philips, and GE scanners (Mikkelsen et al. 2017). Processing using GANNET yielded a coefficient of variation of 12% for GABA+ relative to creatine across the entire cohort. A multilevel analysis of the quantification outcomes demonstrated that most of the variability was from differences between participants within each site (72%), while site-level differences accounted for 20% of the variation, and vendor-level differences only accounted for 8% of the variability.

A follow-up paper that quantified the signals relative to unedited water, accounting for tissue-dependent signal relaxation and water visibility effects (Mikkelsen et al. 2018), yielded a coefficient of variation of 17% for GABA+. Multilevel analysis showed that subject-level differences now accounted for only 36% of the variability, vendor-level differences accounted for 53%, and site-level differences 11%. It is interesting to note that when unsuppressed water was used as the reference, more variability was attributable to vendor differences. The author noted Siemens differences in particular and recommended further standardisation of water reference data to allow for cross vendor comparison.

Table 3-1 - GABA test-retest reliability, reproduced from Shungu et al. (2016)

Reference	Field strength (T)	Subjects	Acquisition sequence	Interval	Analysis	Brain region/voxels	Results, CV for GABA
Evans et al. (2010)	3	8 HC	MEGA-PRESS, 8-channel	2.5h, scans per subject	Frequency-domain spectral fitting, unsuppressed water normalization	OCC & sensorimotor/27 cm^3	Occipital, 6.5% Sensorimotor, 8.8%
(Bogner et al. 2010)	3	11 HC	MEGA-PRESS	Variable; at least 1 day; 2-4 scans per subject	AMARES, jMRUI, referencing to both tCr and unsuppressed water	OCC/22.5 cm^3	GABA/tCR, 13.3% GABA/water, 15.0%
O'Gorman et al. (2011)	3	14 HC	MEGA-PRESS	4 scans within session	LCModel, MATLAB, jMRUI, water referencing	DLPFC/30 cm^3	GABA, 7–12% (Glx, 6–18%)
Geramita et al. (2011)	3	10 HC	MEGA-PRESS single-channel	28-226 days (131±78 days)	Frequency-domain spectral fitting, referencing to both tCr and unsuppressed water	dACC& rFWM/18 cm^3	dACC GABA/W, 5.3%; rFWM GABA/W, 8.7% dACC GABA/tCr, 6.5%; rFWM GABA/tCr, 8.2%
Harada et al. (2011)	3	15 HC	MEGA-PRESS single-channel	1 week	LCModel	Lentiform nuclei, frontal lobe & ACC/27 cm^3	4.6%
Wijtenburg et al. (2013)	7	4 HC	STEAM, MEGA-PRESS, 32-channel	8±2 days	STEAM: LCModel MEGA-PRESS: frequency-domain spectral fitting	AC & DLPFC STEAM 27 cm^3; MEGA-PRESS 34.2 cm^3	STEAM: AC 3.5%, DLPFC 16.2%; MEGA-PRESS: AC 13.6%, DLPFC 13.4%
Near et al. (2014)	3	17 HC, male	MEGA-PRESS	229±42 days	jMRUI; referencing to tCr	OCC / 27 cm^3	0.2 – 12.3%; mean 4.3%
Gaetz et al. (2014)	3	5 HC	MEGA-PRESS	~5 days, 5 scans per subject	jMRUI; referencing to tCr, NAA, and Glx	Motor cortex/27 cm^3, Auditory cortex/24 cm^3, visual cortex/27 cm^3	6–14%; average ~ 10% over regions and referencing methods

Mikkelsen et al. (2016)	3	15 HC x2 cohorts	MEGA-PRESS with and without symmetric editing	15 min	Gannet	dACC/24 cm^3, OCC/27 cm^3	GABA asymmetric editing: 4.0% OCC, 14.8% dACC GABA symmetric editing: 8.6% OCC, 12.6% dACC
Long et al. (2015)	3	5 HC, elderly	MEGA-PRESS	2-28 days	LCModel comparing 2 basis sets	Cerebellum, left and right/15.6 cm^3	4–13%
Shungu et al. (2016)	3	6 HC	MEGA-PRESS, single channel and 8-channel	1 h	Frequency-domain spectral fitting, unsuppressed water normalization	DLPFC/9.6cm^3	GABA: 3.6% single channel, 1.3% 8-channel (Glx, 2.8–3.5%)

CV, coefficient of variation; AC, anterior cingulate; dACC, dorsal anterior cingulate cortex; DLPFC, dorsolateral prefrontal cortex; GABA, γ-aminobutyric acid; Glx, combined glutamate and glutamine; HC, healthy control; MEGA-PRESS, Mescher–Garwood point-resolved spectroscopy; NAA, N-acetyl-L-aspartate; OCC, occipital cortex; rFWM, right frontal white matter; STEAM, stimulated echo acquisition mode; tCr, total creatine/phosphocreatine; W, unsuppressed water.

Recently, Prescot *et al.* (2018) directly compared GABA quantification using 1D edited spectroscopy and 2D spectroscopy (Prescot et al. 2018) in six healthy adult male subjects (mean age ± standard deviation [SD] = 34.2 ± 16.8 years) enrolled in a double-blind, randomized, placebo-controlled study. The study involved the administration of a GABA-amino transferase inhibitor to increase brain GABA concentrations. The study, which was performed on a Siemens 3T Verio scanner, used MEGA-PRESS for the 1D edited spectroscopy and a 2D J-resolved sequence for the 2D data. While GABA levels measured using both methods showed similar changes over time, the coefficient of variation (CV) of creatine levels (relative to water) was greater for data from 2D J-PRESS than MEGA-PRESS (Table 3-2).

Table 3-2 - Mean within-subject CV (%c ± SD) of creatine (Cr; normalised to CSF-corrected unsuppressed water) for both measurement techniques and the two treatment cohorts. The final column shows the effect size for drug-induced changes in GABA levels (normalised to creatine).cc (Prescot et al. 2018).

GABA concentration for variation for MEGA-PRESS and 2D J-Resolved NMR - reproduced from Prescot et al. (2018)			
Cohort	**Technique**	**CV (Cr:water)**	**ΔGABA Effect Size (day7, day 13)**
CPP-115	MEGA-PRESS	4 ± 1	7.2, 2.1
	2D J-Resolved	7 ± 2	4.3, 2.0
Placebo	MEGA-PRESS	5 ± 2	N/A
	2D J-Resolved	9 ± 4	N/A

3.4 Previous GSH studies

Glutathione is most commonly detected with MEGA-PRESS by editing the 4.56 ppm peak on the cysteine moiety. However, this co-edits the NAA-aspartyl peaks, effects that can be minimized by setting the echo time to 68 ms (Terpstra et al. 2003).

Not all recent studies report improvements using editing techniques. A recent study assessing the reproducibility of glutathione measurements in 10 subjects who were repeat scanned using PRESS, SPECIAL, Phase-rotation STEAM (PR-STEAM), and MEGA-PRESS (Wijtenburg et al. 2019), found that PR-STEAM had the lowest mean coefficient of variation (CV) and absolute difference (AD) (5.4 and 7.5%, respectively), followed by PRESS (5.8 and 8.2%, respectively) and SPECIAL (8.0 and 10.1%, respectively). MEGA-PRESS performed the worst (13.5 and 17.1%, respectively).

4 Methodology

This project comprised three major components: (i) porting the HERMES sequence previously implemented by researchers from Johns Hopkins on Philips (Chan et al. 2016) to a Siemens platform (section 4.1), (ii) developing code for signal processing and metabolite quantification of data acquired using this sequence (section 4.2), and (iii) testing and validation of the sequence and metabolite quantification algorithms both in phantoms and *in vivo* (section 4.3).

This project presents a collaboration between the Universities of Cape Town and Prof Edden's group at Johns Hopkins University in Baltimore, USA, where the HERMES sequence was first implemented. Data for this project were acquired according to protocols that had been approved by the Faculty of Health Sciences Human Research Ethics Committee of the University of Cape Town and the Institutional Review Board of Johns Hopkins. All participants provided written informed consent.

4.1 HERMES Sequence Development

Siemens, Philips, and GE have commercially available PRESS sequences. The commercial name for the Siemens PRESS sequence is svs_se, and for their MEGA-PRESS WIP is svs_edit. Since the latter sequence edits only for a single metabolite, the svs_edit.h and svs_edit.cpp source code files were modified to implement HERMES. Sections below describe changes that were made to the sequence user interface, the RF pulse shapes, and sequence timing.

4.1.1 Sequence User Interface

The principal difference between MEGA-PRESS and HERMES is that instead of two sub-experiments with editing pulses ON or OFF, respectively, there are four sub-experiments – one with dual editing pulses (i.e. editing for both metabolites), two with single lobe editing pulses (one for each of the metabolites separately), and one with no editing pulses.

In MEGA-PRESS, the ON and OFF sub-experiments are interleaved. For HERMES it is necessary to interleave four different sub-experiments by applying different combinations of two distinct editing pulses. A checkbox (HERM_GABA_GSH) was therefore added in the svs_edit WIP special card that would, when selected, allow a second editing frequency to be specified (Figure 4-1). This implementation allows the user to run MEGA-PRESS and HERMES using the same sequence. The sequence essentially performs interleaved acquisitions for all possible permutations of the editing pulses (2 permutations in the case of MEGA-PRESS, and 4 for HERMES) without requiring any adjustments to sequence timing or pulse shapes. This is achieved by switching in the sequence between a two-step (MEGA-PRESS) and four-step (HERMES) editing loop ('m_editloop').

In our implementation, the 'Edit Pulse Frequency 1' and 'Edit Off Frequency' boxes always remain active and are set for GABA editing. Their default values are 1.9 ppm (i.e. editing for the GABA-H3 quintet) and 7.5 ppm, respectively. The latter ensures that the editing pulse in the OFF sub-experiment is placed far from the useful portion of the spectrum where no coupled spin systems interfere with the spin systems of interest. Therefore, the first sub-experiment (A) is performed with the first editing frequency (GABA) ON and the second sub-experiment (B) with the first editing frequency OFF. This is the standard MEGA-PRESS acquisition.

Only when the HERM_GABA_GSH checkbox is selected, does the 'Edit Pulse Frequency 2' box become active. The default value of 4.56 ppm allows editing of the GSH cysteine moiety doublet-of-doublets. Sub-experiment

C therefore edits for GSH (GSH ON), and sub-experiment D for both GABA and GSH (i.e. GABA ON and GSH ON), as shown in Table 4-1. The Hadamard matrix for our implementation is therefore given by

$$H = \begin{pmatrix} +1 & -1 \\ -1 & -1 \\ -1 & +1 \\ +1 & +1 \end{pmatrix}.$$

Table 4-1: Order of acquisition of the different edited spectra in our HERMES implementation.

Experiment	Editing Pulses	
	GABA	GSH
A	ON	OFF
B	OFF	OFF
C	OFF	ON
D	ON	ON

All other sequence cards and settings remained unchanged.

Editing pulse parameters are set using Siemens closed-source functions setTypeRefocussing, setDuration, setFlipAngle, setInitialPhase, setFamilyName, setThickness, setFrequency, and setPhase.

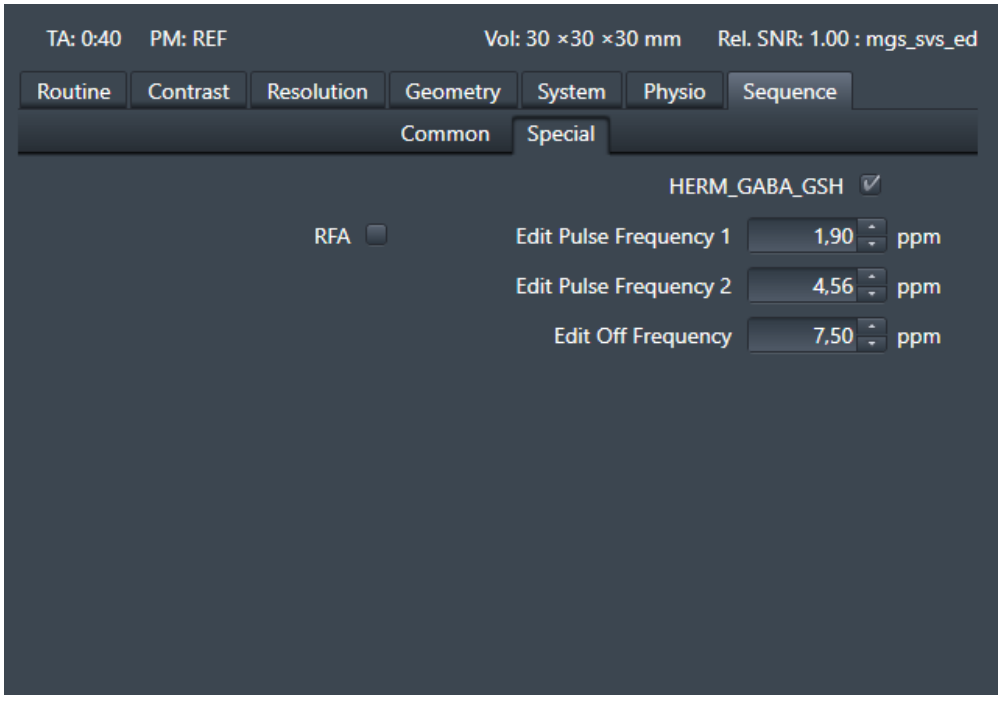

Figure 4-1 - HERMES sequence special card as it appears in the scanner user interface, featuring HERMES checkbox and editing frequency settings.

4.1.2 RF pulse design

Sequence standardisation is an important research focus in MRS as it allows for comparison of data between vendors. Part of this project was to standardise the RF pulse shape and sequence timing of the Siemens HERMES implementation to that used in the previous Philips implementation.

Edited MRS pulse sequences feature 3 types of RF pulses: excitation, refocusing, and editing pulses. In the following sections the pulses used by the Siemens MEGA-PRESS WIP are compared to those selected for the HERMES sequence.

Siemens MEGA-PRESS WIP - 'svs_edit'

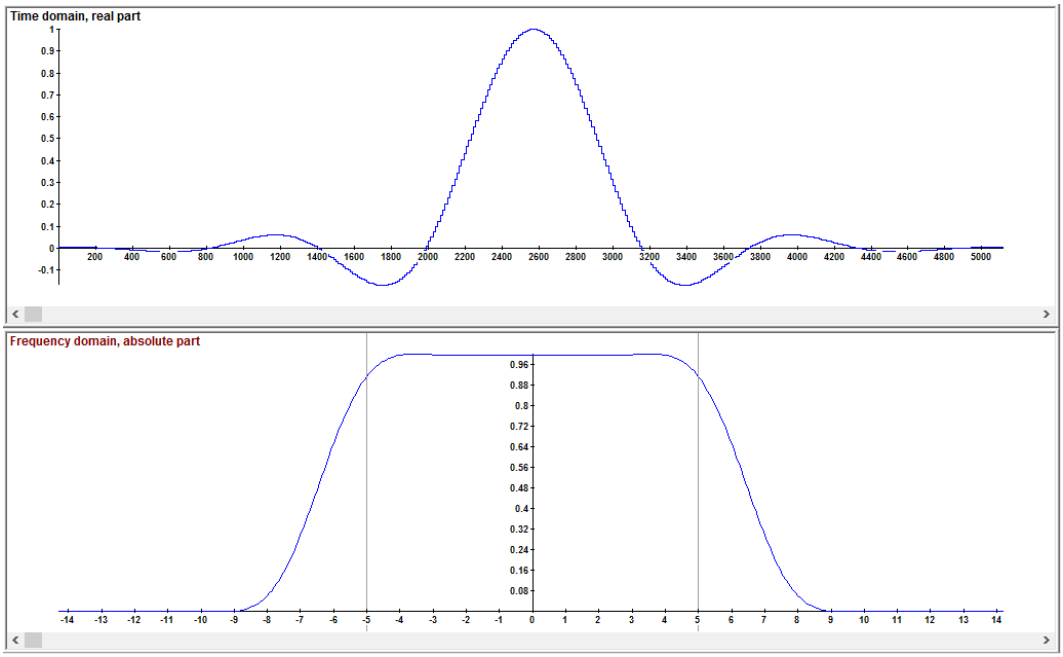

Figure 4-2 - Siemens svs_edit excitation pulse ('hsinc_400_8750')

For excitation, the Siemens MEGA-PRESS WIP (svs_edit) uses a symmetrical hsinc_400_8750 pulse (Figure 4-2) from the hsinc_400_8750 family with 400 samples, integral of the normalised amplitude (AMPINT) 45.490761, integral of the absolute magnitude of the normalised pulse (ABSINT) 66.644113, integral of the calculated power (POWERINT) 41.497912, and logical reference gradient (amplitude of a slice selection gradient required to excite a 10 mm thick slice) as calculated by the Siemens Pulse Tool (REFGRAD) 4.014000.

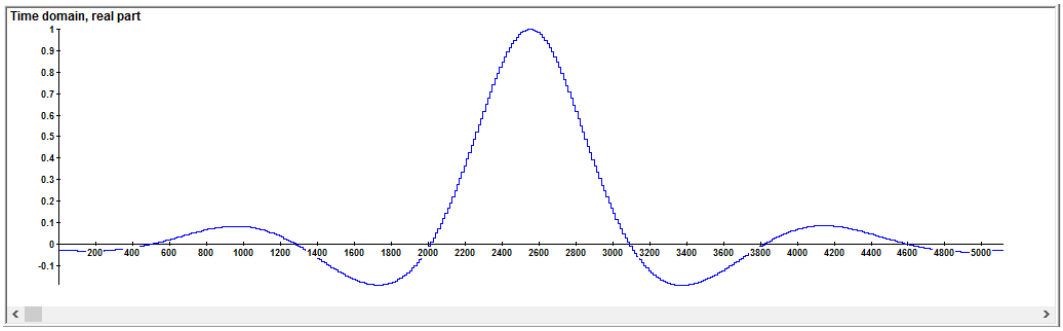

Figure 4-3 - Siemens svs_edit refocussing pulse ('mao_400_4'). Note that the Siemens pulse tool, which generated the points in the figure, uses Fourier Transform techniques to create the frequency domain profile. Fourier Transform methods are inaccurate for inversion and refocussing pulses, and as such only the time domain profile is shown for this pulse.

The refocussing pulse is a symmetrical 180 degree mao_400_4 pulse (Figure 4-3) from the mao_400_4 family with parameters:

Samples :	400
AMPINT:	36.711385
ABSINT:	68.374723
POWERINT:	37.032906
REFGRAD:	2.752000

By contrast, the editing pulses are built within the sequence code rather than importing external pulse shapes.

HERMES

Two major changes required for the HERMES implementation were:

1. Importing the editing pulses from externally generated .rda files rather than manually building them in the sequence code. This makes it easier to update and change the pulses, facilitating standardisation.
2. Replacing all the pulses with 'universal' pulses that closely match those used in the Philips implementation of HERMES. The pulses used were designed and shared by Prof Richard Edden from Johns Hopkins University. Matching the pulse shapes across platforms reduces the potential impact of pulse shape variations on cross vendor comparisons.

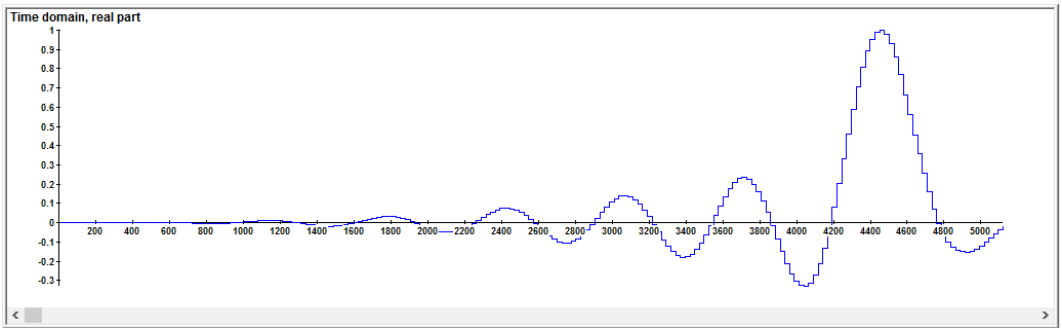

Figure 4-4 – HERMES excitation pulse ('spreddenrex'). Note that the Siemens pulse tool, which generated the points in the figure, uses Fourier Transform techniques to create the frequency domain profile. Fourier Transform methods are inaccurate for inversion and refocussing pulses, and as such only the time domain profile is shown for this pulse.

For excitation, an asymmetrical *spreddenrex* (Figure 4-4) pulse was used with 200 samples, AMPINT 10.023573, ABSINT 23.982528, POWERINT 11.571791, and REFGRAD 7.421000. Refocussing used the *eddenrefo* (Figure 4-5) pulse with 200 samples, AMPINT 24.678796, ABSINT 88.300436, POWERINT 57.209626, and REFGRAD 4.309.

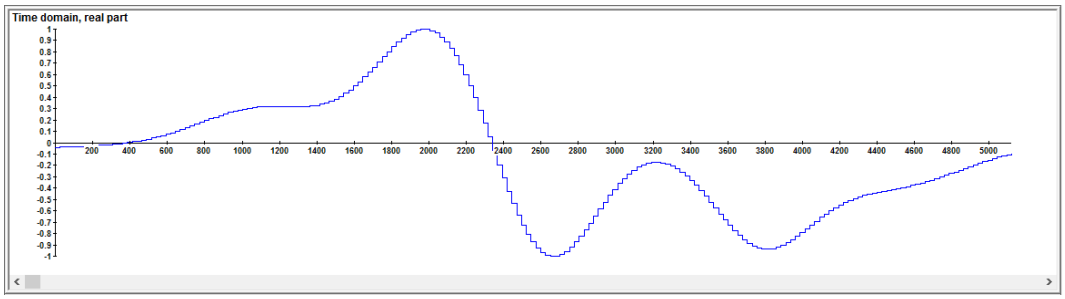

Figure 4-5 – HERMES refocussing pulse ('eddenrefo'). Note that the Siemens pulse tool, which generated the points in the figure, uses Fourier Transform techniques to create the frequency domain profile. Fourier Transform methods are inaccurate for inversion and refocussing pulses, and as such only the time domain profile is shown for this pulse.

Single and dual lobe editing used the *sl_edden_edit* (Figure 4-6) and *DUALBAND2* (Figure 4-7) pulses, respectively, both with 200 samples and REFGRAD 1. For the former, AMPINT was 110.291802, ABSINT 110. 291802, and POWERINT 82.725094, while parameter values for the latter were AMPINT 55.602906, ABSINT 70.385032, and POWERINT 41.466523.

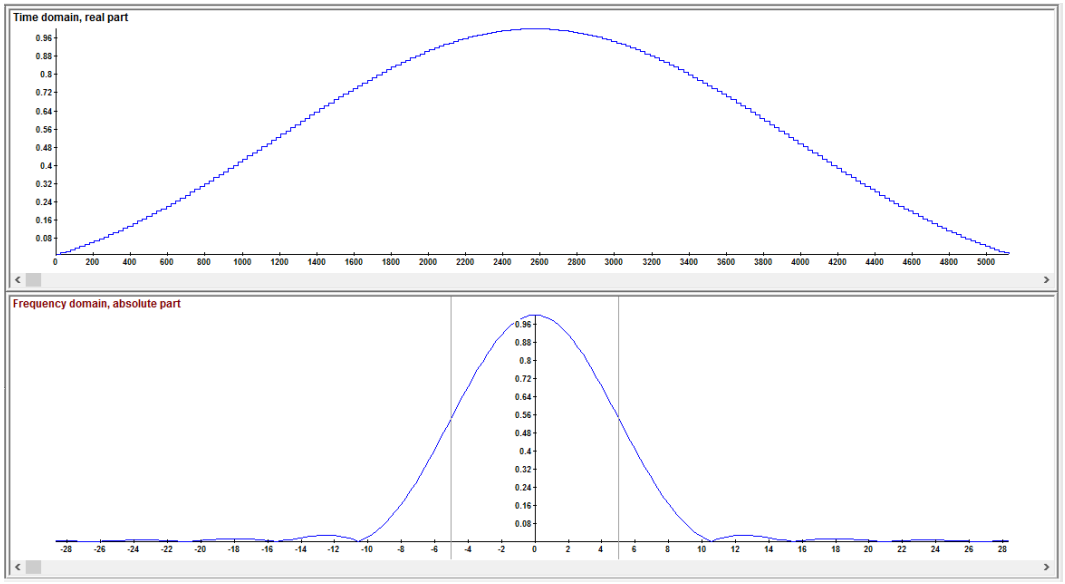

Figure 4-6 - HERMES single lobe editing pulse ('sl_edden_edit')

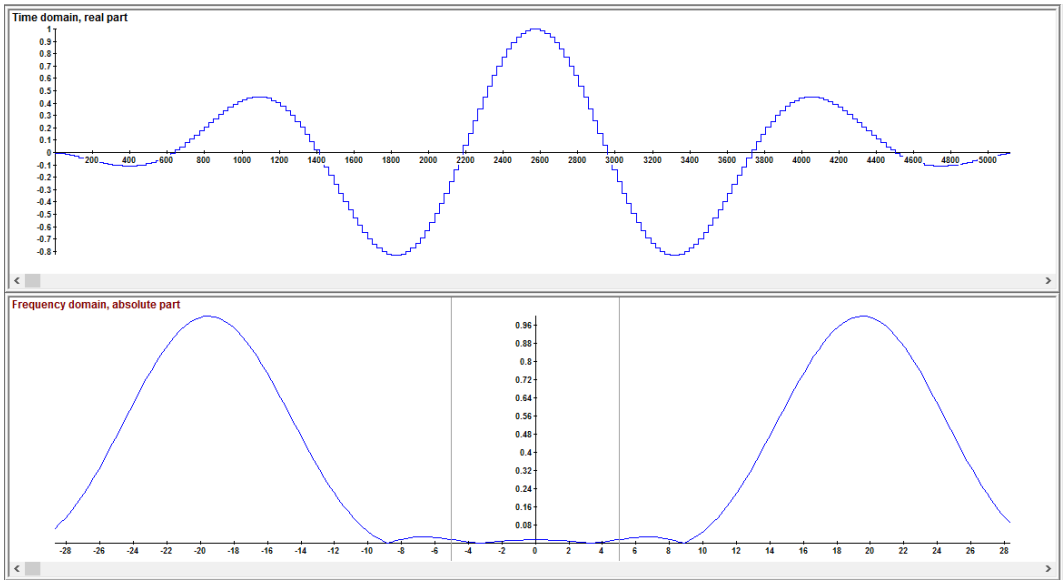

Figure 4-7 - HERMES dual lobe editing pulse ('DUALBAND2')

4.1.3 Sequence timing

Adapting the svs_edit WIP for HERMES involved changing the timings of the editing pulses, the RF excitation, and the first echo.

Editing pulses

Maximum editing efficiency requires that the time between the two editing pulses equals half the total echo time, i.e.

$$T_{Edit\ 2} - T_{Edit\ 1} = \frac{TE}{2} \quad , \qquad \text{(Philips and universal implementation timing),}$$

while maximum echo signal amplitude requires that the editing pulses be placed symmetrically around the second refocussing pulse (Figure 4-8), i.e.

$$\left|T_{Edit1} - T_{Refocus2}\right| = \left|T_{Edit2} - T_{Refocus2}\right|. \qquad \text{(Siemens WIP timing)}$$

In the latter, the spoiler gradients on the x-axis are also typically placed symmetrically about the second refocussing pulse. Due to the editing pulses being long (17.9 ms in the Siemens WIP and 20 ms in the Philips and universal implementations), both the above conditions cannot be met simultaneously, so that sequences typically maximise either editing efficiency (the difference between sub spectra) or echo amplitude. The HERMES implementations by Saleh et al. (2016) on the Philips platform optimised editing efficiency, while the Siemens svs_edit WIP optimises the echo amplitude (Figure 4-8).

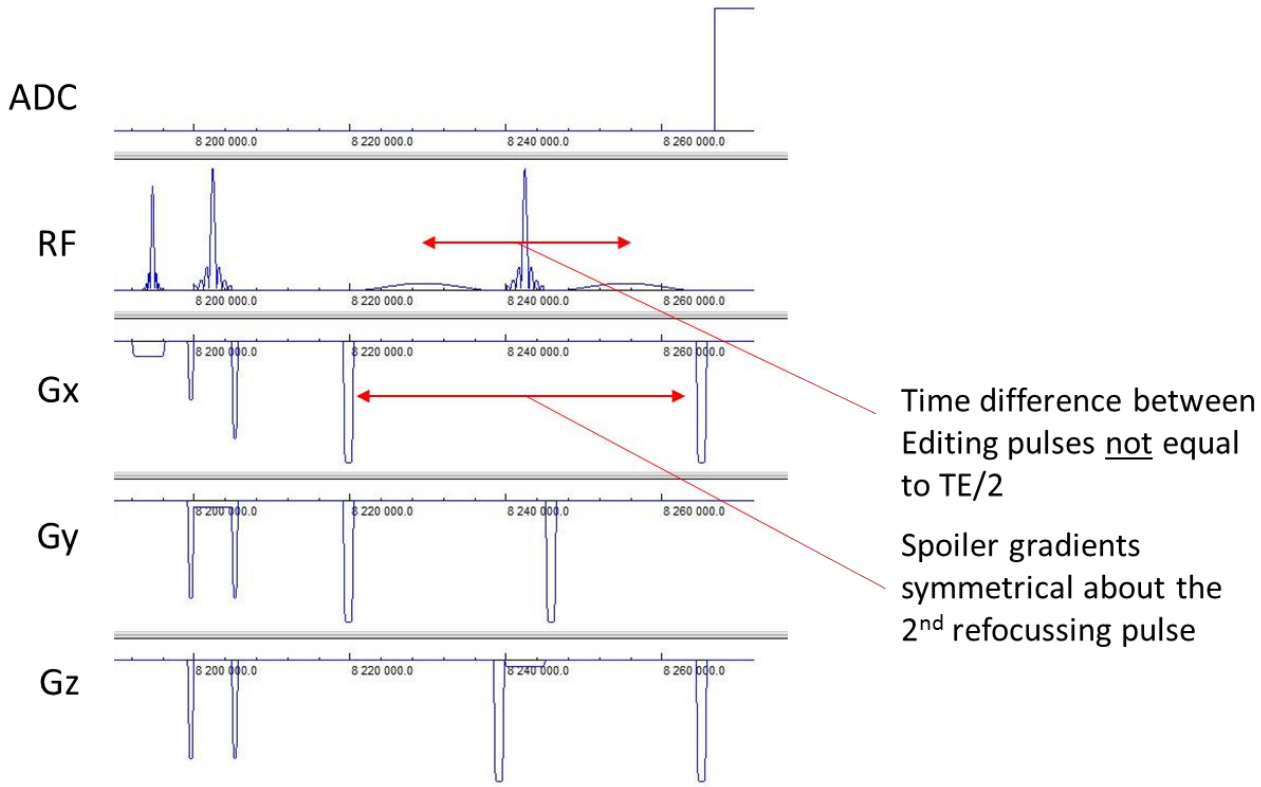

Figure 4-8 – Timing of the Siemens MEGA-PRESS WIP ('svs_edit')

Figure 4-9 shows the HERMES pulse sequence that was adapted from the svs_edit pulse sequence. In addition to replacing the pulses with universal pulses as discussed previously, two new time periods were defined – the interval 'm_postEdit1' between the first editing pulse and the second refocussing pulse, and the time 'm_preEdit2' between the second refocussing pulse and the second editing pulse. These values were chosen such that the difference between the editing pulses would be half the total echo time, while ensuring that the first editing pulse is positioned halfway between the excitation pulse and the second refocussing pulse, i.e.

$$T_{Edit1} = T_{Exc} + \frac{T_{Refocussing2} - T_{Exc}}{2} \qquad \text{(HERMES timing condition)}$$

T_{Edit1} is the time when the first editing pulse is applied, T_{Exc} the time when the excitation pulse is applied, and $T_{Refocussing2}$ the time of the second refocussing pulse.

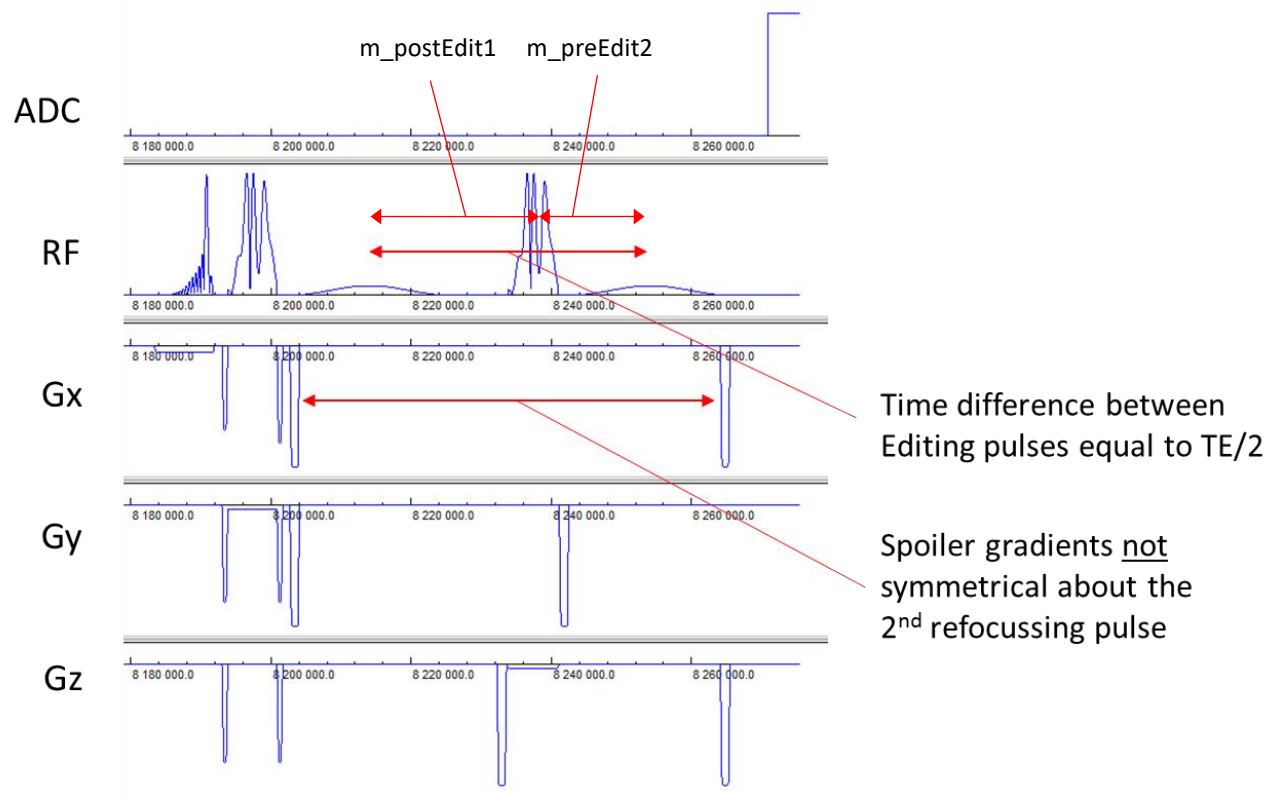

Figure 4-9 – Timing of the HERMES pulse sequence

Excitation pulse

Notably, the use of an asymmetric excitation pulse also affects the sequence timing. Since most of the energy is imparted under the tallest peak, this is the time when excitation is assumed to have occurred in timing calculations. For symmetric pulses, such as the one shown on the right in Figure 4-10, this occurs at the mid-point (0.5) of the pulse duration. In contrast, this happens later for an asymmetric pulse, as shown on the left in Figure 4-10. The asymmetry was set in the sequence code and any subsequent timing references in the original WIP to the mid-point of the excitation pulse were modified to return instead the asymmetry value ('getAsymmetry').

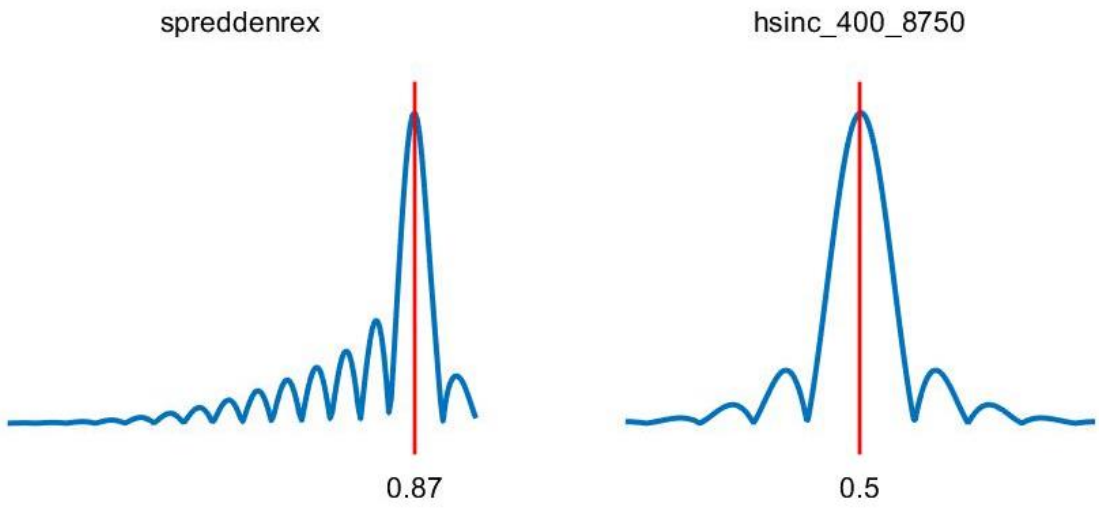

Figure 4-10 - Diagram of the spreddenrex (HERMES sequence) and hsinc_400_8750 (svs_edit sequence) excitation pulses and their asymmetry factors

TE1

The final notable timing change for HERMES compared to the svs_edit WIP was hard coding the time TE1 to 13.1 ms, regardless of the total TE selected. This fixes the timing of the first refocussing pulse. In the original svs_edit WIP, TE1 depended on the pulse duration of the excitation pulse.

4.1.4 Other sequence development details

Simulation and POET

The POET tool in IDEA allows the sequence user interface to be visualised (such as the image in Figure 4-1). Simulation is also possible either from POET directly or using the 'sim' command. Figure 4-8 and Figure 4-9 in the previous section were generated using the 'sim' command.

Unit tests

A useful first check of the newly developed sequence is the Unit Test, which is typically performed before installing the sequence on the scanner. The Unit Test performs a comprehensive test on a number of sequence details. Figure 4-11 shows a sample result from a Unit Test performed on a version of the svs_edit sequence.

```
Unit Test of 'svs_edit_859F'


Sequence DLL:           \n4\x86\prod\bin\svs_edit_859F
Unit source code:       \n4\pkg\MrServers\MrSpecAcq\svs_edit/svs_edit.cpp
Status file:            C:\MIDEA\N4_VE11C_LATEST_20160120\n4\MriSitedata\Skyra-XQ
Protocol:               Initialized by sequence
Analyzed event blocks:  658
Start of Test:          Tue, 04-September-2018 11:06   (by User)

Unit test of svs_edit_859F with protocol 'Initialized' on Skyra-XQ passed successfully.

-------------------
Summary of EGA keys:
-------------------
```

Figure 4-11 - Sample Unit Test results (incomplete) from svs_edit

Compiling binaries and installation

The sequence source code was compiled using IDEA. This can be done in one of three modes: debug, release, and SO (where 'SO' is a reference to the Linux binary file type .so, meaning 'shared object'). The debug compilation can be used to perform various checks from the IDEA command shell. However, the scanner ultimately needs the 'release' binaries (which run on the Windows host - .dll) and the 'SO' binaries (which run on the Linux based Measurement and Reconstruction System (MARS) - .so).

The sequence binaries as well as the ICE reconstruction binaries were installed on the scanner. Notably the ICE reconstruction files were not adjusted for this project. Therefore, Hadamard recombination of sub-experiments, and visualising of difference spectra, could not be done directly on the scanner. Raw data were therefore exported from the scanner using the Twix program and processed offline as described in the next section.

4.2 Development of a Simultaneous Modelling Processing Tool

For this research a quantification technique was developed that simultaneously fits simulated basis sets ('prior knowledge') for all the acquired spectra rather than just the relevant difference spectra. The basis sets were simulated using the FID-A toolkit. In addition, phase cycling was applied to the simulations. The following sections present more details on the modelling technique.

4.2.1 Generating a HERMES Basis set

A HERMES basis set comprising 16 metabolites was generated by simulating with FID-A, at the centre of a 3x3x3 cm^3 voxel, a spectrum for each metabolite for each of the four sub-experiments (A – GABA ON; B – BOTH OFF; C – GSH ON, D – BOTH ON). The metabolites included in the basis set were ascorbic acid (Asc), aspartate (Asp), creatine (Cr), γ-aminobutyric acid (GABA), glycero-phosphocholine (GPC), glutathione (GSH), glutamine (Gln), glutamate (Glu), myo-inositol (Ins), lactate (Lac), N-acetyl aspartyl glutamate (NAAG), N-acetyl aspartate (NAA), phosphocholine (PCh), phosphocreatine (PCr), scyllo-inositol (Scyllo), and water (H_2O). While the spectra generated for sub-experiments A and B (or B and C) can be used to generate a basis set for GABA (or GSH) edited MEGA-PRESS, the unedited sub-experiement (B) cannot be used as a basis set for PRESS due to the fact that the timing and pulses used in the universal HERMES sequence are not the same as those used in the Siemens PRESS sequence ('svs_se') and would lead to inaccurate results.

In all simulations, excitation was assumed to be a perfectly uniform non-frequency selective pulse, while actual sequence timing and RF profiles were used for signal evolution and RF refocussing, respectively. For each basis set simulation, 2048 points were calculated and linewidths were set to 3 Hz. Effects of frequency drift, phase drift and noise were ignored.

Complete phase cycling, where every pulse can have one of four possible phases (i.e. 0, 90, 180 or 270 degrees), requires that each basis set simulation be repeated for all possible combinations of the pulses' phases. The number of unique phase cycling combinations are given by

$$No.of\ phase\ cycling\ combinations = Number\ of\ phases^{Number\ of\ pulses},$$

with the *Number of phases* equal to four.

However, if the number of possible phases for the different pulses differ, the number of possible phase cycling combinations for *k* pulses are given by

$$No.of\ phase\ cycling\ combinations = Pulse1_{Phases} \times Pulse2_{Phases} \times \dots \times Pulsek_{phases},$$

where $Pulsei_{Phases}$ is the number of phases to be cycled through for pulse *i*, and *i* = 1 to *k*.

In addition to repeating each metabolite's simulation for each sub-experiment and all possible phase cycling combinations, the basis set simulation may also need to be repeated for multiple points on the voxel (if desired) to account for within-voxel spatial variation of the metabolite signal (as explained further below).

As such, the total number of simulations (*N*) required to generate a complete basis set is given by

$$N = No.of\ metabolites\ \times No.of\ sub-experiments\ (4\ for\ HERMES)\ \times \\ No.of\ phase\ cycling\ combinations\ \times No.of\ positions\ in\ voxel.$$

As a general rule of thumb within-voxel spatial variation of the metabolite signal arises when the bandwidth of the slice selective pulses are close to the chemical shift difference of the coupled spin-systems (Edden & Barker 2007). In our implementation, the FWHM bandwidth of the refocussing pulse is 1228 Hz and the chemical shift difference for GABA is 144 Hz ((3.012 - 1.889 ppm) × 128 MHz) and for GSH is 209 Hz ((4.561 - 2.926 ppm) × 128 MHz) (Govindaraju et al. 2000). Since FID-A can account for spatial variation, initial simulations were done with 3 spatial distances in each direction of the 3x3x3 cm^3 voxel i.e. x=(-1.5, 0, 1.5)cm, y=(-1.5, 0, 1.5)cm, and z=(-1.5, 0, 1.5)cm – giving 27 points. However, due to the refocussing bandwidth being nearly an order of magnitude larger than the chemical shift difference for GABA and nearly 6 times larger for GSH, and because of the already intensive computational requirements of the simulation, the simulations were performed only at the centre of the voxel for the final basis set i.e. number of positions in voxel = 1.

For HERMES, which comprises 2 refocussing (RP) and 2 editing (EP) pulses, complete phase cycling would involve 256 phase cycling combinations (i.e. 4 phases for each of the 4 pulses). In an effort to reduce the computational burden, the effect that reducing the number of phase cycling steps would have on the spectral lineshapes was examined. This optimisation was performed on a simple singlet before being applied during the final basis set simulation. Figure 4-12 shows sum and difference spectra for a singlet simulated using complete phase cycling (i.e. combining results from 256 simulations), while Figure 4-13 shows the phase distortion present in the GABA difference spectrum for two-step (0, 90 degree) phase cycling (i.e. 2^4 = 16 simulations). Complete phase cycling of one pulse and two-step phase cycling for the other three pulses results in significant distortion of both difference spectra, as shown in Figure 4-14 for different phase cycling combinations. In contrast, two-step phase cycling of the editing pulses and complete phase cycling of the refocussing pulses yields difference spectra (Figure 4-15) with lineshapes indistinguishable from those generated using complete phase cycling (Figure 4-12), while achieving four-fold acceleration (64 phase cycles compared to 256). This strategy was therefore employed when simulating the metabolite spectra for the different sub-experiments to reduce the computation time. In total,

$$N = 16\ (Metabolites) \times 4\ (Sub-experiments) \times 64\ (phase\ cyclings) \times 1(position) = 4096$$

simulations were performed to generate the basis set.

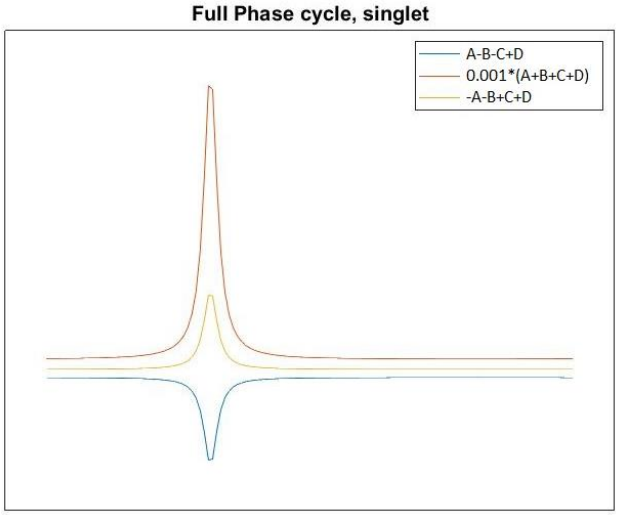

Figure 4-12 - Singlet density matrix simulation for HERMES sequence, showing GABA and GSH weighted difference spectra (A-B-C+D and -A-B+C+D, respectively) and SUM spectrum, for 4-step phase cycling on all refocussing and editing pulses.

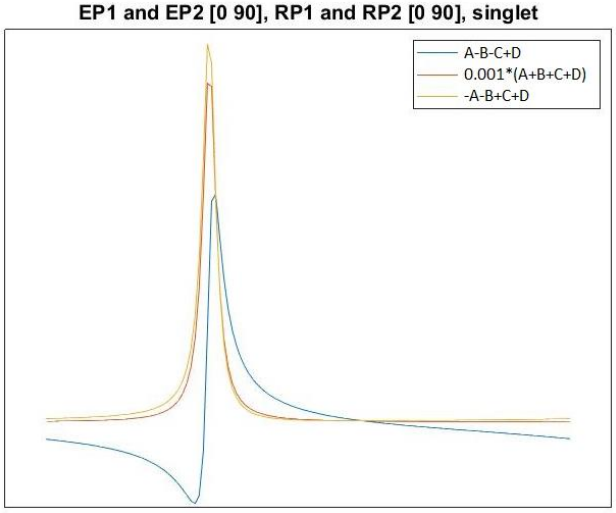

Figure 4-13 - Singlet density matrix simulation for HERMES sequence, showing GABA and GSH weighted difference spectra (A-B-C+D and -A-B+C+D, respectively) and SUM spectrum, for 2-step phase cycling on all refocussing and editing pulses. EP1 and EP2 are the two editing pulses; RP1 and RP2 are the two refocussing pulses.

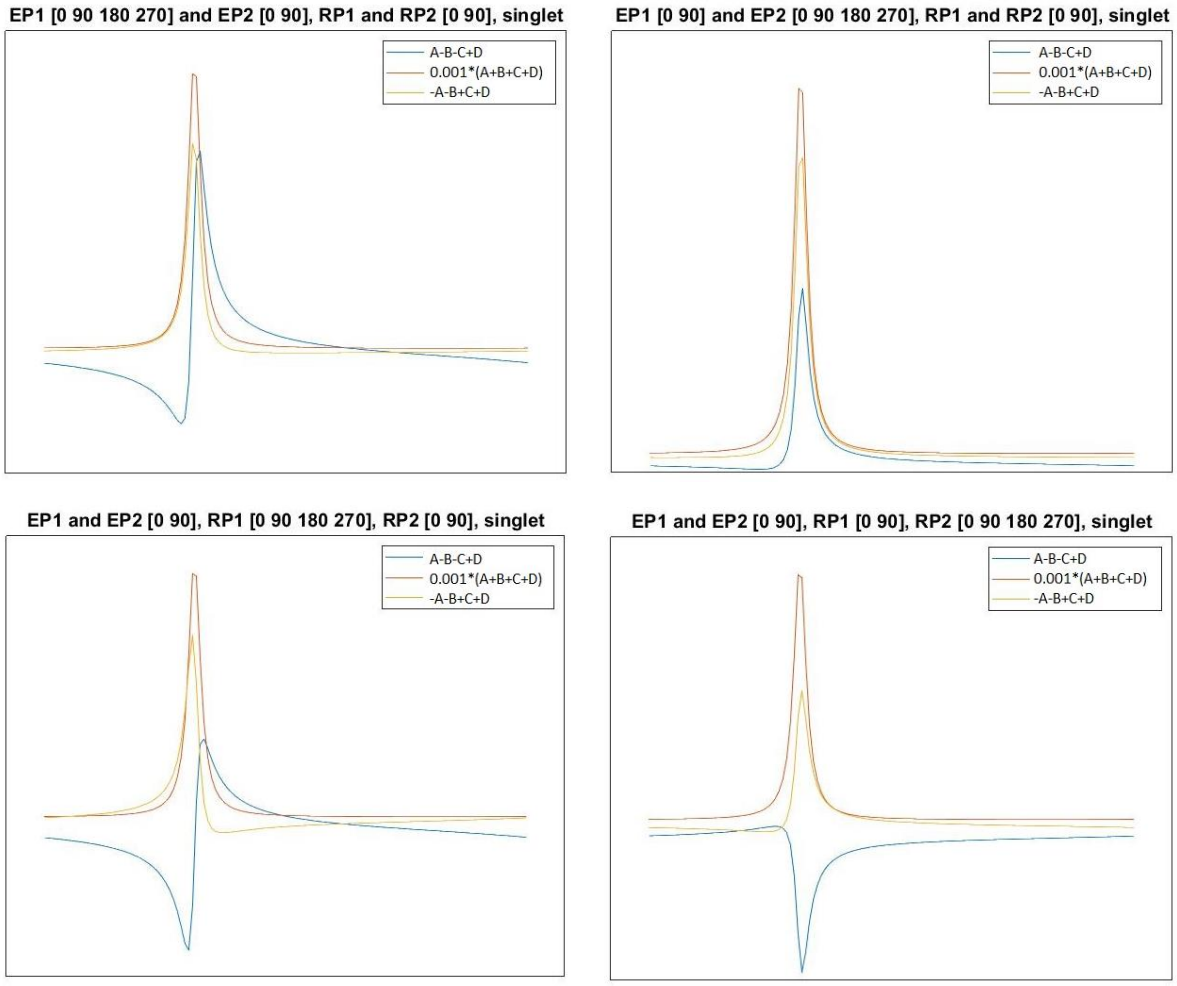

Figure 4-14 - Singlet density matrix simulation for HERMES sequence showing GABA and GSH weighted difference spectra (A-B-C+D and -A-B+C+D, respectively) and SUM spectrum, for three 2-step and one 4-step phase cycles as shown on each figure. EP1 and EP2 are the two editing pulses; RP1 and RP2 are the two refocussing pulses.

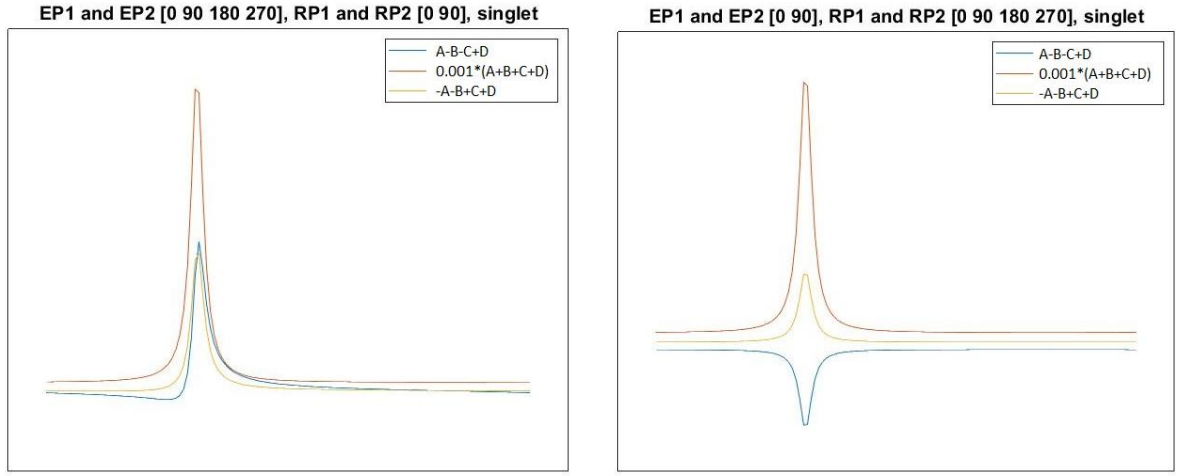

Figure 4-15 - Singlet density matrix simulation for HERMES sequence showing GABA and GSH weighted difference spectra (A-B-C+D and -A-B+C+D, respectively) and SUM spectrum, for two 4-step and two 2-step phase cycles as shown on each figure. EP1 and EP2 are the two editing pulses; RP1 and RP2 are the two refocussing pulses.

Figure 4-16 shows the spectra generated for GABA for each of the HERMES sub-experiments. Note how the two outer peaks of the triplet at 3 ppm are correctly inverted relative to the centre peak when no GABA editing pulse is applied (i.e. sub-experiments B and C), while they are not inverted when a GABA editing pulse is applied (i.e. sub-experiments A and D).

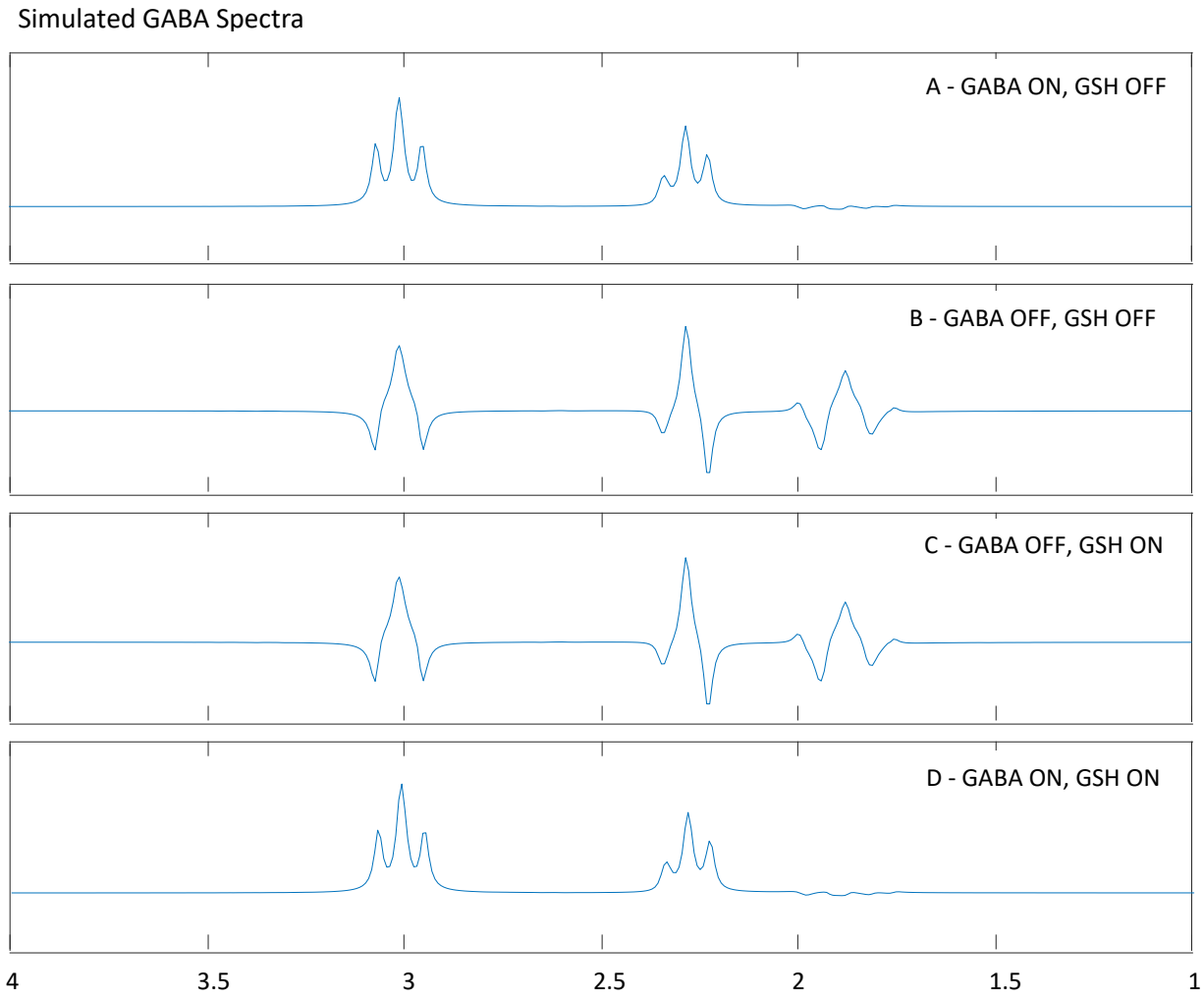

Figure 4-16 - GABA spectra simulated using FID-A for each HERMES sub-experiment.

For all 16 metabolites, spectra simulated for sub-experiment B (GABA OFF, GSH OFF) were compared to lineshapes from literature. A complete HERMES basis set was finally generated by appropriately combining the spectra simulated for the different sub-experiments (sum (A+B+C+D), zero (-A+B-C+D), GSH (-A-B+C+D) and GABA (A-B-C+D)) and concatenating the outputs. Figure 4-17 shows the resulting HERMES basis set comprising 16 metabolites, and figure 4-18 the same for GABA- and GSH edited MEGA-PRESS.

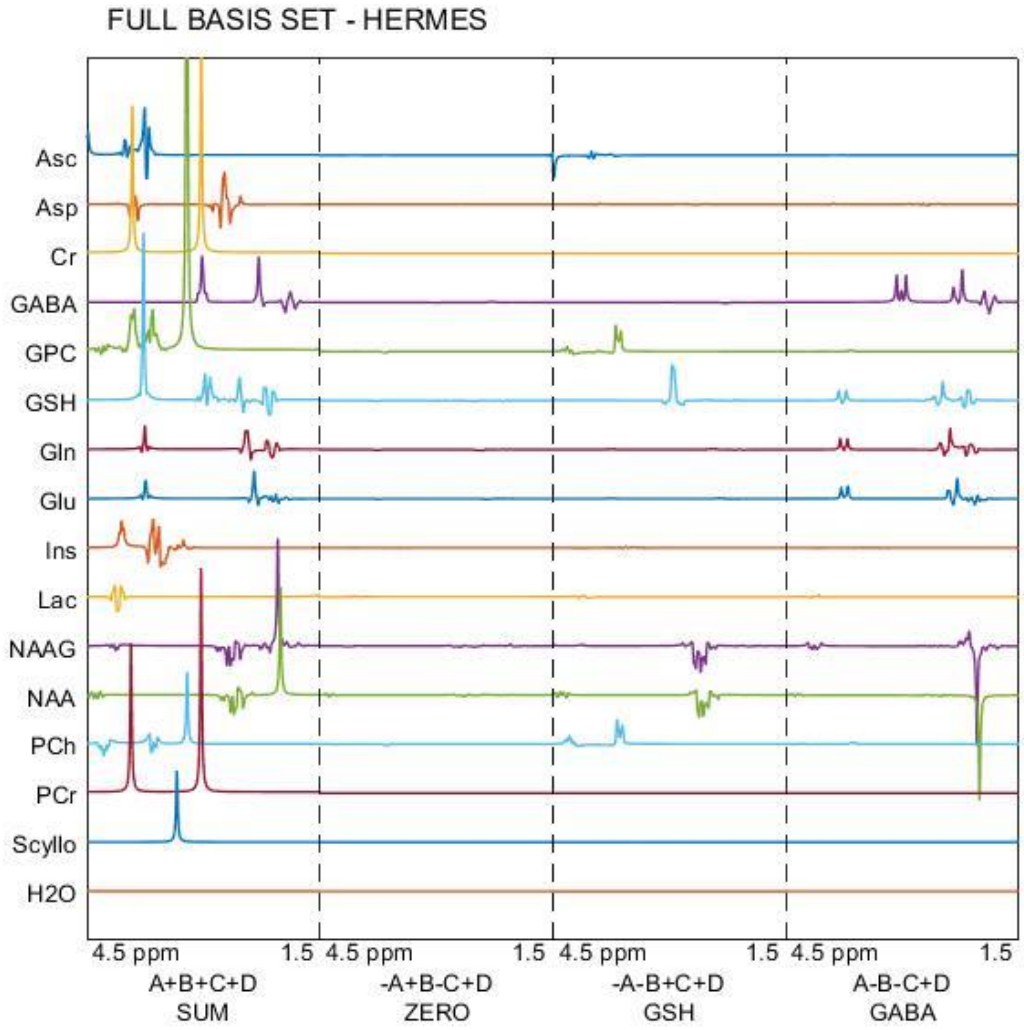

Figure 4-17 – HERMES basis set comprising sum, zero, GSH and GABA spectra for 16 metabolites in the range 1.5 – 4.5 ppm. Spectra simulated for the different sub-experiments were combined according to the Hadamard matrix and the outputs concatenated as shown.

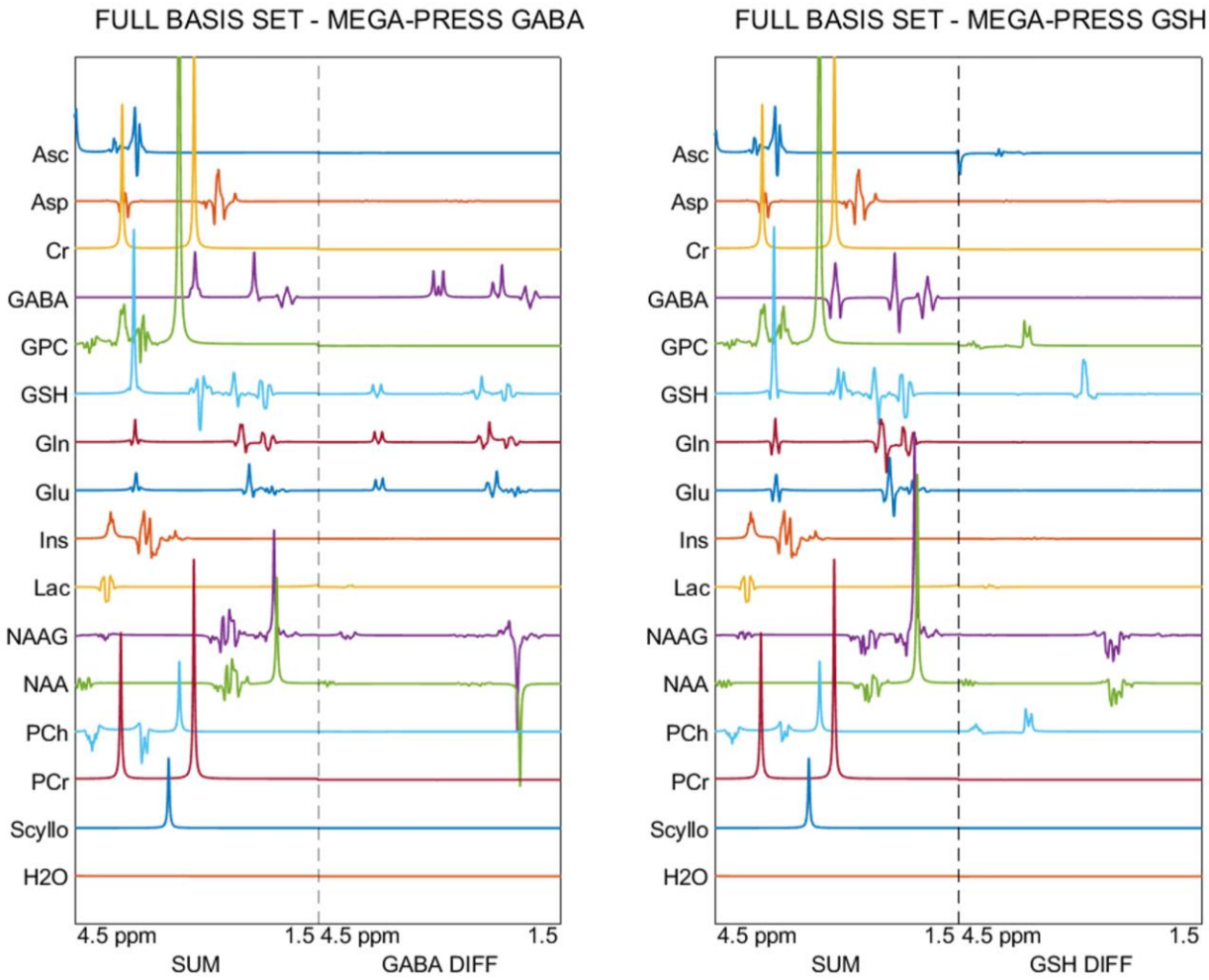

Figure 4-18 – MEGA-PRESS basis sets for GABA and GSH comprising sum and difference spectra for 16 metabolites in the range 1.5 – 4.5 ppm. Spectra simulated for the different sub-experiments (EDIT ON and EDIT OFF) were combined and the outputs concatenated.

4.2.2 Simultaneous linear combination modelling

HERMES data were exported from the scanner in raw format (.dat) using the TWIX program and processed using tools from GANNET, FID-A, SPM, and in-house MATLAB scripts. The processing pipeline is shown in Figure 4-19. The fitting code was written in MATLAB and comprised modules: initialise settings, prepare data, prepare basis sets, fit, quantify, plot, and save outputs. The scripts were written as functions for batching.

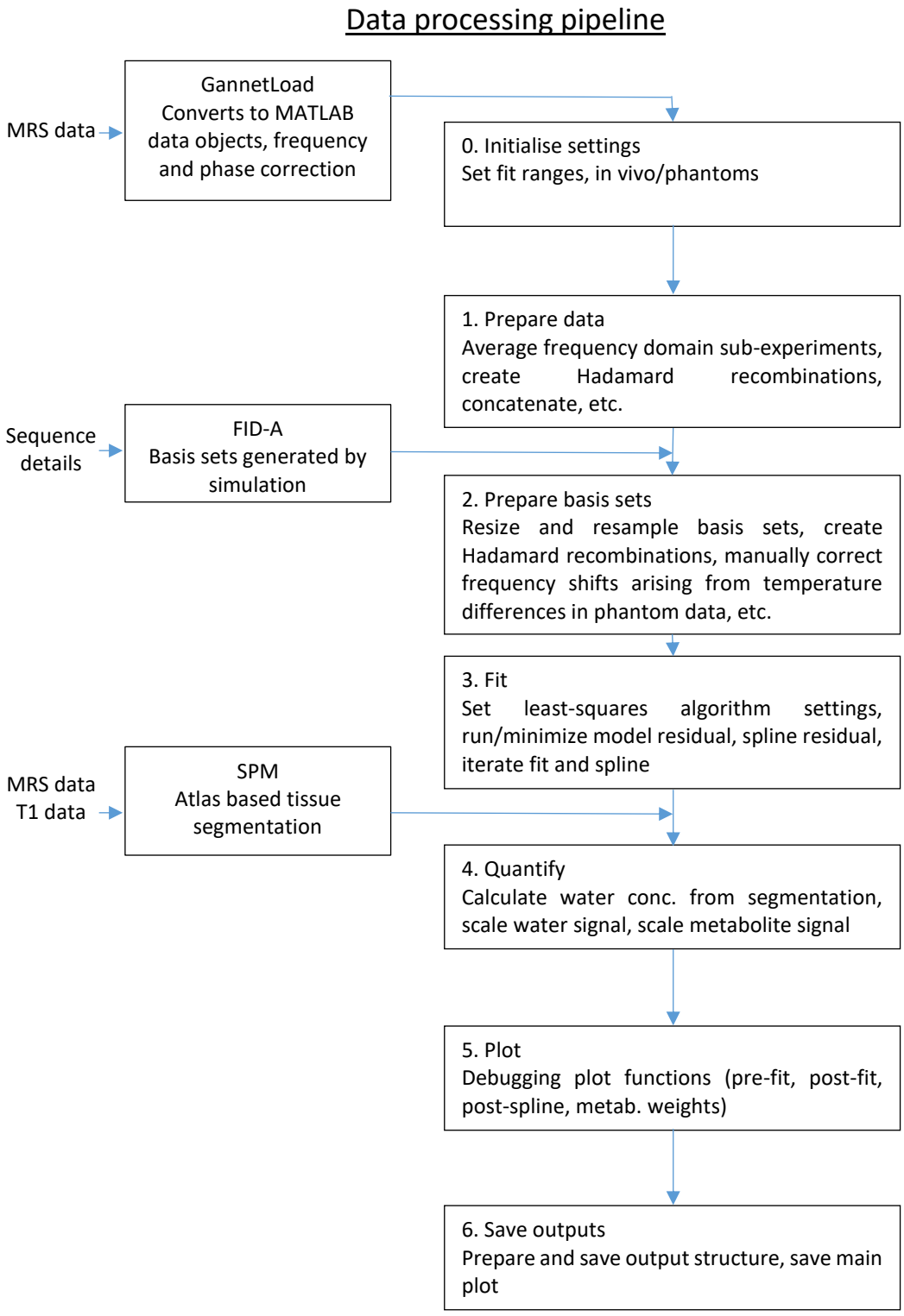

Figure 4-19 – Data processing pipeline.

Some items to note on the modelling approach;

- The simultaneous linear combination modelling pipeline used GannetLoad to import the raw data, to convert the raw scanner data into MATLAB data structures, and to perform frequency and phase correction. The GANNET pipeline would usually then proceed with GannetFit, GannetSegment, and GannetQuantify to fit and quantify the data. These tools were not used in the simultaneous linear combination modelling pipeline.
- SPM was used to segment the voxel into grey matter, white matter, and CSF. This was done by co-registering the voxel coordinates from the header information of the MRS data file on the T1 image. The T1 image was then cropped to the size of the voxel and tissue fractions computed.

The simultaneous linear combination modelling approach developed as part of this project differs from existing methods in that the Hadamard combinations (i.e. the sum, zero, GSH and GABA spectra) were concatenated into a single spectrum prior to fitting. Notably, the basis sets were similarly concatenated. Figure 4-20 shows the model parameters. The model comprised 27 parameters – 16 metabolite weightings (P1 - P16), 8 parameters (P17 – P24) for baseline correction (two parameter estimates per sub-spectrum), 2 for line broadening (P25, P26), and one (P27) to correct small frequency shifts.

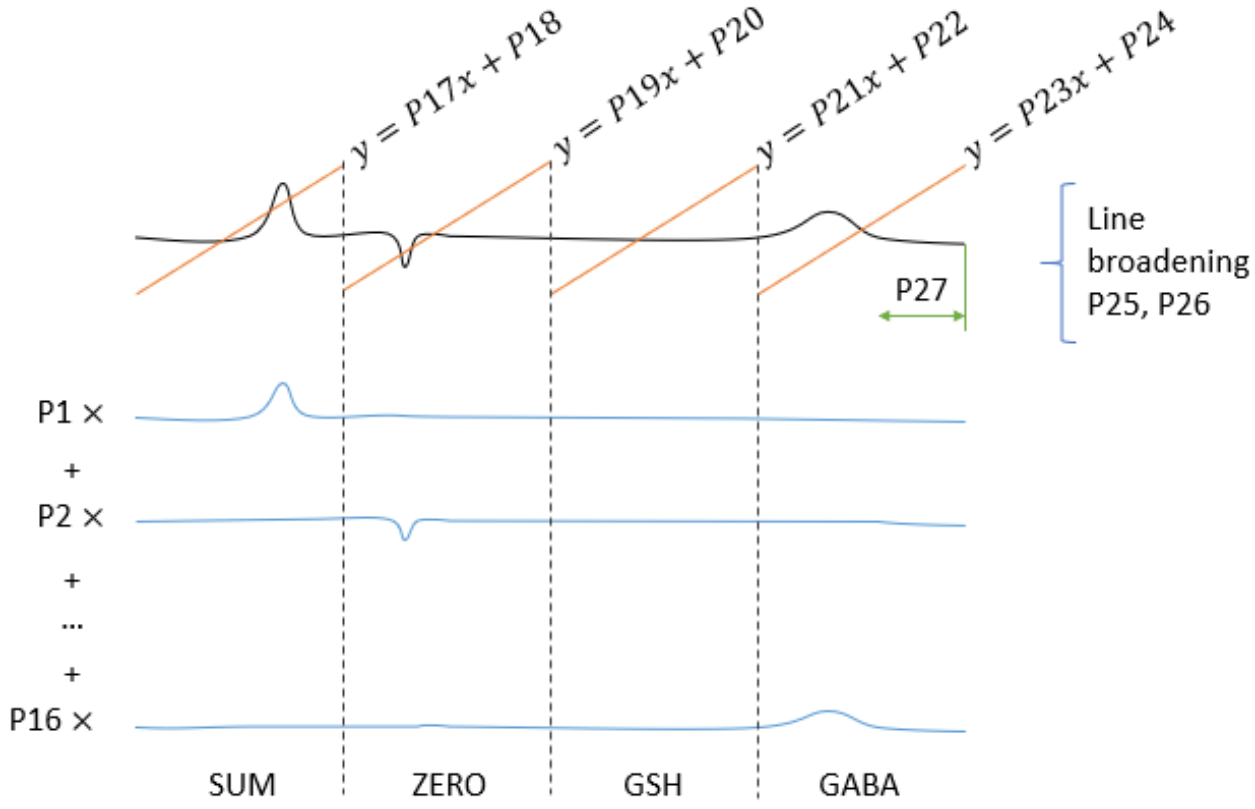

Figure 4-20 - Graphical illustration of the model used in the least squares fitting algorithm, where P denotes a parameter, black lines are data, orange lines are baseline corrections, and blue lines are the basis set

Line broadening involved convolution with Gaussian and Lorentzian functions. The width was set to 1 ppm and the remaining parameters were controlled by the least squares algorithm. A Gaussian function is given by

$$G(x) = ae^{-\frac{(x-b)^2}{2c^2}},$$

where a is the peak height, b is the peak centre, and c is the standard deviation.

A Lorentzian function is given by

$$L(x) = \frac{1}{\pi}\frac{\frac{1}{2}\Gamma}{(x-x_0)^2+\left(\frac{1}{2}\Gamma\right)^2},$$

where Γ is the FWHM, and x_0 is the peak centre.

In the model, the centre points of the Gaussian and Lorentzian were both set to zero, while the remaining three parameters (a, c and Γ) were defined to be functions of model parameters P25 and P26, namely

$$a = \sqrt{\frac{ln2}{\pi}}\frac{2}{P25 \times P26}$$

$$c = \frac{P25 \times P26}{2\sqrt{2ln2}}$$

$$\Gamma = P25 - P25 \times P26$$

Since straight lines cannot adequately remove macromolecule contributions from the baselines, splines were fitted to the residuals iteratively for additional baseline correction as illustrated in Figure 4-21. It should be noted that the splines were fit to the residuals of each recombination separately (SUM, ZERO, GSH, GABA) by reshaping the spectra after the first optimisation, splining, and then concatenating again before the next iteration of the least squares optimisation. This improves the fit at the edges of the separate spectra which is often where significant macromolecule signal is found.

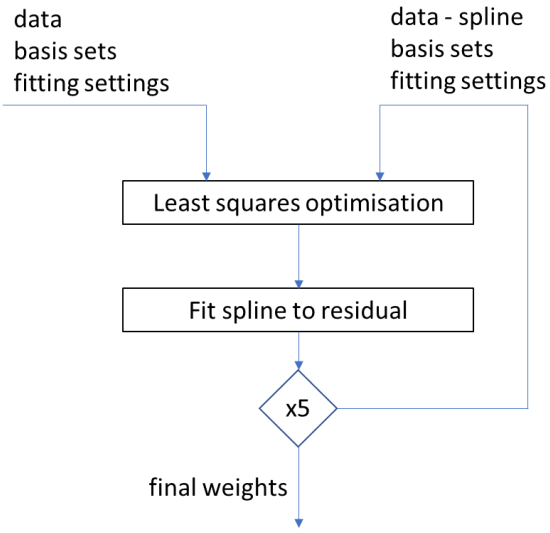

Figure 4-21 - Iterative fitting of splines to the residual for improved baseline correction within the Simultaneous linear combination modelling pipeline

Figure 4-22 shows an example of how this splining procedure improved the fitting of *in vivo* data.

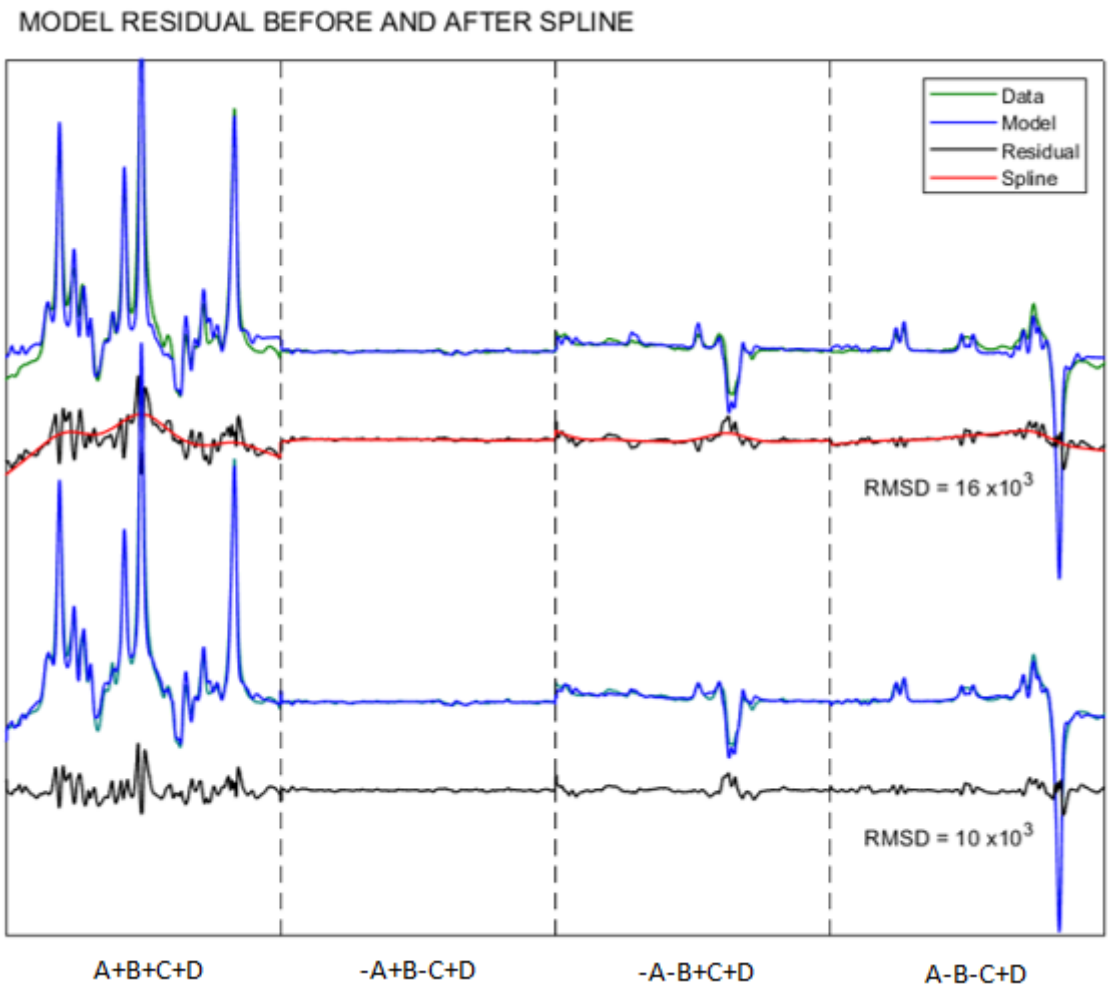

Figure 4-22 - Sample in vivo data showing the initial model solution (top two spectra) and the spline (red line) fitted to the residual, as well as the final iteration of the model and residual (bottom two spectra). The model Root-mean-square Deviation (RMSD) is 38% lower after the splining procedure.

Least squares algorithm

Initial weights for the least squares algorithm were chosen from typical *in vivo* concentrations (Govindaraju et al. 2000). These are listed in Table 4-2. The 'lsqcurvefit' function in MATLAB 2018a was used for the non-linear least-squares regression. The inputs and outputs are summarised in Table 4-3.

Table 4-2 – Initial weights for parameter estimates

LC Model Parameter number	Metabolite		Typical brain concentration (mM/kg_{ww})	X0 for lsqcurvefit	[lower and upper] bounds for lsqcurvefit
	Full name	Abbr.			
P1	Ascorbic acid	Asc	1.0 (de Graaf)	1	[0 1E8]
P2	Aspartate	Asp	1.0 – 1.4	1	[0 1E8]
P3	Creatine	Cr	5.1 – 10.6	8	[0 1E8]
P4	Aminobutyric acid	GABA	1.3 – 1.9	2	[0 1E8]
P5	Glycero-phosphocholine	GPC	1.0	1	[0 1E8]
P6	Glutathione	GSH	2.0	2	[0 1E8]
P7	Glutamine	Gln	3.0 – 5.8	4	[0 1E8]
P8	Glutamate	Glu	6.0 – 12.5	9	[0 1E8]
P9	Myo-inositol	Ins	3.8 – 8.1	6	[0 1E8]
P10	Lactate	Lac	0.4	1	[0 1E8]
P11	N-acetyl aspartyl glutamate	NAAG	0.6 – 2.7	2	[0 1E8]
P12	N-acetyl aspartate	NAA	10.3	10	[0 1E8]
P13	Phosphocholine	PCh	0.6	1	[0 1E8]
P14	Phosphocreatine	PCr	3.2 – 5.5	4	[0 1E8]
P15	Scyllo-inositol	Scy	0.3 – 0.6	1	[0 1E8]
P16	Water	H2O		10	[0 1E8]
	Property description				
P17	Y-intercept of SUM baseline			0	[-1 1]E6
P18	Y-intercept of ZERO baseline			0	[-1 1]E6
P19	Y-intercept of GSH baseline			0	[-1 1]E6
P20	Y-intercept of GABA baseline			0	[-1 1]E6
P21	Gradient of SUM baseline			0	[-1 1]E6
P22	Gradient of ZERO baseline			0	[-1 1]E6
P23	Gradient of GSH baseline			0	[-1 1]E6
P24	Gradient of GABA baseline			0	[-1 1]E6
P25	Convoluted Lorentzian and Gaussian combined parameters See formula above			1	[0.01 1]
P26				0.5	[0 1]
P27	Frequency shift (Hz)			0	[-200 100]

Table 4-3 - Non-linear regression analysis function inputs and outputs explained

MATLAB function [x, resnorm, residual, exitflag, output, lambda, jacobian] = lsqcurvefit(fun, x0, xdata, ydata, lb, ub, options)		
Input	**General description**	**Description for this use-case**
fun	Non-linear function fun(x,xdata)	MRS model as illustrated in Figure 4-20.
x0	Initial weights.	Initial weights for parameter estimates (Table 4.2).
xdata	Input data for the model.	The basis set resampled to the length of the data.
ydata	Response data from the model y=fun(x,xdata)	The concatenated MRS spectrum.
lb	Lower bounds.	Zero concentrations, baseline shift, line broadening, and frequency shift.
ub	Upper bounds.	Metabolite weights two orders above expected, etc.
options	Optimisation options.	Max fit iterations = 1e6 Function tolerance = 1e-8 Max. function evaluations = 4e3

Quantification

The fitting model quantifies metabolite levels in absolute terms by using the water scan as an internal reference according to the relationship given previously (Chapter 1), i.e.

$$[m] = \left(\frac{S_m}{S_r}\right)[r]C_n C_{av} C_{gain}.$$

The parameter estimates P1-P15 are used as the metabolite signal strengths S_m, and the water parameter estimate P16 (from the water reference scan) as the reference signal S_r.

C_n: In the basis set generated, signal amplitudes were already adjusted for the number of nuclei, i.e. in each basis spectrum (e.g. GABA) the height of the peaks were scaled according to the number of active nuclei at that shift/frequency. These weights come directly from the FID-A 'sys' matrices. As such, no further adjustment was necessary and C_n=1.

C_{av}: The correction for the number of averages was also not necessary as the sub-experiment scans were averaged not summed, i.e. the spectra were essentially rescaled to the size of the individual scans prior to fitting regardless of the number of averages acquired (16 for water reference and 320 for metabolite scans).

C_{gain}: The receiver gain was the same for both the metabolite and water reference scans, so no correction was needed.

[r]: Tissue fractions (*GM*, *WM* and *CSF*) were obtained from segmentation of the voxel on the co-registered T1 weighted image. The water concentration is then given by

$$[r] = 55.5\ (GM \times 0.82 + WM \times 0.73 + CSF \times 0.98)$$

Phantom data

The code also features the option to switch between phantom and *in vivo* data. While the intention was to process the phantom and *in vivo* data as similarly as possible so as to avoid bias, two changes were required when processing phantom data, namely

- Enabling a manual frequency shift for phantom data: the code plots the data alongside the metabolite basis set (scaled by the initial weights) and allows the user to manually shift the frequency of the basis set upon reviewing the plot. The temperature of phantoms is not the same as *in vivo* tissue, which causes a frequency shift. When the phantom is taken from a fridge at 5 degrees Celsius, the frequency shift is of the order of 0.2 ppm. Although the model allows the frequency to be shifted by 200 Hz in either direction (P27 from Figure 4-20), this is sometimes less than the temperature-related frequency shift that has occurred. Since widening the upper and lower bounds for P27 causes unstable fitting, a manual frequency shift was rather allowed.
- Bypassing tissue segmentation: the segmentation section of the code is bypassed for phantom data and the water concentration is assumed to be that of pure water.

4.3 Testing

HERMES sequence and simultaneous linear combination modelling algorithm were tested in both phantoms and *in vivo*.

4.3.1 Phantom testing

Three sets of phantoms were constructed (Table 4-4). Design guidance was obtained from the LCmodel manual (Provencher 2018), in particular regarding the inclusion of the pH correcting and preservative compounds HK_2PO_4, H_2KPO_4, and N_3Na, respectively. Quantities of reagents were calculated using the published molar mass values, the known container volume, and the desired concentration according to

$$m = [reagent]MV,$$

where m is the mass in grams, [reagent] is the desired reagent concentration in mols/litre, M is the molar mass of the reagent in grams/mol, and V is the container volume in litres.

Table 4-4 - Details of phantom sets used in the testing and evaluation of the sequence and fitting routine

	[metabolite] (mM/l)	[HK_2PO_4] (mM/l)	[H_2KPO_4] (mM/l)	[N_3Na] (g/l)	Volume (mL)
Phantom set #1					
1	GABA 25 GSH 25	72	28	1	1165
2	GABA 25	72	28	1	1165
Phantom set #2					
1	Cr 20	72	28	1	50
2	GABA 10	72	28	1	50
3	GABA 10 GSH 10	72	28	1	50
4	GABA 10 GSH 20	72	28	1	50
5	GABA 20 GSH 10	72	28	1	50
6	GABA 20 GSH 20	72	28	1	50
7	GSH 10	72	28	1	50
8	NAA 10	72	28	1	50
Phantom set #3					
1	GABA 20 GSH 10 NAA 20 Cr 20 Cho 20	72	28	1	1165

Initial phantom scans during early stages of sequence development were performed at Johns Hopkins University on a 3T Siemens Prisma scanner running software version VE11B. Subsequent sequence testing was done at the Cape Universities Body Imaging Centre (CUBIC) on a 3T Siemens Skyra running software version VE11C using phantom set #1.

Phantom sets #2 and #3 were used to validate the accuracy of the fitting algorithm and absolute quantification.

4.3.2 *In vivo* Testing

All scanning was conducted according to protocols that had been approved by the Human Research Ethics Committee of the Faculty of Health Sciences at the University of Cape Town.

Table 4-5 - Scanning protocol

Sequence Name	TR (ms)	TE (ms)	AVGS	Water Suppression	Sequence Version	Edit Frequency (ppm)	Expected Scan Time (mins)
Localizer	-	-	-	-	-	-	2.5
Calibration and Shimming	-	-	-	-	-	-	4
MPRAGE	-	-	-	-	-	-	5
svs_se (PRESS)	2000	80	64	SWS	Siemens	-	4
MEGA-PRESS GABA	2000	80	320	SWS	Universal	1.9	10
MEGA-PRESS GABA water	2000	80	16	Only RF off	Universal	1.9	2
MEGA-PRESS GSH	2000	80	320	SWS	Universal	4.56	10
MEGA-PRESS GSH water	2000	80	16	Only RF off	Universal	4.56	2
HERMES	2000	80	320	SWS	Universal	1.9 and 4.56	10
HERMES water	2000	80	16	Only RF off	Universal	1.9 and 4.56	2
						Total	**51.5**

SWS = strong water suppression, AVGS = averages, RF = radio frequency

24 healthy adult participants (12 male, mean age 26 ± 2 yr) were scanned on the 3T Siemens Skyra MRI with a 32-channel head coil at the Cape Universities Body Imaging Centre (CUBIC) in Cape Town using the protocol detailed in Table 4-5. All participants provided written informed consent. MRS acquisitions were performed in a single 3 × 3 × 3 cm^3 midline parietal region with 20-ms editing pulses, 2048 data points and 2 kHz spectral width. In three participants, the scanning session was repeated three times. Figure 4-23 shows typical voxel placement for the midline parietal region.

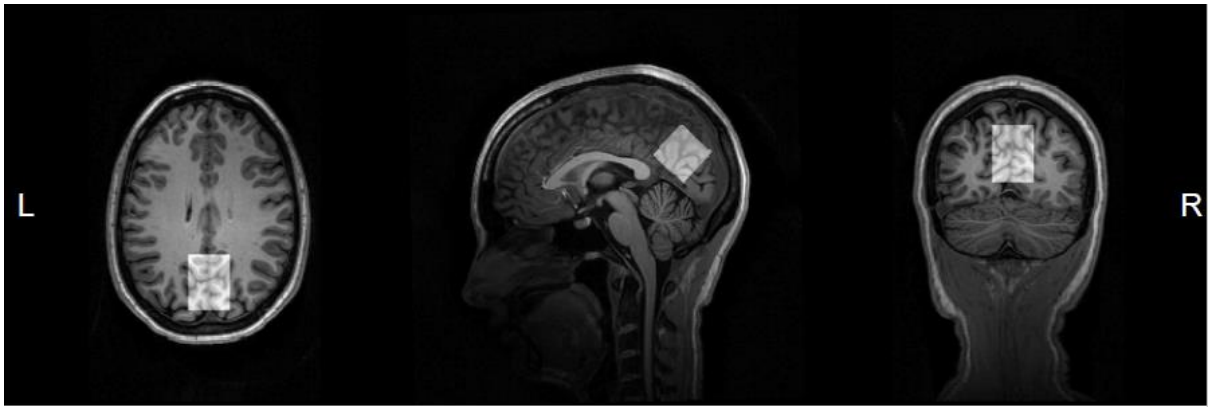

Figure 4-23 - Sample midline parietal voxel placement shown for subject G13.

Data were analysed using our simultaneous linear combination fitting algorithm.

To compare MEGA-PRESS and HERMES data, without biasing the latter by the improvement inherent to fitting to four Hadamard re-combinations rather than two (sum and difference) as in MEGA-PRESS, HERMES data were first processed using only two re-combinations, namely the sum spectrum (A+B+C+D) and either the combinations for GSH- (-A-B+C+D) or GABA- (A-B-C+D) editing. In this way we could directly compare GABA- (or GSH) edited MEGA-PRESS to GABA- (or GSH) HERMES using the identical fitting routine. Metabolite levels from two-recombination fitting of HERMES data were then compared separately to metabolite levels from GABA- and GSH-edited MEGA-PRESS, respectively, using a Mann-Whitney U test.

Subsequently, HERMES data were quantified by fitting to all four Hadamard re-combinations, namely sum (A+B+C+D), zero (-A+B-C+D), GSH (-A-B+C+D) and GABA (A-B-C+D) spectra. Metabolite levels from HERMES were compared separately to those obtained from fitting to sum and difference spectra of GABA- and GSH-edited MEGA-PRESS, respectively, using Mann-Whitney U tests, as well as Spearman rank and intraclass correlation.

4.3.3 Reproducibility

To compare reproducibility's for the different sequences, three subjects were scanned three times using all three sequences, namely GABA-edited MEGA-PRESS, GSH-edited MEGA-PRESS, and HERMES. Data were processed using the fitting routine and reproducibility assessed using coefficients of variation (CVs). Un-edited spectroscopy (such as PRESS) typically gives good reproducibility (over 95%) for total N-acetylaspartate (NAA + NAAG = tNAA), total creatine (Cr + PCr = tCr), choline containing compounds (GPC + PCh = Cho), and myo-inositol (Ins). The signals of glutamate and glutamine are also detectable with un-edited spectroscopy, but typically give less reproducible results than tNAA, tCr, Cho, and Ins.

4.3.4 Comparison of simultaneous and multiple independent fittings

To evaluate the potential benefit of our simultaneous fitting approach compared to multiple independent fittings, both procedures were applied to HERCULES data that had been previously acquired from two 3 × 3 × 3 cm^3 voxels (one white-matter-rich (WM) voxel in the centrum semiovale, and one grey-matter-rich (GM) voxel over the cingulate cortex) in 10 healthy adult participants (5 male, mean age 29.3 ± 2.9 yr) using a 32-channel head coil on the 3T Philips Achieva MRI at John's Hopkins University (Oeltzschner et al. 2019). Acquisition parameters were TE/TR 80/2000 ms; 20-ms editing pulses; 320 averages (i.e. 80 averages for each sub-

experiment), 2048 data points; 2 kHz spectral width; and VAPOR water suppression. A non-water-suppressed reference scan (16 averages) was also acquired in each voxel.

Analysis of Variance (ANOVA) was used to compare metabolite levels obtained from simultaneous fitting to values obtained from multiple separate fittings.

5 Results

5.1 Phantom testing

Scans with phantom set #2 yielded low SNR, presumably due to the small voxel size imposed by the phantom's design, possible signal contamination from the plastic container, and poor shimming. Phantom set #3 was therefore used in all subsequent experiments aimed at validating the processing algorithm.

The phantom was at 5 degrees Celsius when scanned. Manual shimming yielded a FWHM for the water peak of 2.0 Hz immediately prior to the start of the edited MRS protocol. The frequency of the editing pulses was not adjusted to account for chemical shift changes resulting from the phantom being at a low temperature.

Figure 5-1 shows the GABA (left) and GSH (right) difference spectra for Phantom #3 obtained from HERMES and GABA- or GSH-edited MEGA-PRESS acquisitions, respectively. Simulated spectra for GABA and GSH are also shown for both (left) GABA- and (right) GSH-edited MEGA-PRESS. Figure 5-2 shows a comparison of actual metabolite levels to estimates obtained for each acquisition using the simultaneous linear combination model. During fitting the frequency was manually shifted by 150 Hz. While metabolite level estimates of tNAA from all acquisitions were similar to actual values, HERMES yielded the most reliable estimate of total choline levels. Estimates for creatine from all three acquisitions were about 25% lower than actual levels, and for GSH and GABA, concentration estimates from all three acquisitions were more than 50% too low.

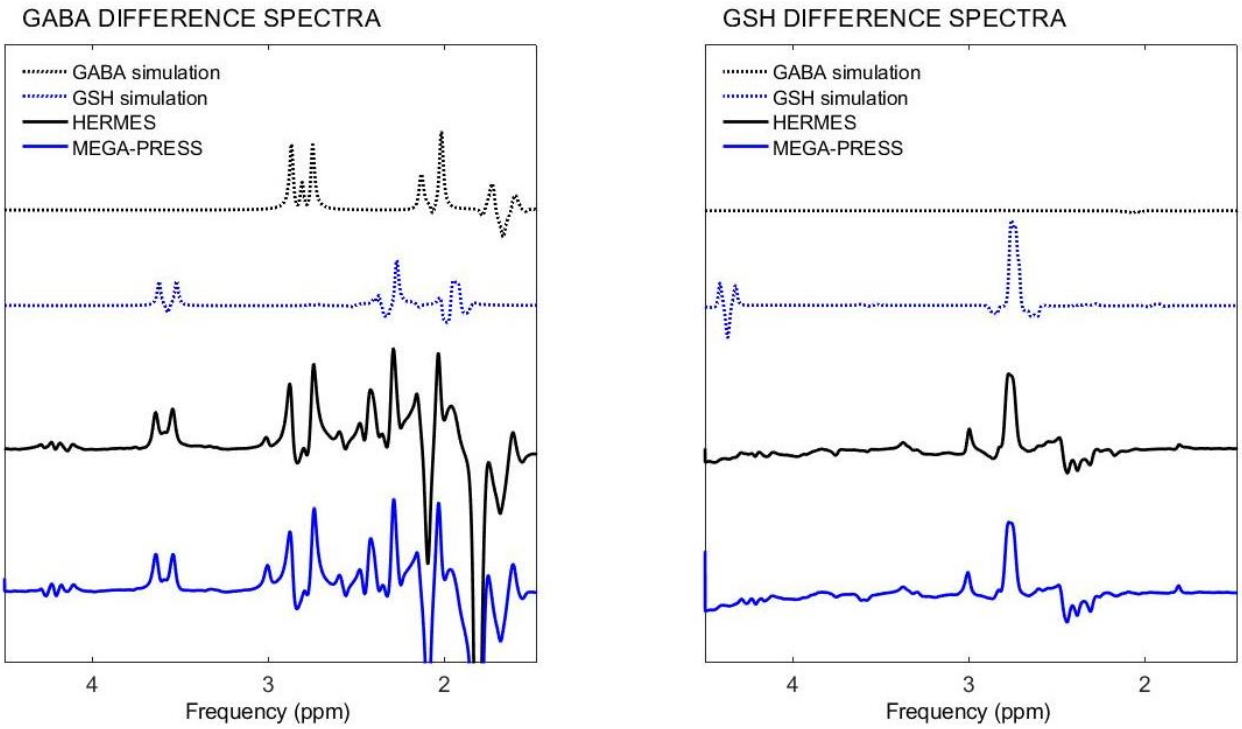

Figure 5-1 – GABA (left) and GSH (right) difference spectra (plotted in solid lines) for phantom #3 from HERMES and (left) GABA- or (right) GSH-edited MEGA-PRESS acquisitions, respectively. (Left) The GABA difference spectrum is obtained using (A-B-C+D) for HERMES data and EDIT ON – EDIT OFF for GABA-edited MEGA-PRESS. (Right) The GSH difference spectrum is given by (-A-B+C+D) for HERMES data and EDIT ON – EDIT OFF for GSH-edited MEGA-PRESS. The dotted lines show simulated GABA and GSH difference spectra for (left) GABA- and (right) GSH-edited MEGA-PRESS, respectively.

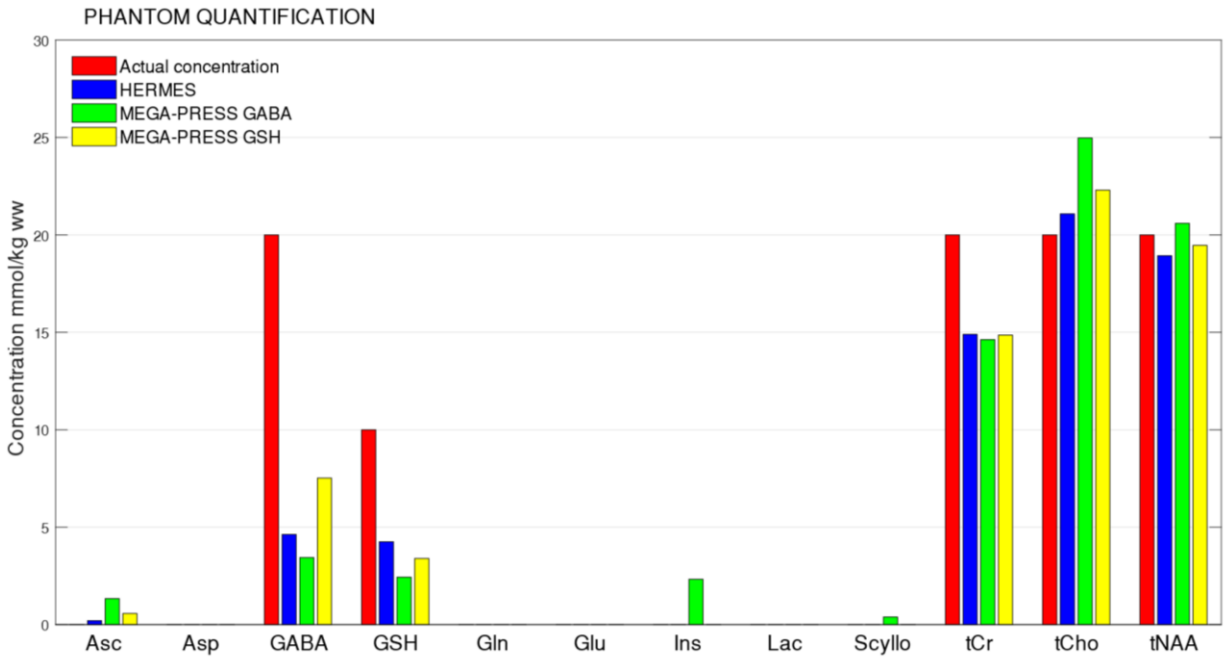

Figure 5-2 - Bar graph comparing the known metabolite concentrations in phantom #3 to the metabolite level estimates obtained from HERMES, GABA- and GSH-edited MEGA-PRESS acquisitions using the simultaneous linear combination model.

5.2 *In vivo* testing

In vivo scans were performed over 9 scanning sessions and are summarised in Table 5-1. The first 6 scans (S01-S06) were all unsuccessful due to an incorrect B1 power setting and sequence error. Data from a further 3 scans (G01, G06 and G12) could not be used. As such, data acquired in 15 participants were used to validate the sequence and quantification tool.

Table 5-1 – Scanning record

Code	Weight	Age	Sex	Height	Repeats	Comment	Valid/invalid data
S01	47,5	26	Female	152	0	B1 power setting incorrect. Sequence pulse file prior to 12 July patch	Invalid
S02	56,5	28	Male	174,5	0		Invalid
S03	60,4	26	Female	173	0		Invalid
S04	51,1	24	Male	169	0		Invalid
S05	68,3	27	Male	174	0		Invalid
S06	55	28	Female	168	0		Invalid
G01	80	26	Male	186	0	Significant field inhomogeneity. Scans followed DTI scans. Potential coil heating issue.	Invalid
G02	64	24	Male	162	0		Valid
G03	102	24	Female	178	0		Valid
G04	54	24	Female	177	0		Valid
G05	79	24	Male	189	0		Valid
G06	47,5	26	Female	152	2	Subject requested to be removed from the study	Invalid
G07	66	24	Female	174	2		Valid
G08	65	23	Female	171	2		Valid
G09	55	21	Female	169	0		Valid
G10	71	26	Male	170	2		Valid
G11	79	24	Male	180	0		Valid
G12	82	29	Male	188	0	Subject became claustrophobic. Scan was not completed.	Invalid
G13	61	27	Female	177	0		Valid
G14	92	27	Male	179	0		Valid
G15	57	29	Female	162	0		Valid
G16	72	29	Male	180	0		Valid
G17	49	26	Female	159	0		Valid
G18	79	32	Male	177	0		Valid
						Total number of scans	32
						Number of valid scans	21
						Number of subjects providing usable data	15

Figures 5-3 to 5-5 present GABA- and GSH-edited MEGA-PRESS and HERMES data, respectively, acquired in the same subject (G04). Sub-plots A show the individual acquisitions, sub-plots B show the averages for each sub-experiment, and sub-plots C (and D for HERMES) show the difference (or Hadamard recombined for HERMES) spectra. In sub-plots C (and D for HERMES), the edited peaks around 3 ppm have been highlighted. Notably, in this subject, the Hadamard recombined GABA and GSH spectra from HERMES (Figure 5-5 C and D) are comparable to the difference spectra obtained from the two separate GABA- and GSH-edited MEGA-PRESS acquisitions (Figures 5-3C and 5-4C). Figure 5-6 shows the HERMES GABA and GSH spectra and those from separate GABA- and GSH-edited MEGA-PRESS acquisitions averaged across all 15 participants. Figure 5-7 shows the parameter estimates of each metabolite obtained using our simultaneous linear combination modelling algorithm for the GABA-edited MEGA-PRESS data acquired in participant G04.

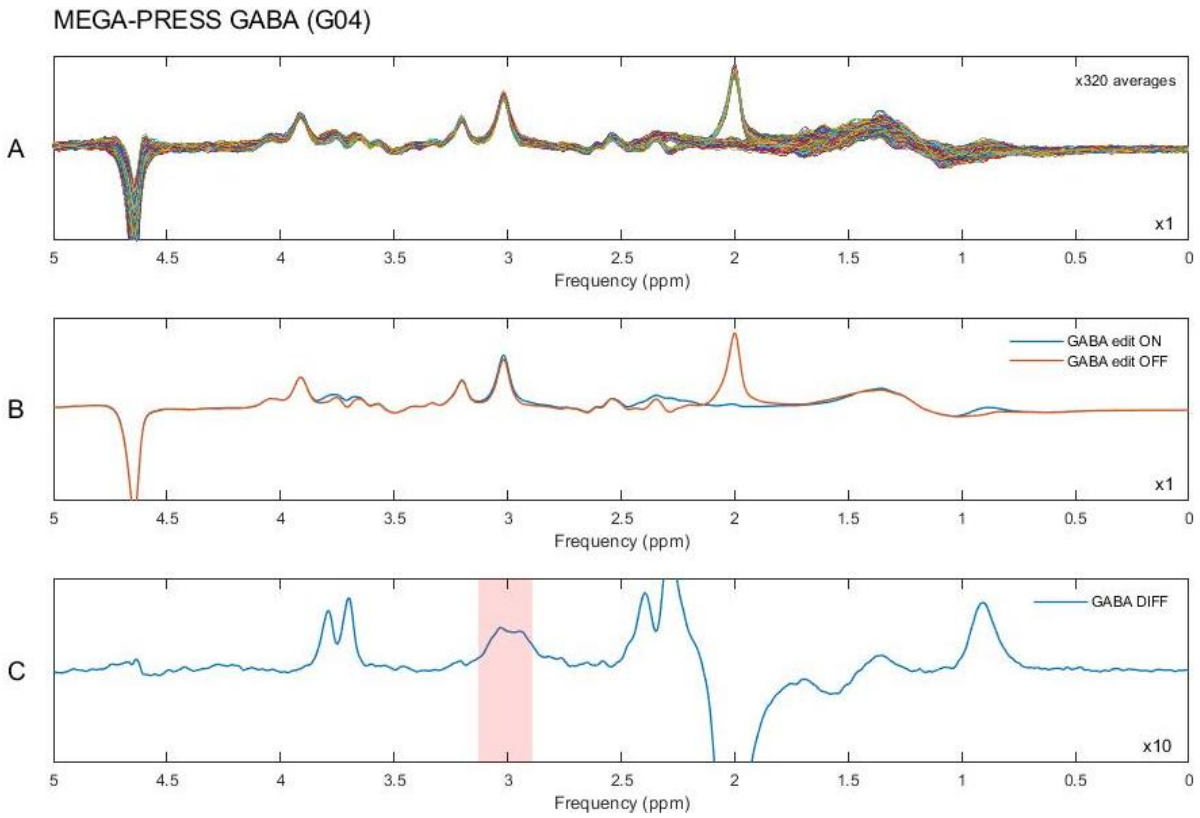

Figure 5-3 - Spectra from the GABA-edited MEGA-PRESS acquisition in subject G04. A shows all 320 acquisitions, B the averaged spectra for each sub-experiment, and C the difference spectrum with the edited GABA peak highlighted. Note that the spectrum in C was scaled to highlight the edited GABA peak at 3.01 ppm.

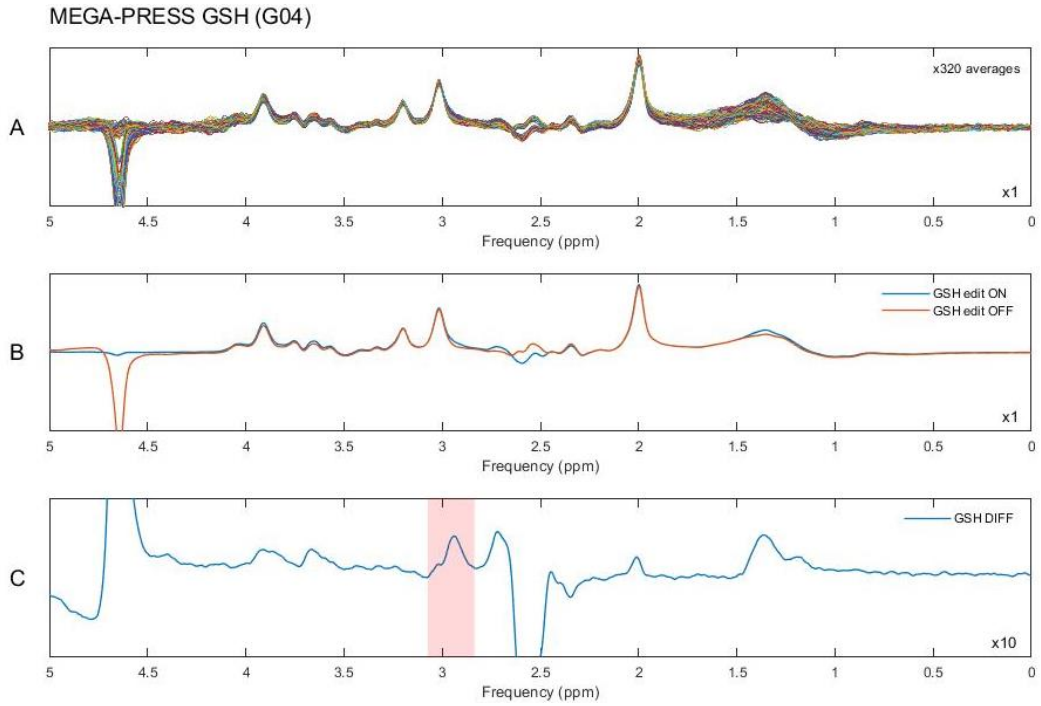

Figure 5-4 – Spectra from the GSH-edited MEGA-PRESS acquisition in subject G04. A shows all 320 acquisitions, B the averaged spectra for each sub-experiment, and C the difference spectrum with the edited GSH peak highlighted. Note that the spectrum in C was scaled to highlight the edited GSH peak at 2.995 ppm.

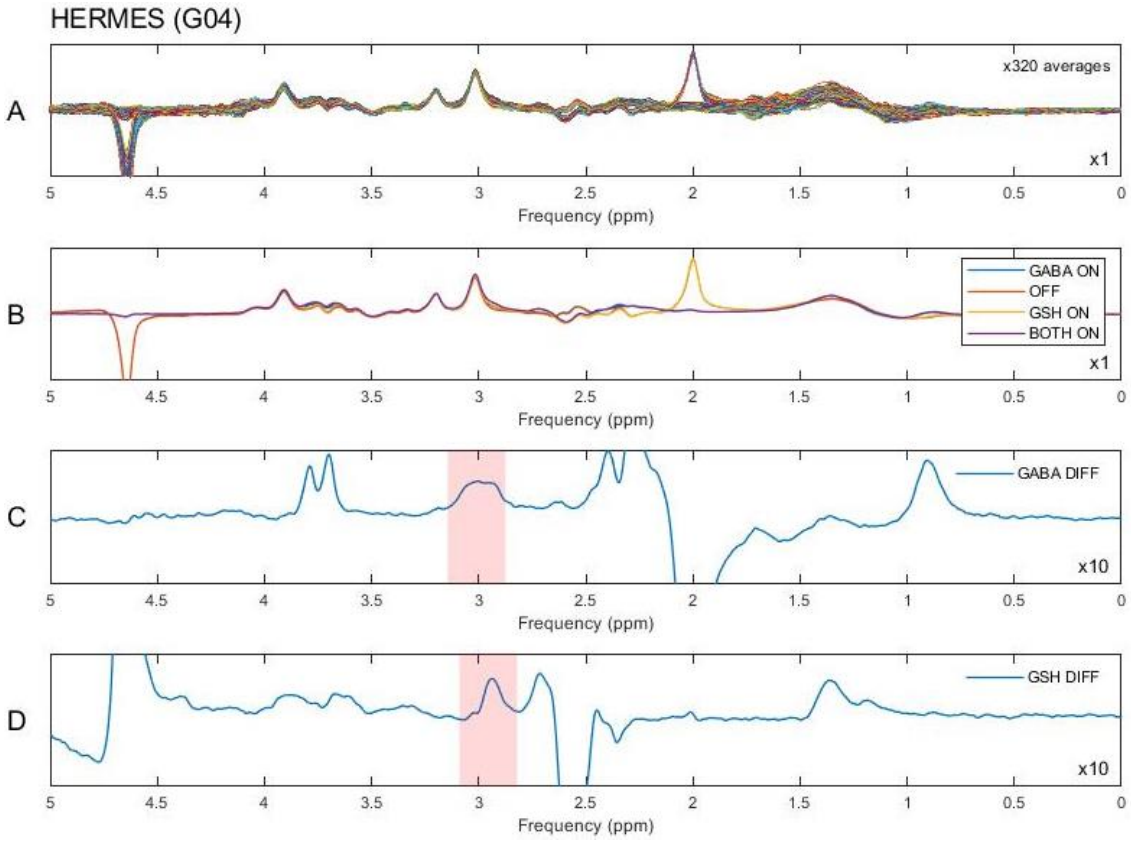

Figure 5-5 – Spectra from the HERMES acquisition in subject G04. A shows all 320 acquisitions, B the averaged spectra for each sub-experiment, C the Hadamard recombined spectrum for GABA, and D the Hadamard recombined spectrum for GSH. The GABA and GSH edited peaks are highlighted in C and D, respectively. The spectra in C and D were scaled to highlight the two edited peaks.

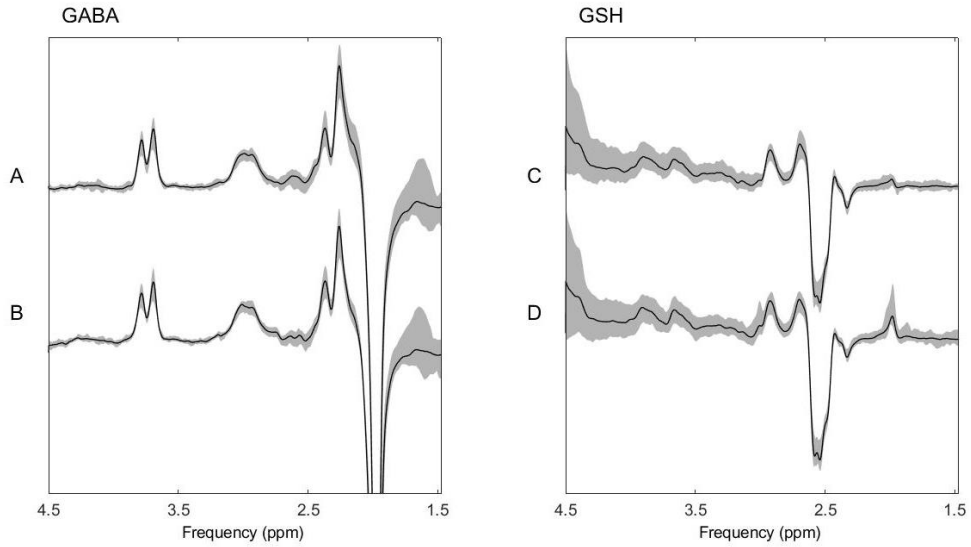

Figure 5-6 – GABA (left) and GSH (right) spectra from HERMES (A, C) and GABA- or GSH-edited MEGA-PRESS (B or D, respectively) averaged across all 15 participants. The grey shading shows the variance.

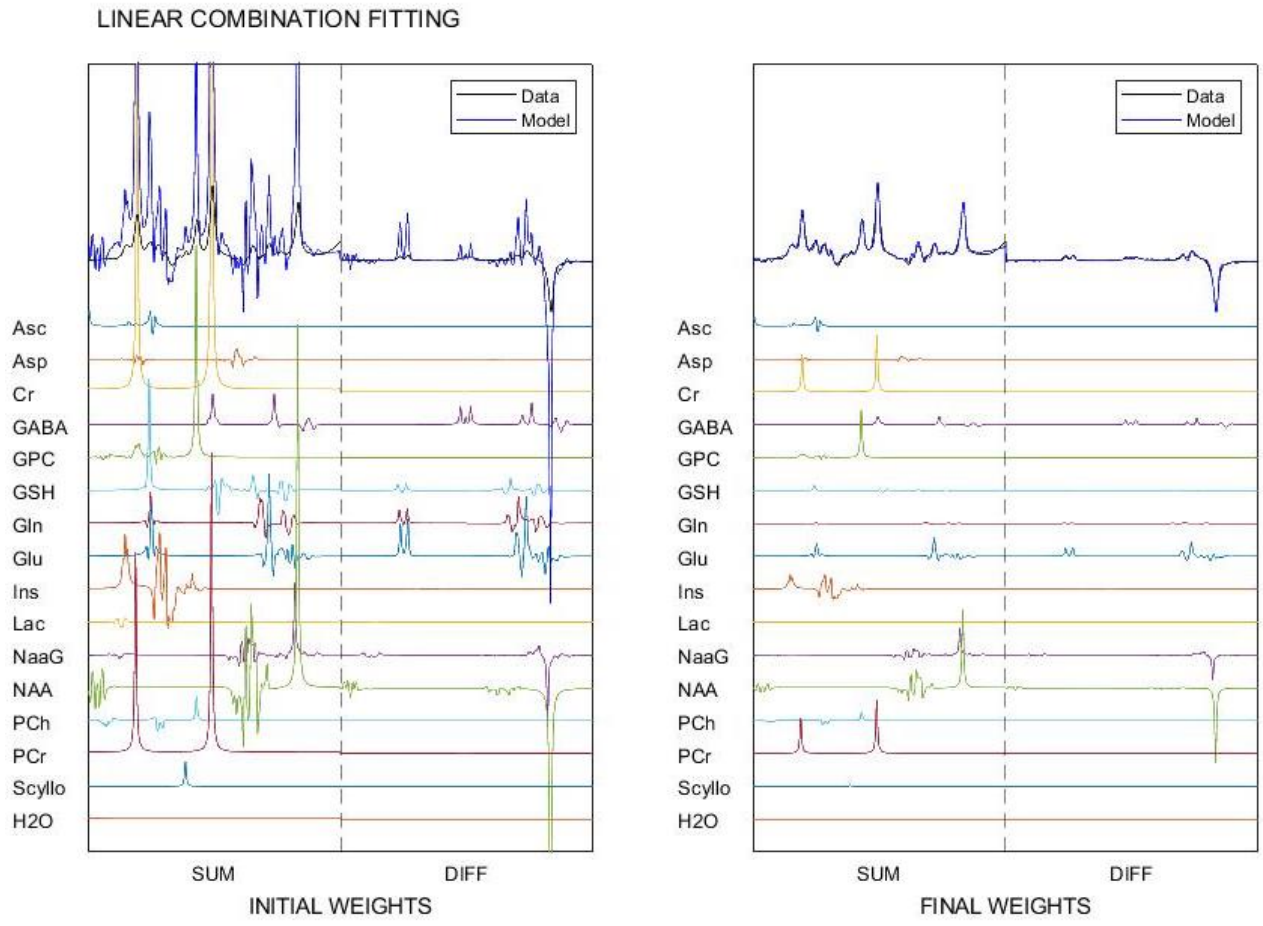

Figure 5-7 – Results from the linear combination fitting of GABA-edited MEGA-PRESS data acquired in subject G04. The initial parameter estimates (x0 in lsqcurvefit) are shown on the left, and the final parameter estimates on the right. The model spectrum was corrected with a baseline spline.

As described previously, HERMES data were first analysed using fitting to only two re-combinations, namely sum and either GSH (-A-B+C+D) or GABA (A-B-C+D) difference spectra, to allow direct comparison with MEGA-PRESS data that are also fit simultaneously to only two combinations (sum and difference). Table 5-2 compares metabolite levels obtained from MEGA-PRESS and HERMES data when using identical simultaneous two-combination fitting routines. Notably, mean concentrations across the 15 subjects obtained from HERMES and MEGA-PRESS data differed for about half the metabolites. Asc, GSH, NAAG, NAA, Scyllo, tCr, tCho, and tNAA levels did not differ significantly between GABA-edited MEGA-PRESS and HERMES, and for GSH-edited MEGA-PRESS and HERMES, levels of Ins, Lac, NAAG, NAA, Scyllo, tCr, and tNAA were similar.

Table 5-2 - Mean (and standard deviations) of absolute metabolite concentrations across 15 subjects. Fitting routine used only SUM and GABA- or GSH-difference spectra from both MEGA-PRESS and HERMES data. Since more than half the metabolites and fitting combination datasets had skewness greater than 2, the Mann-Whitney Test was used to compare means.

	GABA-edited MEGA-PRESS	HERMES (GABA-edited difference and SUM only)	Mann-Whitney Test p-value	GSH-edited MEGA-PRESS	HERMES (GSH-edited difference and SUM only)	Mann-Whitney Test p-value
	mean (stdev) (mmol/kg ww)	mean (stdev) (mmol/kg ww)		mean (stdev) (mmol/kg ww)	mean (stdev) (mmol/kg ww)	
Asc	1,9 (1,8)	2,7 (3,1)	0,803	3,3 (1,4)	1,7 (2,1)	**0,008**
Asp	1,9 (0,7)	0,6 (0,4)	**<0.001**	1,2 (0,6)	0,5 (0,4)	**<0.001**
GABA	5,5 (2,7)	4,2 (1,4)	**0,018**	0,0 (0,0)	4,0 (1,6)	**<0.001**
GSH	1,7 (1,2)	2,4 (1,0)	0,068	1,6 (0,5)	2,7 (0,9)	**<0.001**
Gln	1,9 (1,1)	1,1 (0,7)	**0,046**	0,1 (0,1)	1,0 (0,8)	**<0.001**
Glu	17,6 (7,5)	13,3 (4,7)	**0,001**	7,9 (1,6)	11,8 (4,4)	**<0.001**
Ins	13,0 (5,0)	10,4 (3,5)	**0,004**	9,2 (1,2)	10,2 (3,5)	0,481
Lac	0,0 (0,0)	0,0 (0,0)	**0,042**	0,0 (0,1)	0,0 (0,0)	0,32
NAAG	5,7 (1,8)	5,2 (1,8)	0,32	5,0 (0,9)	4,5 (1,6)	0,051
NAA	19,1 (7,4)	17,1 (6,0)	0,481	15,6 (2,9)	16,9 (5,9)	0,455
Scyllo	1,8 (2,6)	0,7 (1,0)	0,229	0,5 (0,7)	0,8 (1,1)	0,455
tCr	12,9 (4,9)	11,6 (3,7)	0,431	10,7 (1,6)	11,7 (3,7)	0,561
tCho	5,3 (2,4)	5,3 (1,8)	0,591	2,3 (0,5)	2,9 (0,7)	**0,013**
tNAA	24,8 (9,1)	22,2 (7,6)	0,300	20,5 (3,6)	21,4 (7,4)	0,678

* Bold denotes significance at p <0.05

Subsequently, HERMES data were quantified by fitting to all four Hadamard re-combinations. All least squares optimisations stopped due to convergence and iteration limits were not reached. Data from repeat scans were not included when calculating mean metabolite levels. Figure 5-8 shows in a single subject how metabolite levels obtained from HERMES data compare to those obtained from GABA- and GSH-edited MEGA-PRESS. Table 5-3 and Figure 5-9 compares mean metabolite levels across all 15 participants obtained from HERMES data using simultaneous fitting to four spectral re-combinations to metabolite levels obtained from simultaneous two-combination fitting of GABA- and GSH-edited MEGA-PRESS data, respectively. Except for Asc, GSH, Lac, and NAA (for which levels were similar), levels for all other metabolites obtained from HERMES data were significantly

lower than those from GABA-edited MEGA-PRESS. Levels from GSH-edited MEGA-PRESS and HERMES were similar for Ins, NAAG, NAA, Scyllo, tCr, tCho and tNAA, but differed for all other metabolites.

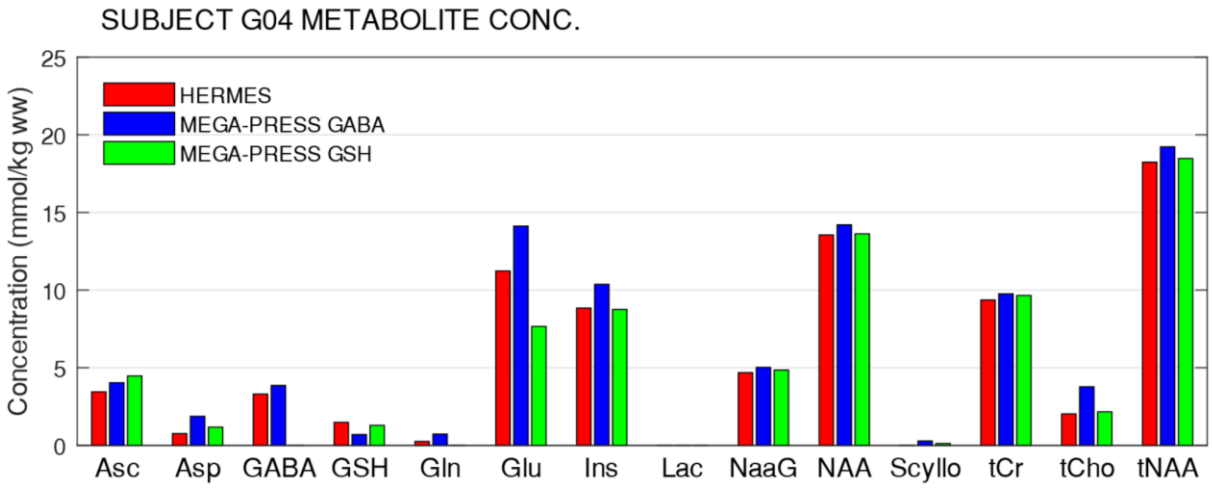

Figure 5-8 – Comparison of metabolite levels obtained in a single subject (G04) from simultaneous linear combination fitting of HERMES (red), GABA- (blue) and GSH-edited (green) MEGA-PRESS data.

Table 5-3 - Mean (and standard deviations) of absolute metabolite concentrations across 15 subjects. For HERMES data, the fitting routine used all four re-combination spectra (SUM, zero, GSH, and GABA). For MEGA-PRESS data, two re-combinations (SUM and difference) were used in the fitting routine. Since more than half the metabolites and fitting combination datasets had skewness greater than 2, the Mann-Whitney Test was used to compare means.

Metabolite	GABA-edited MEGA-PRESS	GSH-edited MEGA-PRESS	HERMES (simultaneous four recombination fitting)	p-values from Pairwise Comparisons using Mann-Whitney Test	
	mean (stdev) (mmol/kg ww)	mean (stdev) (mmol/kg ww)	mean (stdev) (mmol/kg ww)	GABA MEGA-PRESS vs. HERMES	GSH MEGA-PRESS vs. HERMES
Asc	1,9 (1,8)	3,3 (1,4)	2,2 (1,2)	0,678	**0,020**
Asp	1,9 (0,7)	1,2 (0,6)	0,6 (0,3)	**<0,001**	**0,001**
GABA	5,5 (2,7)	0,0 (0,0)	3,6 (0,6)	**<0,001**	**<0,001**
GSH	1,7 (1,2)	1,6 (0,5)	1,9 (0,6)	0,340	**0,028**
Gln	1,9 (1,1)	0,1 (0,1)	0,9 (0,4)	**0,002**	**<0,001**
Glu	17,6 (7,5)	7,9 (1,6)	11,6 (1,0)	**<0,001**	**<0,001**
Ins	13,0 (5,0)	9,2 (1,2)	8,8 (0,7)	**<0,001**	0,561
Lac	0,0 (0,0)	0,0 (0,1)	0,0 (0,0)	0,074	**0,034**
NAAG	5,7 (1,8)	5,0 (0,9)	4,4 (0,6)	**0,010**	0,074
NAA	19,1 (7,4)	15,6 (2,9)	15,0 (1,2)	0,106	0,901
Scyllo	1,8 (2,6)	0,5 (0,7)	0,3 (0,5)	**0,018**	0,407
tCr	12,9 (4,9)	10,7 (1,6)	10,1 (0,6)	**0,023**	0,089
tCho	5,3 (2,4)	2,3 (0,5)	2,2 (0,5)	**<0,001**	0,507
tNAA	24,8 (9,1)	20,5 (3,6)	19,3 (1,3)	**0,038**	0,340

* Bold denotes significance at p <0.05

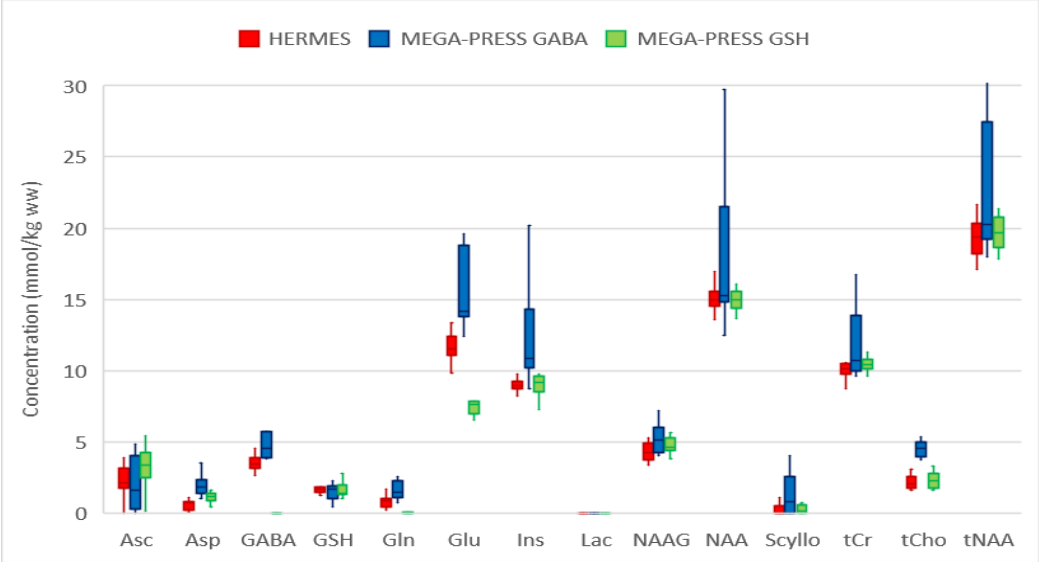

Figure 5-9 – Comparison of mean metabolite levels in 15 participants (not including data from repeat scans) obtained from linear combination fitting of HERMES (red), GABA- (blue) and GSH-edited (green) MEGA-PRESS data.

Despite absolute agreement being poor for most metabolites, levels from GABA-edited MEGA-PRESS and HERMES showed moderate correlation (Spearman correlation: 0.42 - 0.79) for all metabolites except three (Asp, Gln and Lac), and moderate consistency (ICC: 0.45 – 0.76) for all metabolites except 5 (Asp, Gln, Lac, Glu & Ins) (Table 5-4). For GSH-edited MEGA-PRESS and HERMES, correlation was moderate (>0.39) to strong (<0.94), and consistency moderate (ICC: 0.44 – 0.76), for all metabolites except GABA. Figure 5-10 shows how the coefficients of variation (CVs) across the 15 participants compared for each metabolite for the three different acquisitions.

Table 5-4 – Spearman's rank and Intraclass correlation coefficients (and p-value) of metabolite levels obtained from MEGA-PRESS and HERMES acquisitions in 15 subjects.

	GABA-edited MEGA-PRESS vs HERMES		GSH-edited MEGA-PRESS vs HERMES	
	Spearman's rank correlation coefficient (p-value)	Intraclass correlation coefficient (p-value)	Spearman's rank correlation coefficient (p-value)	Intraclass correlation coefficient (p-value)
Asc	**0,64 (0,013)**	**0,69 (0,004)**	**0,59 (0,022)**	**0,58 (0,022)**
Asp	0,17 (0,541)	0,24 (0,399)	**0,86 (<0.001)**	**0,76 (0,001)**
GABA	0,42 (0,119)	**0,69 (0,005)**	0,18 (0,524)	-0,10 (0,733)
GSH	**0,53 (0,044)**	**0,73 (0,002)**	0,49 (0,067)	**0,61 (0,016)**
Gln	0,27 (0,333)	0,10 (0,716)	**0,59 (0,022)**	**0,68 (0,005)**
Glu	0,50 (0,062)	0,15 (0,59)	**0,74 (0,003)**	**0,64 (0,011)**
Ins	0,51 (0,056)	0,28 (0,321)	**0,57 (0,029)**	0,44 (0,1)
Lac	-0,11 (0,705)	-0,11 (0,688)	0,39 (0,148)	**0,53 (0,041)**
NAAG	**0,74 (0,002)**	**0,61 (0,016)**	**0,83 (<0.001)**	**0,62 (0,015)**
NAA	**0,79 (0,001)**	0,48 (0,073)	**0,94 (<0.001)**	**0,75 (0,001)**
Scyllo	**0,58 (0,026)**	0,45 (0,09)	**0,55 (0,035)**	**0,69 (0,004)**
tCr	**0,75 (0,002)**	**0,76 (0,001)**	**0,81 (<0.001)**	**0,54 (0,04)**
tCho	**0,55 (0,038)**	0,48 (0,069)	**0,74 (0,003)**	**0,65 (0,009)**
tNAA	**0,78 (0,001)**	**0,62 (0,013)**	**0,93 (<0.001)**	**0,72 (0,002)**

* Bold denotes significance at p <0.05

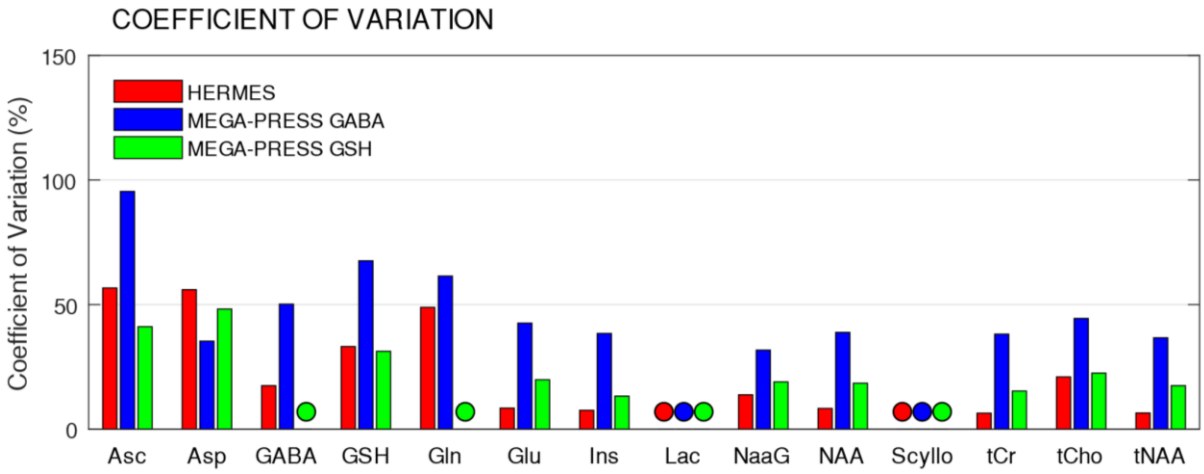

Figure 5-10 - Coefficients of variation (CVs) of the metabolite levels across the 15 subjects for each of the three acquisitions: HERMES, GABA-edited MEGA-PRESS, and GSH-edited MEGA-PRESS. Coloured dots are used where CVs are over 150%.

The metabolite concentrations obtained from the HERMES data had the lowest CVs for GABA, Gln, Glu, Ins, NAAG, NAA, tCr, tCho, and tNAA. Metabolite concentrations from GABA-edited MEGA-PRESS had the lowest CV for Asp, and GSH-edited MEGA-PRESS had the lowest CV for Asc and GSH.

5.3 Reproducibility

Figure 5-11 shows good agreement between metabolite levels obtained in three subjects from HERMES acquisitions in three different scanning sessions. Greater variance across scanning sessions were evident for metabolite levels obtained from GABA-edited MEGA-PRESS acquisitions in subjects G08 and G10 (Figure 5-12). Coefficients of variation within and across subjects are compared for 8 metabolites in Table 5-5 and Figure 5-13 for GABA- and GSH-edited MEGA-PRESS and HERMES acquisitions.

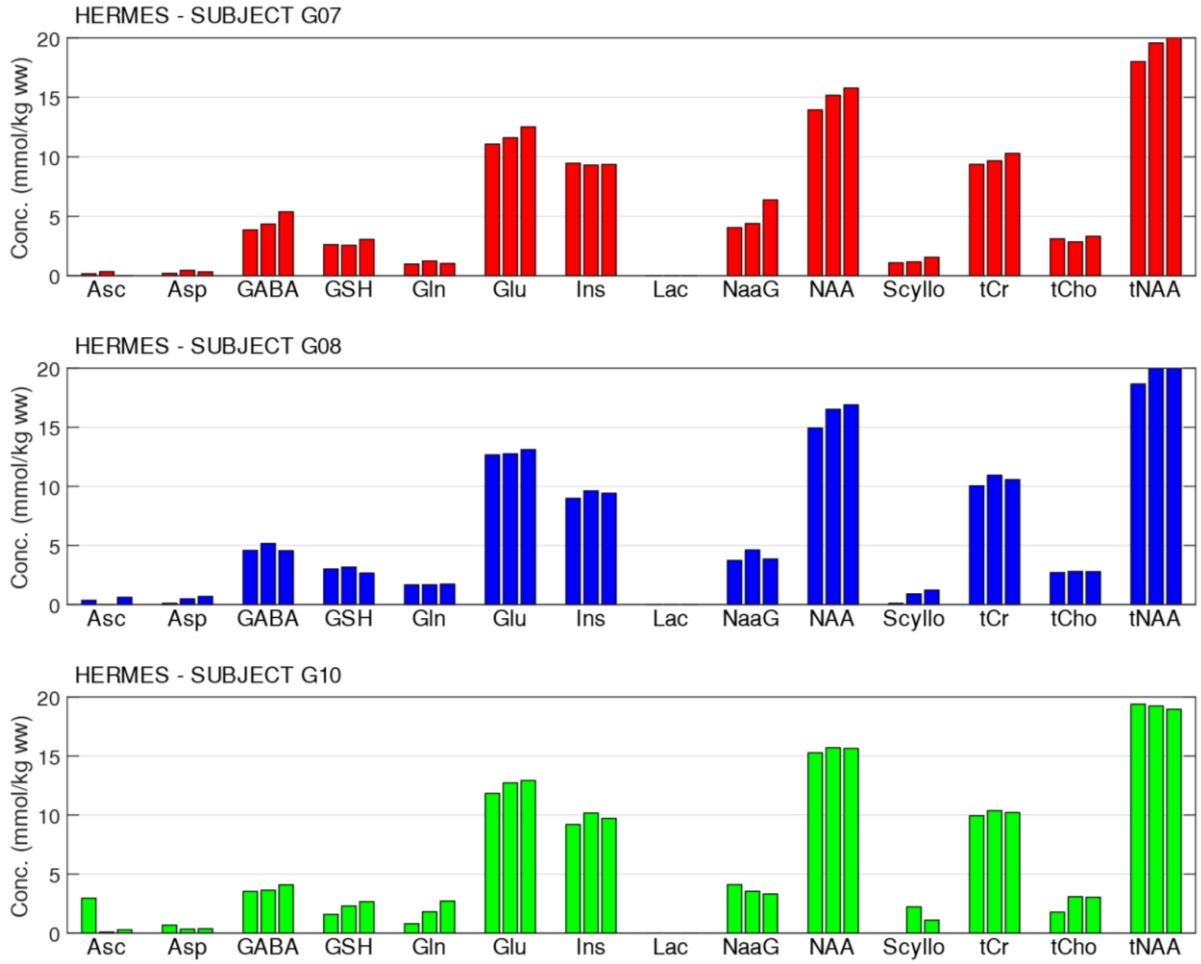

Figure 5-11 – Comparison in three subjects of metabolite concentrations obtained from HERMES acquisitions performed in three different scanning sessions.

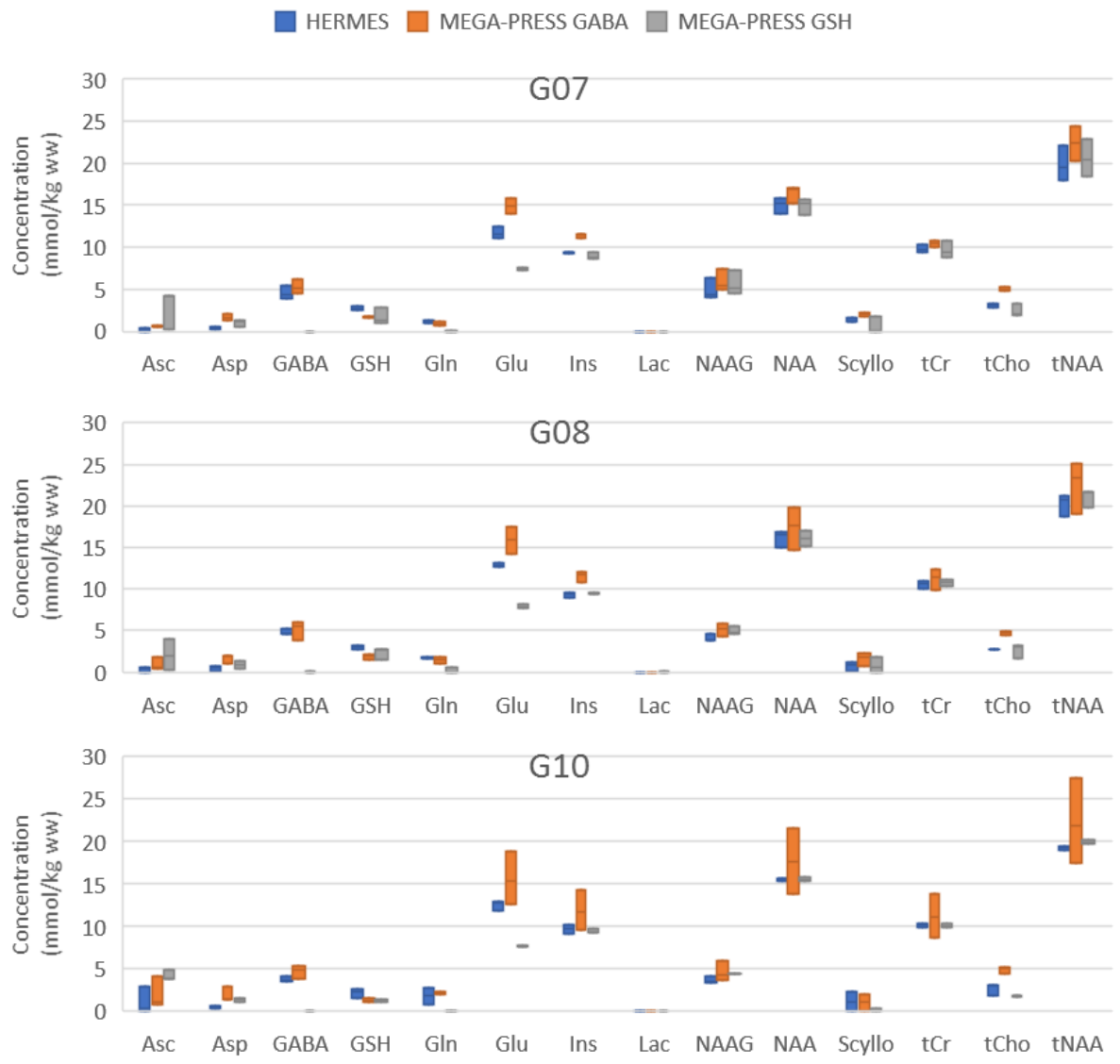

Figure 5-12 – Box and whisker plots for three subjects showing how metabolite levels vary across three scanning sessions for HERMES, and GABA- and GSH-edited MEGA-PRESS acquisitions, respectively.

Table 5-5 - Coefficients of variation within and across subjects of tNAA, tCr, tCho, Ins, Glu, Gln, GABA, and GSH levels obtained in three different scanning sessions from HERMES, GABA- and GSH-edited MEGA-PRESS acquisitions, respectively.

		Coefficients of variation of metabolite levels obtained with each sequence in 3 separate scanning sessions (%)							
Sequence	**Subject**	**tNAA**	**tCr**	**tCho**	**Ins**	**Glu**	**Gln**	**GABA**	**GSH**
HERMES	G07	10.6	4.7	6.5	1.1	6.0	10.8	17.1	10.4
	G08	6.5	4.4	2.1	3.3	1.6	0.0	7.2	8.5
	G10	1.3	2.5	27.5	5.2	4.7	53.8	8.6	25.3
	Across subjects	6.8	4.5	15.2	3.6	5.6	38.7	15.2	18.2
GABA-edited MEGA-PRESS	G07	9.6	3.5	5.0	2.0	6.0	24.7	16.1	3.3
	G08	13.8	11.3	5.4	5.3	10.4	30.7	20.8	22.3
	G10	22.5	23.3	7.4	19.8	1.5	9.5	17.4	24.1
	Across subjects	14.0	13.8	6.2	10.7	31.2	38.3	16.6	23.2
GSH-edited MEGA-PRESS	G07	10.9	10.6	34.4	5.5	2.1	undef	undef	61.4
	G08	4.9	3.3	30.9	1.1	2.9	undef	undef	28.9
	G10	1.3	2.0	3.1	2.4	1.5	undef	undef	16.7
	Across subjects	6.5	7.2	29.2	4.2	3.4	undef	undef	46.5

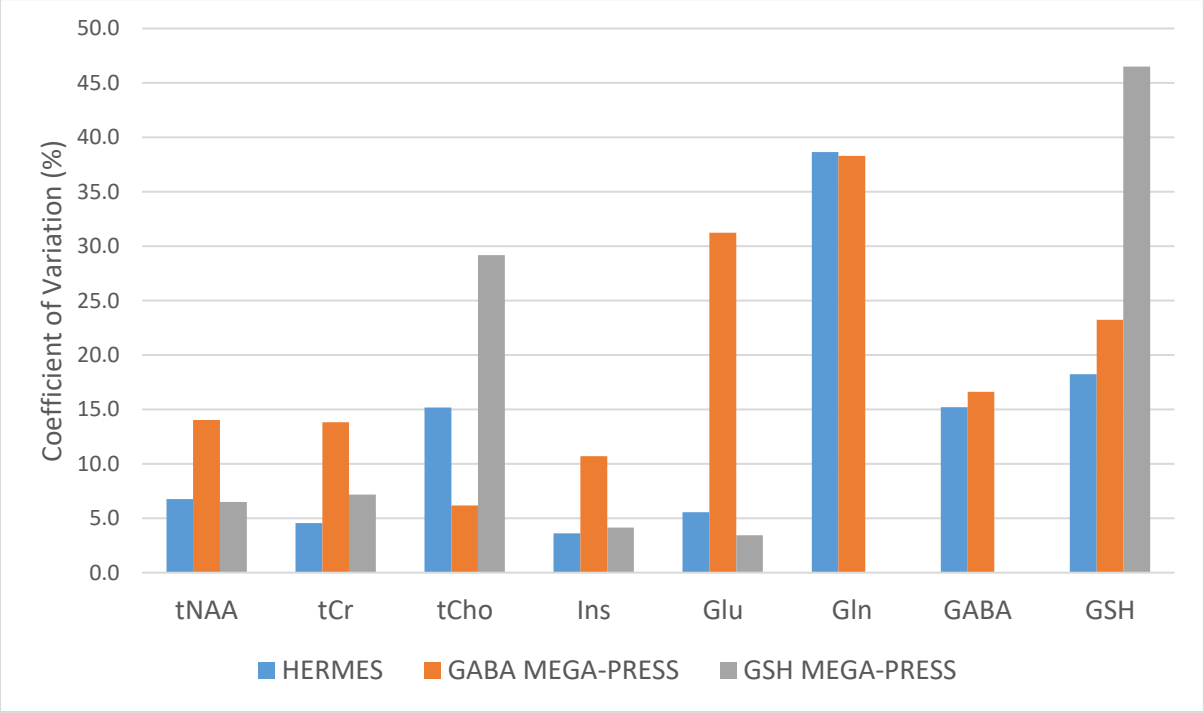

Figure 5-13 – Comparison for different metabolites of coefficients of variation across subjects and scanning sessions for HERMES, and GABA- and GSH-edited MEGA-PRESS acquisitions.

5.4 Comparison of simultaneous and multiple independent fittings

Figure 5-14 demonstrates the four fitting algorithms that are being compared, namely simultaneous fitting to concatenated sum, GSH, GABA and zero spectra (top row), or separate fittings to either the SUM, GSH difference or GABA difference spectra, respectively. Table 5-6 shows metabolite ratios relative to total creatine estimated using each of the different fitting routines from HERCULES data acquired in 10 subjects in two voxels – one white matter (WM) rich voxel in the centrum semiovale and one grey matter (GM) rich voxel positioned over the cingulate cortex. Figures 5-15 and Figure 5-16 are box and whisker plots showing the metabolite levels obtained using each fitting approach for the grey- and white matter rich voxels, respectively. Figures 5-17 and 5-18 show the coefficients of variation of the metabolite levels for each fitting approach in the grey matter and white matter rich voxels, respectively.

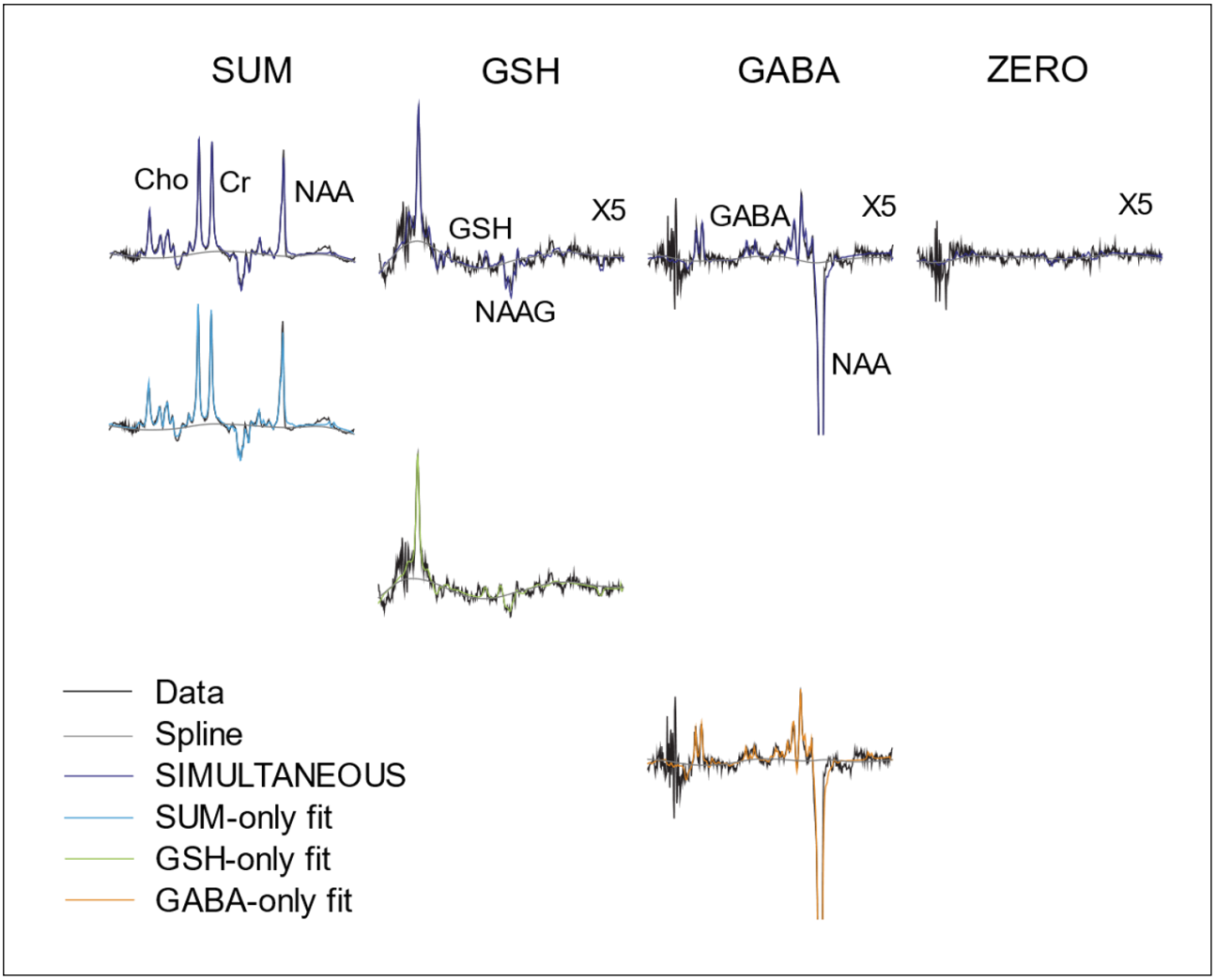

Figure 5-14 – Illustration of simultaneous fitting versus multiple independent fittings of HERCULES data.

Table 5-6 - Mean metabolite concentration values relative to tCr for a grey matter rich (Cingulate Cortex) voxel (top) and a white matter rich (Centrum Semiovale) voxel (bottom) are shown. The last column shows ANOVA p values with values less than 0.05 highlighted in green. Since fewer than 15% of the datasets had skewness above or below 2 or -2, Analysis of Variance (ANOVA) was used.

Metabolite	Simultaneous spectra fit (Stdev)	SUM spectrum fit (Stdev)	GABA spectrum fit (Stdev)	GSH spectrum fit (Stdev)	ANOVA p-value
Grey Matter rich voxel (Cigulate Cortex)					
Asc	0.07 (0.12)	0.01 (0.04)	2.53 (1.96)	0.13 (0.19)	**<0,001**
Asp	0.10 (0.04)	0.04 (0.06)	0.78 (0.61)	0.34 (0.22)	**<0,001**
GABA	0.31 (0.06)	0.34 (0.06)	0.31 (0.29)	0.07 (0.03)	**0,001**
GSH	0.25 (0.02)	0.26 (0.04)	0.20 (0.16)	0.11 (0.09)	**0,005**
Gln	0.15 (0.05)	0.20 (0.07)	0.17 (0.13)	0.20 (0.53)	0,973
Glu	1.19 (0.10)	1.08 (0.18)	1.28 (1.02)	0.67 (1.17)	0,332
Ins	0.91 (0.08)	0.87 (0.08)	3.13 (3.94)	1.37 (1.15)	0,060
Lac	0.20 (0.12)	0.40 (0.25)	0.83 (1.96)	0.11 (0.10)	0,379
NAAG	0.26 (0.08)	0.30 (0.10)	0.24 (0.18)	0.19 (0.11)	0,246
NAA	1.57 (0.13)	1.47 (0.15)	1.92 (1.10)	1.49 (0.84)	0,462
Scyllo	0.19 (0.14)	0.15 (0.13)	16.70 (47.5)	34.9 (34.8)	**0,037**
tCho	0.36 (0.09)	0.41 (0.13)	1.78 (1.42)	0.23 (0.18)	**<0,001**
tNAA	1.83 (0.10)	1.77 (0.13)	2.15 (1.21)	1.68 (0.91)	0,534
White Matter rich voxel (Centrum Semiovale)					
Asc	0.07 (0.11)	0.05 (0.12)	1.38 (1.36)	0.11 (0.18)	**<0,001**
Asp	0.04 (0.05)	0.07 (0.12)	0.72 (0.76)	0.25 (0.23)	**0,002**
GABA	0.27 (0.03)	0.37 (0.06)	0.22 (0.19)	0.08 (0.04)	**<0,001**
GSH	0.22 (0.04)	0.22 (0.05)	0.16 (0.15)	0.44 (0.70)	0,329
Gln	0.18 (0.06)	0.30 (0.16)	0.18 (0.17)	0.79 (1.41)	0,193
Glu	1.01 (0.24)	0.98 (0.27)	1.00 (0.91)	0.77 (1.53)	0,928
Ins	0.81 (0.16)	0.79 (0.15)	3.72 (4.00)	0.77 (0.55)	**0,004**
Lac	0.10 (0.03)	0.18 (0.09)	0.15 (0.31)	0.07 (0.05)	0,485
NAAG	0.60 (0.13)	0.59 (0.13)	0.56 (0.25)	0.49 (0.32)	0,698
NAA	1.67 (0.12)	1.58 (0.13)	1.99 (1.61)	1.79 (1.89)	0,896
Scyllo	0.22 (0.22)	0.20 (0.25)	22.7 (50.6)	5.74 (7.30)	0,175
tCho	0.47 (0.10)	0.49 (0.12)	3.39 (5.34)	0.27 (0.21)	**0,038**
tNAA	2.27 (0.16)	2.17 (0.15)	2.55 (1.82)	2.28 (2.17)	0,942

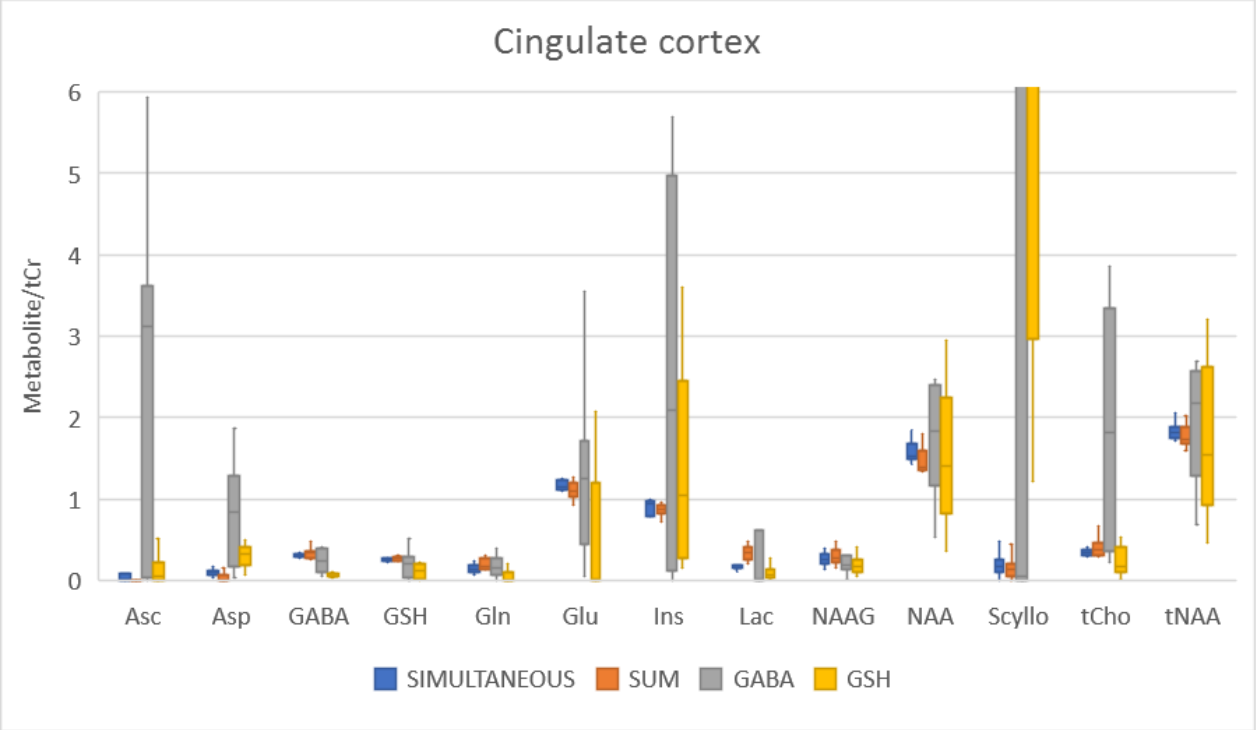

Figure 5-15 – Metabolite concentrations relative to total creatine in 10 subjects from HERCULES data in a grey matter rich voxel (cingulate cortex). Plot compares quantification by fitting all data simultaneously, and fitting to just the SUM, GABA or GSH re-combinations, respectively.

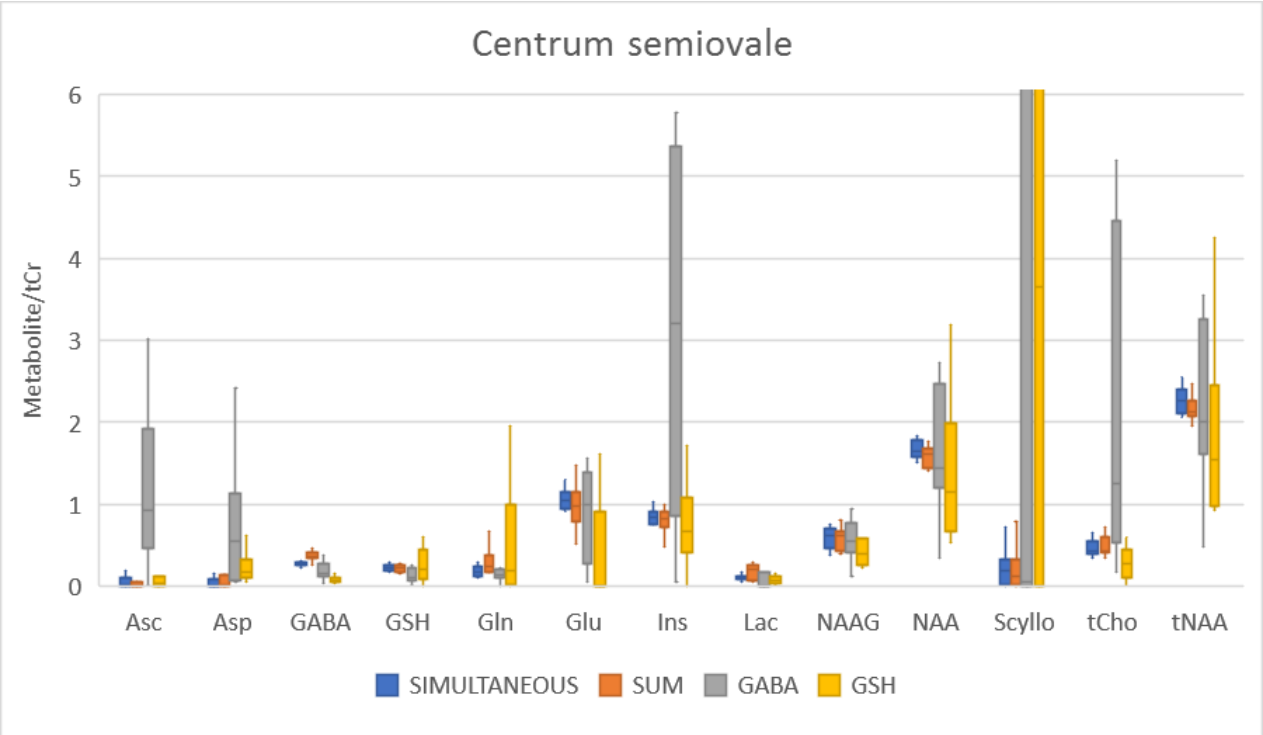

Figure 5-16 - Metabolite concentrations relative to total creatine in 10 subjects from HERCULES data in a white matter rich voxel (centrum semiovale). Plot compares quantification by fitting all data simultaneously, and fitting to just SUM, GABA or GSH re-combinations, respectively.

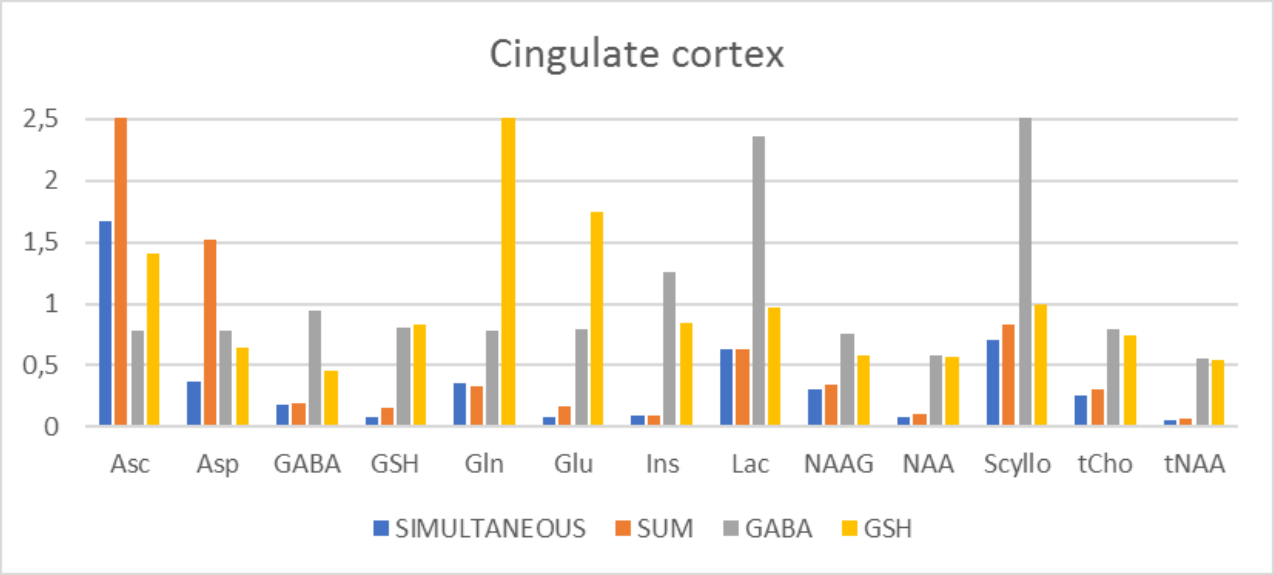

Figure 5-17 – Comparison of coefficients of variation of metabolite ratios relative to total creatine in a grey matter rich voxel (cingulate cortex) in 10 subjects obtained from simultaneous modelling of the HERUCLES data, and separate modelling to SUM, GABA, or GSH difference spectra.

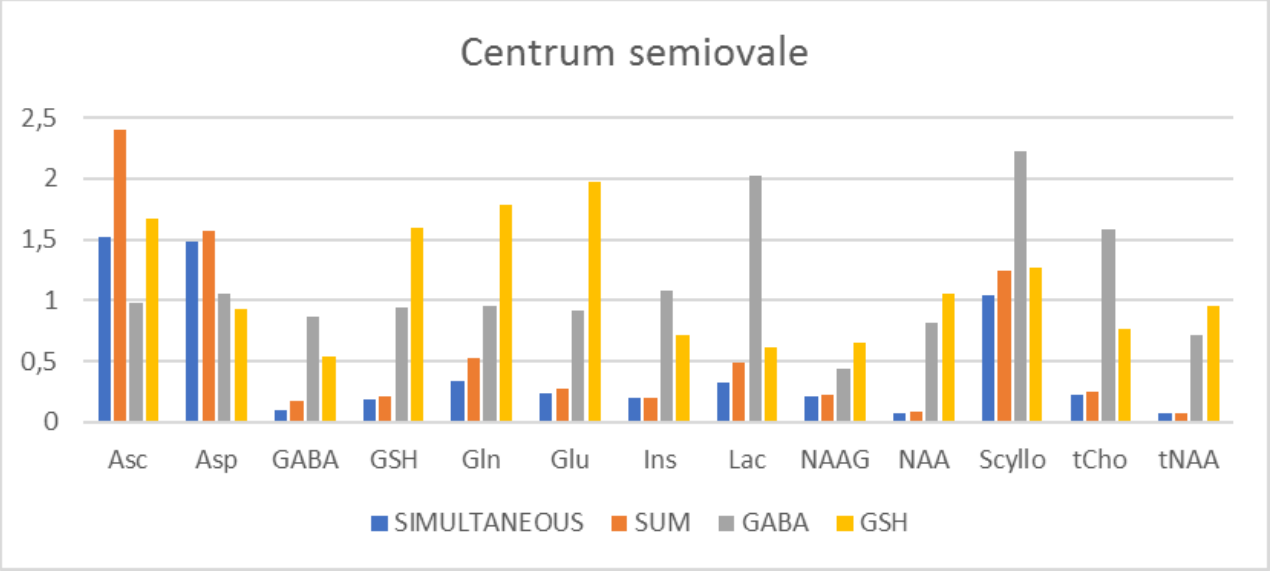

Figure 5-18 - Comparison of coefficients of variation of metabolite ratios relative to total creatine in a white matter rich voxel (centrum semiovale) in 10 subjects obtained from simultaneous modelling of the HERUCLES data, and separate modelling to SUM, GABA, or GSH difference spectra.

6 Discussion

6.1 HERMES Sequence Implementation

A feature of the current HERMES implementation, is the ability to acquire MEGA-PRESS data by de-selecting the check-box for a second editing pulse in the 'special' card on the user interface. This MEGA-PRESS acquisition differs from the standard Siemens WIP in that it uses standardised RF pulse shapes and altered sequence timing (similar to that of the Philips HERMES implementation), thereby facilitating direct comparison of HERMES and MEGA-PRESS data, as well as between vendor platforms.

Phantom Testing

Phantom testing demonstrated that HERMES and the two (GABA- and GSH-edited) MEGA-PRESS acquisitions are able to accurately quantify total NAA. HERMES provided the most reliable estimate of total choline, with levels from GABA- and GSH-edited MEGA-PRESS being too high by about 25% and 12%, respectively. Data from all three acquisitions underestimated creatine levels by roughly 25% and failed to accurately quantify GABA or GSH levels, which were more than 50% lower than actual levels. Additionally, GABA-edited MEGA-PRESS incorrectly detected low levels of Asc, Ins and Scyllo, while HERMES and GSH-edited MEGA-PRESS incorrectly detected low levels of Asc only.

The low levels of GABA and GSH may, in part, be due to poor editing efficiency resulting from temperature-related frequency shifts as the phantoms were at 5 degree Celsius when scanned. Editing efficiency refers to the percentage of signal that is correctly inverted in the difference spectra. Any temperature-related frequency shift would cause the coupled spin systems to not be completely inverted. Poor editing efficiency can be accounted for retrospectively by measuring the frequency shift and calculating the loss of editing efficiency from the pulse profile. The editing efficiency for a 5 Hz shift would, for example, be roughly 50% (Figure 4-6). Prospective correction is also possible by shifting the frequency of the editing pulses before acquisition, following an initial unedited calibration scan (PRESS SVS) to determine the frequency shift. Since prospective adjustment will not correct for efficiency loss due to field inhomogeneity and drift, retrospective scaling adjustment should still be performed. The absence of editing efficiency correction in the present work may contribute to underestimation of GABA and GSH levels.

Despite absolute agreement of GABA and GSH levels being poor, line shapes of the GABA- and GSH-difference spectra obtained from HERMES and MEGA-PRESS acquisitions were comparable and features from the relevant basis spectra were clearly visible, albeit shifted by roughly 0.2 ppm to the right. This shift is presumably also due to the phantom being at lower temperature than *in vivo* tissue. Although LCModel allows for each individual metabolite basis spectrum to be shifted independently, our simultaneous linear combination fitting routine that only applies a single shift to all the basis spectra yielded good fits and signal isolation.

In vivo Testing

In vivo data demonstrated successful GABA and GSH editing with both the MEGA-PRESS and HERMES sequences (Figures 5-3 to 5-6), and comparable line shapes across 15 participants. Consistent with other *in vivo* studies, we observe a single rounded peak in the GABA difference spectra at 3 ppm rather than the 'pseudo doublet' seen on simulations and phantom data (Mikkelsen et al. 2017), while the co-edited Glx doublet peaks of glutamine and glutathione are evident at 3.75 ppm. Overall, our GABA difference spectra from both the HERMES and MEGA-PRESS acquisitions closely match typical GE and Philips GABA spectra (Mikkelsen et al. 2017), while the characteristic 'bump' normally seen in Siemens MEGA-PRESS data to the left of the GABA peak at 3 ppm (Mikkelsen et al. 2017) is less visible, indicating that its origin may be the RF pulse shape and timing used in the Siemens WIP rather than being hardware-related. The very large negative peak at 1.9 ppm observed in both the HERMES and MEGA-PRESS spectra is caused directly by the editing pulse rather than through coupling as with

the 3 ppm peak. The intensity range shown by the grey shading was generated from the maximum and minimum intensities at each frequency across subjects. The large intensity variation seen at and to the right of the negative peak at 1.9 ppm may be due to field drift, causing the centre frequency and bandwidth of the editing pulse to shift thereby creating subtraction differences between acquisitions.

With regards the GSH difference spectra in Figure 5-6, MEGA-PRESS shows a more pronounced peak at 2 ppm than HERMES data. This peak could either be a subtraction artefact from the NAA signal, or a co-edited GABA signal from the 2.283 or 1.889 ppm GABA peaks. However, the latter is unlikely, since those two peaks are coupled to the 1.889 and 3.012 ppm spins, respectively, neither of which will be edited by the 4.56 ppm editing pulse applied in the GSH-edited MEGA-PRESS sequence. Additionally, this peak is located closer to 2 ppm and shows substantial inter-subject variation, indicating that it is more likely an NAA subtraction artefact. It is not clear why this peak is more pronounced in MEGA-PRESS than HERMES data. Notably, the GSH edited peak at 2.995 ppm appears similarly in the MEGA-PRESS and HERMES GSH difference spectra. Another noteworthy feature is that the inter-subject variance of the GSH difference spectra (for both HERMES and MEGA-PRESS) is greater than the variance observed in the GABA difference spectra. This is particularly noticeable at frequencies above 3 ppm (left of the 3 ppm GSH peak), and may, in part, be due to subtraction artefacts from the editing pulse at 4.56 ppm (similar to the variance observed around the 1.9 ppm editing pulse frequency in the GABA difference spectra). Another contributing factor may be sidebands resulting from incomplete water suppression as shown in Figure 2-7 (de Graaf 2007). Since the editing pulses applied in the edit-ON measurements may have a water suppression effect, a greater portion of the variance observed in the difference spectra is likely from the edit-OFF measurements.

Using simultaneous fitting to *two* re-combinations for MEGA-PRESS and HERMES data, quantification values from GABA-edited spectra differed for 6 of 14 metabolites, and for 7 of 14 metabolites for GSH-edited spectra. Simultaneous fitting to *four* re-combinations for HERMES yielded quantification values that were significantly different from GABA-edited MEGA-PRESS levels for 10 of 14 metabolites, and from GSH-edited MEGA-PRESS levels for 7 of 14 metabolites. Notably, GABA levels from GABA-edited MEGA-PRESS and HERMES differed significantly, as well as GSH levels from GSH-edited MEGA-PRESS and HERMES. These findings suggest that four re-combination fitting does not improve quantification agreement between MEGA-PRESS and HERMES data. A limitation of the current study is that we do not have actual metabolite levels to determine which method is most accurate. At most, we are able to conclude that the three acquisitions yield largely different results, irrespective of the fitting routine. Four re-combination fitting of HERMES data did, however, yield lower CVs across 15 subjects than the two MEGA-PRESS acquisitions for 9 of 14 metabolites, suggesting that this method might be most reliable.

In a study with GABA MEGA-PRESS data from 25 research sites and a total of 284 volunteers the cohort wide coefficient of variation for GABA+ was 10%, and for macromolecule suppressed quantification it was 29% (Mikkelsen et al. 2018). The term GABA+ refers to GABA quantification where macromolecule suppression has not been applied (as is the case in the present study also). Comparatively this research found CV values of 50% and 17% for GABA(+) using MEGA-PRESS and HERMES, respectively.

Concentrations of tNAA and tCr in the brain typically range from 10.9 – 13 and 5.1 – 10.6 mmols/kg_{ww}, respectively, while the tCho concentration in the brain is roughly 1.6 mmols/kg_{ww} (Govindaraju et al. 2000). Across all participants, all three our acquisitions yielded substantially higher levels for tNAA and tCho, and levels of tCr at the upper limit. Levels obtained for Asc and Ins from all three acquisitions were higher than typical *in vivo* concentrations (see Table 4-2), while only levels from GABA-edited MEGA-PRESS were higher than typical concentrations for Asp, Glu and Scyllo. All three sequences yielded Gln and Lac levels that were lower than typical brain concentrations.

Of specific relevance to this work is the accuracy of the edited GABA and GSH concentration estimates. Typical GABA and GSH concentrations in the brain are 1.3 – 1.9 and 2 mmols/kg_{ww}, respectively. HERMES and GABA-edited MEGA-PRESS yielded GABA levels that were roughly two and three times higher, respectively, while GSH-edited MEGA-PRESS and HERMES both yielded GSH levels similar to the expected value.

Despite absolute agreement being poor, the fact that metabolite levels from the different acquisitions were moderately correlated increases confidence that one might be able to distinguish group differences in study populations.

GABA-edited MEGA-PRESS demonstrated poorer reproducibility than GSH-edited MEGA-PRESS and HERMES across scanning sessions in two of three participants who each completed three scanning sessions. Across scanning sessions and participants, CVs from HERMES were lowest for 4 of the 8 metabolites that were compared (tCr, Ins, GABA and GSH). Within-subject CVs for GABA ranged from 7.2 to 17.1%, and from 8.5 to 25.3% for GSH. GABA-edited MEGA-PRESS yielded the lowest CVs for tCho and Gln, and GSH-edited MEGA-PRESS for tNAA and Glu. Although GABA MEGA-PRESS had the highest CVs for 4 of the 8 metabolites (tNAA, tCr, Ins and Glu), CVs for Gln, GABA and GSH were similar to those from HERMES. Specifically, within-subject CVs for GABA from GABA-edited MEGA-PRESS ranged from 16.1 to 20.8%, and for GSH from 3.3 to 24.1%. Within-subject CVs of GSH from GSH-edited MEGA-PRESS ranged from 16.7 - 61.4%. Notably, Gln and GABA levels were undetectable on the GSH-edited MEGA-PRESS data, yielding undefined CVs. CVs for GABA from our HERMES and GABA MEGA-PRESS acquisitions were of the same order as reproducibilities reported in the 11 studies summarised in Table 3-1, where test-retest CVs for GABA from GABA MEGA-PRESS ranged from 0.2 to 16.2%. Using universal pulses, Saleh et al. (2019) reported within-subject CVs for GABA across different scanners of 3% using both MEGA-PRESS and HERMES. For GSH, Wijtenburg et al. (2019) reported CVs between two scanning sessions using MEGA-PRESS of 13.5%, while CVs using PRESS, PR-STEAM and SPECIAL were lower at 5.8%, 5.4% and 8%, respectively. In 2 of 3 subjects, CVs for GSH using HERMES were comparable, and in 1 of 3 subjects using GABA MEGA-PRESS. All other acquisitions yielded higher within-subject CVs for GSH.

6.2 Simultaneous Modelling Technique

Concentrations relative to tCr from simultaneous and three separate independent fittings agreed for 7 of 13 metabolites in a grey matter rich voxel, and 8 of 13 metabolites in a white matter rich voxel. In the grey matter rich voxel, the simultaneous fitting routine yielded the lowest CVs for all metabolites except Asc and Gln, with the CV for Gln being comparable to the lowest CV obtained from fitting to the SUM spectrum only. In the white matter rich voxel, CVs from simultaneous fitting were lowest for all metabolites except Asc and Asp. These findings support that simultaneous fitting to the sum and difference spectra improves the accuracy of metabolite quantification.

6.3 Limitations

The fitting routine failed to correct frequency shifts that may have affected editing efficiency. Inclusion of this may have improved quantification accuracy, specifically for GABA and GSH, which would be most severely impacted by such shifts. The basis sets also did not include spectra for macromolecule signal.

The fact that no standard Siemens MEGA-PRESS WIP data were acquired also limits our ability to compare our results with findings from other studies, and performance of the newly implemented sequence with the current standard.

Finally, acquisitions were always performed in the same order, namely GABA-edited MEGA-PRESS, followed by GSH-edited MEGA-PRESS, and finally, HERMES, which is not ideal. Failure to randomise the order of acquisitions could have resulted in systematic drift due to heating of the gradient coils and fatigue-related increases in subject motion towards the end of the scanning session. Although MRS is not gradient intensive and as such would likely not itself cause gradient coil heating, the T1 scan performed prior to the MRS acquisitions is gradient intensive and may have resulted in slight temperature-related frequency drifts. Any frequency shifts would result in reduced editing efficiency.

7 Conclusions and Recommendations for Future Work

Although the HERMES sequence implemented on the Siemens platform as part of this project was able to successfully edit both GABA and GSH, and generate line shapes consistent with the work by Saleh *et al.* (Saleh et al. 2016), quantification accuracy was disappointing. In the phantom data, GSH and GABA concentrations were both roughly 50% of known levels. Since the actual concentrations *in vivo* were not known, we were not able to establish accuracy, but quantification agreement between the MEGA-PRESS and HERMES sequences was poor for most metabolites. Specifically, GABA levels were two to three times higher than expected values using both HERMES and GABA-edited MEGA-PRESS. Despite poor absolute agreement, concentrations from HERMES and MEGA-PRESS data were moderately correlated, and HERMES data showed lower coefficients of variation across subjects, suggesting that it may be more reliable. HERMES was also more reproducible across scanning sessions and participants for more metabolites than GABA- or GSH-edited MEGA-PRESS.

Our findings also show that simultaneous fitting using the sum and difference spectra produces lower coefficients of variation for most metabolites than fittings to sum and difference spectra separately.

Future work might include:

- Implementing HERMES (or other multiplexed edited spectroscopy sequences) on a cross platform development tool. This would help with standardisation and quick implementation between the scanners particularly as HERMES is improved.
- Data acquisition from the same healthy subjects at different research sites with different scanner manufacturers. This would be the best way to compare the results from two scanners as physiological changes in metabolite levels of the same subject would be negligible.
- Standardising the water suppression technique used on the Philips and Siemens implementations. The water suppression technique was not altered for this project and simply used the vendor native technique.
- Corrections for editing efficiency should be incorporated into the fitting routine. This may improve the absolute quantification of the edited signals of GABA and GSH.
- The basis sets should be simulated at more than a single point in the middle of the voxel. This will increase computational demands of the simulations.
- Alternative modelling algorithms for the data processing technique should be considered. Least squares optimisation was not robust and required very careful handling of data in particular when switching between phantom and *in vivo* data.
- The data processing technique could also undergo calibration using a more extensive set of phantom tests. This methodology would need to be carefully designed to make the code applicable to *in vivo* data.
- Deep learning may be a strong candidate for consideration in future data processing techniques given the move to simultaneously considering more of the data. This data could ultimately be given to the deep learning algorithm in a less processed form, which would reduce the risk that the underlying signal is being modified in the pre-processing steps.
- And finally, it is recommended that multiplexed editing sequences further differentiate the signal evolution by adding more sub-experiments that feature different editing pulses. These pulses could still be Hadamard encoded as a Hadamard matrix is defined for any arbitrary square matrix size. But it is the opinion of the author that even linearly spaced editing pulses varied from one acquisition to the next would improve signal isolation. The upper limit of this is the number of averages i.e. 320 different sub-experiments with different editing pulses.

References

Banerjee, A. & Chandrakumar, N., 2014. Volume localized spin echo correlation spectroscopy with suppression of ‘ diagonal ’ peaks. *Journal of Magnetic Resonance*, 239, pp.69–74. Available at: http://dx.doi.org/10.1016/j.jmr.2013.12.001.

Blüml, S. & Panigrahy, A., 2013. MR spectroscopy of pediatric brain disorders. *MR Spectroscopy of Pediatric Brain Disorders*, pp.1–401.

Bogner, W. et al., 2010. In vivo quantification of intracerebral GABA by single-voxel 1 H-MRS — How reproducible are the results ? &. *European Journal of Radiology*, 73(3), pp.526–531. Available at: http://dx.doi.org/10.1016/j.ejrad.2009.01.014.

Bottomley, P.A., 1987. Spatial Localization in NMR Spectroscopy in Vivo. *Annals of the New York Academy of Sciences*, 508(1), pp.333–348.

Chan, K.L. et al., 2016. HERMES: Hadamard encoding and reconstruction of MEGA-edited spectroscopy. *Magnetic Resonance in Medicine*, 76(1), pp.11–19.

Edden, R.A.E. et al., 2014. Gannet: A Batch-Processing Tool for the Quantitative Analysis of Gamma-Aminobutyric Acid – Edited MR Spectroscopy Spectra. *Journal of Magnetic Resonance Imaging*, 1452, pp.1445–1452.

Edden, R.A.E. & Barker, P.B., 2007. Spatial Effects in the Detection of gamma-Aminobutyric Acid: Improved Sensitivity at High Fields Using Inner Volume Saturation. *Magnetic Resonance in Medicine*, 1282(December 2006), pp.1276–1282.

Ernst, T. & Hennig, J., 1995. Improved Water Suppression for Localized in Vivo1H Spectroscopy. *Journal of Magnetic Resonance, Series B*, 106(2), pp.181–186.

Evans, C.J., Mcgonigle, D.J. & Edden, R., 2010. Diurnal Stability of g -aminobutyric Acid Concentration in Visual and Sensorimotor Cortex. *Journal of Magnetic Resonance Imaging*, 209, pp.204–209.

Ford, T.C. & Crewther, D.P., 2016. A Comprehensive Review of the 1H-MRS Metabolite Spectrum in Autism Spectrum Disorder.(Report)(Author abstract). *Frontiers in Molecular Neuroscience*.

Frahm, J., Merboldt, K.-D. & Hanicke, W., 1987. Localized proton spectroscopy using stimulated echoes. *Journal of Magnetic Resonance*, 72(3), pp.502–508.

Fuchs, A. et al., 2013. SPECIAL Semi-LASER with Lipid Artifact Compensation for 1 H MRS at 7 T. *Magnetic Resonance in Medicine*, 612, pp.603–612.

Gaetz, W. et al., 2014. GABA estimation in the brains of children on the autism spectrum : Measurement precision and regional cortical variation. *NeuroImage*, 86, pp.1–9. Available at: http://dx.doi.org/10.1016/j.neuroimage.2013.05.068.

Garwood, M. & Delabarre, L., 2001. The Return of the Frequency Sweep : Designing Adiabatic Pulses for Contemporary NMR. *Journal of Magnetic Resonance*, 177, pp.155–177.

Geramita, M. et al., 2011. Reproducibility of prefrontal g -aminobutyric acid measurements with J -edited spectroscopy y. *NMR in Biomedicine*, (November 2010), pp.1089–1098.

Govindaraju, V., Young, K. & Maudsley, A.A., 2000. Proton NMR chemical shifts and coupling constants for brain metabolites. *NBM NMR in Biomedicine*, 13(3), pp.129–153.

Van Der Graaf, M., 2010. In vivo magnetic resonance spectroscopy: basic methodology and clinical applications. *Eur Biophys*, pp.527–540.

de Graaf, R.A., 2007. *in vivo NMR Spectroscopy: Principles and Techniques* 2nd ed., Connecticut: John Wiley &

Sons, Ltd.

de Graaf, R.A. & Nicolay, K., 1998. Adiabatic water suppression using frequency selective excitation. *Magnetic Resonance in Medicine*, 40(5), pp.690–696.

Haase, A. et al., 1985. 1H NMR chemical shift selective (CHESS) imaging. *Physics in medicine and biology*, 30(4), pp.341–344. Available at: http://stacks.iop.org/0031-9155/30/i=4/a=008.

Harada, M. et al., 2011. Measurement of Variation in the Human Cerebral GABA Level by In Vivo MEGA-Editing Proton MR Spectroscopy using a Clinical 3 T Instrument and its Dependence on Brain Region and the Female Menstrual Cycle. *Human Brain Mapping*, 833(July 2010), pp.828–833.

Harris, A.D., Saleh, M.G. & Edden, R.A.E., 2017. Edited 1 H Magnetic Resonance Spectroscopy In Vivo: Methods and Metabolites. *Magnetic Resonance in Medicine*, 1389(December 2016), pp.1377–1389.

Johann, G., 2011. The normalized sinc (blue) and unnormalized sinc function (red) shown on the same scale. Available at: https://en.wikipedia.org/wiki/Sinc_function#/media/File:Si_sinc.svg.

Kupce, E. & Freeman, R., 2003a. Fast multi-dimensional Hadamard spectroscopy. *Journal of Magnetic Resonance, Series A*, 163, pp.56–63.

Kupce, E. & Freeman, R., 2003b. Two-dimensional Hadamard spectroscopy. *Journal of Magnetic Resonance, Series A*, 162, pp.300–310.

Long, Z. et al., 2015. Reproducibility and effect of tissue composition on cerebellar γ -aminobutyric acid (GABA) MRS in an elderly population. *NMR in Biomedicine*, (February), pp.1315–1323.

Mclean, M.A. et al., 2002. In Vivo GABA+ Measurement at 1.5T Using a PRESS-Localized Double Quantum Filter. *Magnetic Resonance in Medicine*, 241(March), pp.233–241.

Mescher, M. et al., 1998. Simultaneous in vivo spectral editing and water suppression. *NMR in biomedicine*, 11(6), pp.266–72.

Mescher, M. et al., 1996. Solvent Suppression Using Selective Echo Dephasing. *Journal of Magnetic Resonance, Series A*, 123(2), pp.226–229.

Mikkelsen, M. et al., 2018. Big GABA II: Water-Referenced Edited MR Spectroscopy at 25 Research Sites. *NeuroImage*.

Mikkelsen, M. et al., 2016. Comparison of the Repeatability of GABA-Edited Magnetic Resonance Spectroscopy with and without Macromolecule Suppression. *Magnetic Resonance in Medicine*, 953, pp.946–953.

Mikkelsen, M. et al., 2017. NeuroImage Big GABA : Edited MR spectroscopy at 24 research sites. , 159(July), pp.32–45.

Mullins, P.G. et al., 2014. Current practice in the use of MEGA-PRESS spectroscopy for the detection of GABA. *NeuroImage NeuroImage*, 86(2), pp.43–52.

Naressi, A. et al., 2001. Java-based graphical user interface for the MRUI quantitation. *Magnetic Resonance Matierals in Physics, Biology and Medicine*, 12, pp.141–152.

Near, J. et al., 2014. Long-term reproducibility of GABA magnetic resonance spectroscopy. *NeuroImage*, 99, pp.191–196. Available at: http://dx.doi.org/10.1016/j.neuroimage.2014.05.059.

Nordmann, A., 2007. full width at half maximum. Available at: https://en.wikipedia.org/wiki/Full_width_at_half_maximum#/media/File:FWHM.svg [Accessed August 20, 2018].

O'Gorman, R.L. et al., 2011. In Vivo Detection of GABA and Glutamate With MEGA-PRESS : Reproducibility and Gender Effects. *Journal of Magnetic Resonance Imaging*, 1267, pp.1262–1267.

Oeltzschner, G. et al., 2019. NeuroImage Advanced Hadamard-encoded editing of seven low-concentration brain metabolites : Principles of HERCULES. *NeuroImage*, 185(March 2018), pp.181–190. Available at: https://doi.org/10.1016/j.neuroimage.2018.10.002.

Ogg, R.J., Kingsley, P.B. & Taylor, J.S., 1994. WET, a T1- and B1-Insensitive Water-Suppression Method for in Vivo Localized 1H NMR Spectroscopy. *Journal of Magnetic Resonance, Series B*, 104(1), pp.1–10.

Poggetto, G.D. et al., 2016. A new tool for NMR analysis of complex systems: selective pure shift TOCSY. *Royal Society of Chemistry*, 6(October), pp.100063–100066. Available at: http://dx.doi.org/10.1039/C6RA22807K.

Prescot, A.P. et al., 2018. Two-Dimensional Proton Magnetic Resonance Spectroscopy versus J -Editing for GABA Quantification in Human Brain : Insights from a GABA-Aminotransferase Inhibitor Study. *Scientific Reports*, (January), pp.1–12. Available at: http://dx.doi.org/10.1038/s41598-018-31591-3.

Provencher, S., 2018. LCModel & LCMgui User's Manual. Available at: http://lcmodel.ca.

Ryner, L.N., Sorenson, J.A. & Thomas, M.A., 1995a. 3D localised 2D NMR spectroscopy on an MRI scanner. *Journal of Magnetic Resonance, Series B*, 107, pp.126–137.

Ryner, L.N., Sorenson, J.A. & Thomas, M.A., 1995b. Localized 2D J-Resolved H MR Specroscopy: Strong coupling effects in vitro and in vivo. *Magnetic Resonance Imaging*, 13(6), pp.853–869.

Saleh, M.G. et al., 2019. Multi-vendor standardized sequence for edited magnetic resonance spectroscopy. *NeuroImage*, 189(July 2018), pp.425–431.

Saleh, M.G. et al., 2016. Simultaneous edited MRS of GABA and glutathione. *NeuroImage*, 142, pp.576–582. Available at: http://dx.doi.org/10.1016/j.neuroimage.2016.07.056.

Shungu, D.C. et al., 2016. Brain γ -aminobutyric acid (GABA) detection in vivo with the J -editing 1 H MRS technique: a comprehensive methodological evaluation of sensitivity enhancement , macromolecule contamination and test – retest reliability. *NMR in Biomedicine*, (March), pp.932–942.

Simpson, R. et al., 2017. Advanced processing and simulation of MRS data using the FID appliance (FID-A)—An open source, MATLAB-based toolkit. *Magnetic Resonance in Medicine*, 77(1), pp.23–33.

Sklenar, V. & Starcuk, Z., 1982. 1-2-1 Pulse train: A new effective method of selective excitation for proton NMR in water. *Journal of Magnetic Resonance*, 50(3), pp.495–201.

Stagg, C. & Rothman, D.L., 2013. *Magnetic resonance spectroscopy: tools for neuroscience research and emerging clinical applications*, Academic Press.

Star-Lack, J. et al., 1997. Improved Water and Lipid Suppression for 3D PRESS CSI Using RF Band Selective Inversion with Gradient Dephasing (BASING). *Magnetic Resonance in Medicine*, (38), pp.311–321.

Star-Lack, J. et al., 1998. In Vivo Lactate Editing with Simultaneous Detection of Choline, Creatine, NAA, and Lipid Singlets at 1.5 T Using PRESS Excitation with Applications to the Study of Brain and Head and Neck Tumors. *Journal of Magnetic Resonance, Series A*, l, pp.243–254.

Terpstra, M. et al., 2006. Detection of an antioxidant profile in the human brain in vivo via double editing with MEGA-PRESS. *Magnetic Resonance in Medicine*, 56(6), pp.1192–1199.

Terpstra, M., Henry, P. & Gruetter, R., 2003. Measurement of Reduced Glutathione (GSH) in Human Brain Using LCModel Analysis of Difference-Edited Spectra. *Magnetic Resonance in Medicine*, 23(August 2002), pp.19–23.

Tkáč, I. et al., 1999. In vivo 1H NMR spectroscopy of rat brain at 1 ms echo time. *Magnetic Resonance in Medicine*, 41(4), pp.649–656.

Vanhamme, L., van den Boogaart, A. & Huffel, S. Van, 1997. Improved Method for Accurate and Efficient Quantification of MRS Data with Use of Prior Knowledge. *Journal of Magnetic Resonance*, 43(129), pp.35–43.

van der Veen, J.W.C. et al., 1988. Accurate quantification of in vivo 31P NMR signals using the variable projection method and prior knowledge. *Magnetic Resonance in Medicine*.

Wendt, M., 2000. Second Order Shimming of High Field Magnets. *MRI Hot Topics*. Available at:

http://mriquestions.com/uploads/3/4/5/7/34572113/siemens_brochure_on_shimming.pdf.

Wijtenburg, S.A. et al., 2019. Comparing the Reproducibility of Commonly Used Magnetic Resonance Spectroscopy Techniques to Quantify Cerebral Glutathione. *International Society for Magnetic Resonance in Medicine*, pp.1–8.

Wijtenburg, S.A. et al., 2013. Reproducibility of Brain Spectroscopy at 7T Using Conventional Localization and Spectral Editing Techniques. *Journal of Magnetic Resonance Imaging*, 467, pp.460–467.